Journal of Chromatography A, 1221 (2012) 2–40

Contents lists available at ScienceDirect

Journal of Chromatography A

journal homepage: www.elsevier.com/locate/chroma

Review

Mass transfer kinetics, band broadening and column efficiency

Fabrice Gritti, Georges Guiochon*

Department of Chemistry, University of Tennessee, Knoxville, TN 37996, USA

ARTICLE INFO

Article history:
Available online 10 May 2011

Keywords:
Longitudinal diffusion
Eddy dispersion
External film mass transfer
Trans-particle mass transfer coefficient
Totally porous and core–shell particles
Monolithic columns

ABSTRACT

Important progress was recently made in our understanding of the physico-chemical aspects of mass transfer kinetics in chromatographic columns, in methods used for accurate determination of the different contributions to the height equivalent to a theoretical plate (HETP), and in the application of these advances to the elucidation of mass transfer mechanisms in columns packed with recent chromatographic supports (sub-2 μm fully porous particles, sub-3 μm core–shell particles, and monoliths). The independent contributions to the HETP are longitudinal diffusion, eddy dispersion, liquid–solid mass transfer (including trans-particle or trans-skeleton mass transfer and external film mass transfer), and the contributions caused by the thermal heterogeneity of the column. The origin and importance of these contributions are investigated in depth. This work underlines the areas in which improvements are needed, an understanding of the contribution of the external film mass transfer term, a better design of HPLC instruments providing a decrease of the extra-column band broadening contributions to the apparent HETP, the development of better packing procedures giving more radially homogeneous column beds, and new packing materials having a higher thermal conductivity to eliminate the nefarious impact of heat effects in very high pressure liquid chromatography (vHPLC) and supercritical fluid chromatography (SFC).

Contents

DOI of original article: 10.1016/j.chroma.2011.11.004.
* Corresponding author. Tel.: +1 865 974 0733; fax: +1 865 974 2667.
E-mail address: guiochon@utk.edu (G. Guiochon).

0021-9673/$ – see front matter © 2011 Elsevier B.V. All rights reserved.
doi:10.1016/j.chroma.2011.04.058

1. Introduction

Mass transfer kinetics has long been recognized as an important factor in the performance of the columns used in gas, liquid, and supercritical chromatography. Bohart and Adams [1] seem to have been the first authors to write a mass balance equation for chromatography, in 1920. They were studying the adsorption of chlorine from an air stream on various samples of charcoals, using frontal analysis to estimate the saturation capacity and the adsorption kinetics of chlorine on these charcoals and the interference of water and hydrochloric acid. They recognized the existence of constant pattern behavior. Later Wicke [2] gave an analytical solution of the mass balance equation, assuming irreversible adsorption and the control of mass transfer kinetics by the diffusion rate inside the particles. Diffusion and dispersion were ignored in these early models, which were simplified forms of the ideal model, solved by Wilson [3], who showed that the ideal model explains the formation and propagation of discontinuities, and by DeVault who derived the correct solution for the diffuse boundaries of elution profiles [4]. Then, attention drifted to the more realistic reaction models.

Different models of mass transfer kinetics were developed. The first such model was the Thomas or reaction model, based on Langmuir kinetics [5], which was solved by Goldstein [6]. Later came the transport model, the reaction-dispersive, and the transport-dispersive models [7–9], which combines axial dispersion to the kinetics expression of the Thomas or the transport models. Finally, the general rate model [10] accounts for most of all the kinetic factors involved in the band migration along a chromatographic column. Lapidus and Amundson [9] provided the first general solution of equilibrium-dispersive model for one compound. This solution was reformulated by van Deemter et al. in the case when band spreading is limited and the column efficiency is not really small [11]. This was the foundation for the well-known van Deemter equation, which also established a bridge between the solutions of the mathematical models of chromatography and the empirical concept of height equivalent to a theoretical plate (HETP) introduced by Martin and Singe in 1941 [12]. This bridge lead to the multiplication of fundamental and empirical investigations of band spreading in chromatography. Rapidly, however, the groups of chemical engineers drifted to the study of nonlinear chromatography [13] while analysts focused on the theory of column efficiency under linear conditions in gas [14] then liquid chromatography.

The theory of the dynamics of zone migration in chromatography was systematically investigated in depth by Giddings in the 1960s [15]. Giddings approached the problem of band broadening from three different angles, the simple random walk model [16,17], the rigorous stochastic theory [18], and the generalized non-equilibrium theory [19–22]. All three approaches were used to derive the HETP of columns. The first of these approaches merely lead to a useful didactic tool. The second was generalized by McQuarrie [23], and was later extended by Dondi and his group [24–28], who named it the stochastic-dispersive model (see Section 2.2.4). However, Giddings found the third approach, which he could easily braid with the theoretical plate concept and elaborate upon, the most attractive. He actively pursued its development [15].

The interplay of three main random processes was recognized early and too often used in the past in a loose empirical fashion to determine the extent of zone spreading along chromatographic columns. These processes are: (1) the ordinary molecular diffusion that takes place in the fluid phase used as the eluent and along the adsorbent surface on which molecules are adsorbed (the B/u_0 term in the original van Deemter equation); (2) the mass transfer kinetics, which accounts for the delay in achieving local equilibrium between the two phases of the system (the Cu_0 term in the van Deemter equation); and (3) the dispersion that originates from the different irregularities in the velocity distribution in the interparticulate space (the A term in the van Deemter equation). The van Deemter equation was modified by Knox in order to empirically account for the complex flow-dependence of the eddy dispersion term [29]. Numerous variants of the van Deemter equation were suggested, using different expressions of the eddy dispersion term. They include the coupling theory of eddy dispersion of Giddings, [15], the Huber model [30,31], the Horváth model [32], and the Bouchaud model [33]. Although all these models are fundamentally correct because they include the essence of the mass transfer processes in chromatographic columns, they all remain quantitatively inaccurate.

It turns out that all experimental data fit really well or reasonably well to the van Deemter equation. Despite this good fit, it is generally recognized that the best parameters provided by this mathematical exercise are purely empirical and generally void of physical sense [34]. There are two reasons for that. First, most experimental data are inaccurate and imprecise, in so far as they assume that eluted peaks have a Gaussian profile and neglect the contribution of the peak tailing (see Figures 6.9 and 6.10 in [13]). Second, the conventional models of interpretation of the van Deemter equation are wanting for their lack of sophistication which prevents them from properly describing the detailed structure of both the bulk and the stationary phases. Replacing the equilibrium-dispersive model with the general rate model provides a major improvement in the understanding of the band spreading process because it provides clear distinction between different steps that should be accounted for separately [13]. This model separates longitudinal and eddy dispersion, often mixed into a lumped axial dispersion coefficient, D_L. It accounts for a series of distinct, successive non-equilibrium effects like the diffusion of the sample molecules across the stationary film of eluent surrounding the porous particles, the effective diffusivity of the sample molecules through the volume of the particles which results from the combination of pore and surface diffusion, and the adsorption–desorption kinetics between the stagnant eluent inside the particles and the adsorbent surface. It is now realized that chromatographic columns are no longer operated under either isobaric or isothermal conditions as they used to be thirty years ago. These new practical constraints are inevitable with the advent of very high pressure liquid chromatography (vHPLC) [35–39] and the current renaissance of supercritical fluid chromatography (SFC) [40]. Therefore, the oversimplified and superficial description of the mass transfer mechanisms in chromatographic columns that prevailed during the early developments of HPLC and lasted for too long has now been replaced by a more sophisticated and realistic picture.

The purpose of this review is to shed light on the results of recent studies that have lead to marked improvements of our understanding of mass transfer mechanisms in HPLC. These new investigations were essentially triggered by the major breakthroughs made by the manufacturers of chromatographic media who introduced new promising products during the last decade. While the conventional columns packed with 5 μm fully porous particles were prevailing during the mid 1980s and the whole 1990s, monolithic columns made of a highly permeable solid block of bimodal porous silica (with macropores or through-pores to ensure easy percolation of the eluent stream and mesopores to provide a sufficiently large surface area promoting retention) appeared as a potentially successful product in 2000. Unfortunately, because monoliths shrink (silica) or expand (polymers) considerably during their synthesis, the beds obtained are not radially homogeneous, the radial heterogeneity of the velocity distribution warps the bands that migrate at different velocities in the column center and close to its wall, and the lack of improved fabrication processes has limited the efficiency of monolithic columns to ca. 100 000 plates/m [41,42]. For that all, this problem has triggered renewed interest for trans-column eddy dispersion [43–46].

The threat brought by the initial success of monolithic columns and the considerable interest devoted to them triggered new efforts by manufacturers of chromatographic media, locked out of the monolithic bed area by strong patents and other difficulties [41,47]. In the mid-2000s, columns packed with sub-2 μm fully porous particle were successfully offered [48]. Soon thereafter, their systematic use in vHPLC (very high pressure liquid chromatography) to perform rapid analyses of low molecular weight compounds forced chromatographers to evaluate the impact of the effects of the high pressure and mobile phase velocity required on the column efficiency [49]. They discovered that retention factors are pressure dependent and that the diffusion across the column of the heat generated by the friction of the eluent and/or absorbed by its expansion during its decompression causes the formation of significant radial and axial temperature gradients. The so-called friction–expansion HETP term was derived to account for these effects. Finally, in the late 2000s, the forty-year old concept of pellicular particles [50–52] was reborn with the preparation of sub-3 μm superficially porous particles [53,54]. The unexpectedly high performance of columns packed with these new particles has forced the reconsideration of the role of the solid core of the particles and of some of their other properties in the relative importance of the different terms of the HETP equations [55–59].

This review is divided into three main sections. Firstly, we describe the current status of the theory of band broadening in liquid chromatography and report on recent theoretical progress made on the expressions accounting for the longitudinal diffusion, the eddy dispersion, the liquid–solid mass transfer resistance, and the friction–expansion contributions to the column HETP. Secondly, we review new, most accurate experimental techniques allowing the measurements of each one of these individual HETP contributions. Finally, we explain how appropriate combinations of these theoretical and experimental developments have allowed the elucidation of many details of the mass transfer mechanisms in monolithic columns of the first generation, in HPLC columns packed with sub-2 μm fully porous and sub-3 μm superficially porous particles, and in SFC columns. The future challenges that we expect to encounter in attempts to further column technology, through investigations of the mass transfer mechanisms in chromatography and the development of preparation processes of improved particles and of ways of packing them better are finally discussed.

2. Theory

A thorough understanding of the mechanisms involved in the mass transfer of analytes through chromatographic columns requires a brief review of the models of chromatography followed by an account of how our understanding of these mechanisms progressed from the crude empiricism of the early times to the sophisticated knowledge that we have now reached and allows quantitative predictions of column HETPs.

2.1. Early history and the basics of mass transfer kinetics

The finite rate of the mass transfer kinetics between the two phases was very early recognized as a major source of band broadening in chromatography. Bohart and Adams included the corresponding term in their mass balance equation of a column [1]. Later, Thomas [5] developed the first lumped model, in which he ignored axial dispersion and the mass transfer kinetics the way we understand it now but assumed that the rate of adsorption and desorption of the analyte are finite and given by the second-order Langmuir kinetics

$$\frac{\partial C_s}{\partial t} = k_a(q_s - C_s)C - k_d C_s \quad (1)$$

where k_a and k_d are the rate constants of adsorption and desorption, respectively, C_s is the stationary phase concentration averaged over the entire particle [60], and q_s is the specific saturation capacity of the adsorbent, or amount needed to form a saturated monolayer. If we assume that the mass transfer kinetics is fast, C in this equation is the same as C_p in the equation of the general rate model. Thomas [5] derived an analytical solution of this model for a step function input (i.e., for frontal analysis) and later, Goldstein [6] derived an analytical solution for a pulse injection.

Lapidus and Amundson combined the mass balance equation of the equilibrium dispersive model (see later, Eq. (16)) with a slightly

different kinetic equation to form what is now called the lumped kinetic model. This kinetic equation is

$$\frac{\partial C_s}{\partial t} = k_a C - k_d C_s \tag{2}$$

where k_a and k_d are the adsorption and desorption rate constants, respectively. Two similar but simpler models have also been used.

The solid film linear driving force model:

$$\frac{\partial C_{s,i}}{\partial t} = k_f(q_i - C_{s,i}) \tag{3}$$

where q_i is the equilibrium value of $C_{s,i}$ for a mobile phase concentration equal to C_i and k_f is the lumped mass transfer coefficient. This model was often used by Glueckauf and Coates [61], Hiester and Vermeulen [62], Lin et al. [63], and Golshan-Shirazi et al. [64].
The liquid film linear driving force model:

$$\frac{\partial C_{s,i}}{\partial t} = k_m'(C_i - C_i^*) \tag{4}$$

where C_i^* is the solute concentration in the eluent that is in equilibrium with the solid phase concentration $C_{s,i}$. Thus, C_i^* is derived from the isotherm equation. Under linear conditions, $C_i^* = q_i/a$ where a is the slope of the isotherm ($a = k_0'/F$, F, phase ratio), and k_m' is the apparent (lumped) mass transfer coefficient.

In linear chromatography, these two kinetic models are particular cases of the Lapidus and Amundson model [9] and give the same solution. In contrast, these lumped kinetic models give different solutions in nonlinear chromatography. Investigations of the properties of these models and especially of the relationship between the band profiles and the value of the kinetic constants have been carried out for many single-component problems [13].

Lapidus and Amundson [9] derived an analytical solution to their model. Van Deemter et al. [11] simplified this analytical solution in the case of linear chromatography and showed that, if the rate controlling step of the mass transfer kinetics in the chromatographic column is not very slow, this solution can be reduced to a Gaussian profile. By comparing their simplified solution to that of the plate theory [12] they derived a landmark relationship between the height equivalent to a theoretical plate of the plate model, the axial dispersion coefficient, and the lumped mass transfer coefficient of their linear driving force model, the *van Deemter equation*, which can be written in the modern terminology

$$h = \frac{B}{\nu} + A + C\nu \tag{5}$$

where h is the reduced plate height, ν the reduced velocity, A, B, and C numerical coefficients related to the parameters of the column. A considerable effort, lead by Giddings [15,19–22,65], Knox [29,66], and Poppe [67] has been devoted for over fifty years to the elaboration and refinement of these relationships. These efforts were hampered for a long time by the lack of suitable methods allowing the accurate measurements of the different steps involved in the mass transfer kinetics and of systematic investigations of these steps. Systematic efforts carried out during the last ten years has brought considerable progress.

Gunn investigated the mechanisms of axial and radial mixing in random packed beds, like chromatographic columns, catalytic reactor beds, etc. [68–70]. Mixing was described as a stochastic process and Gunn developed a probability theory that incorporates the influences of both convection and diffusion [68]. Axial dispersion is due to the combination between dispersion due to convection and to molecular diffusion. To estimate the contribution of convection, consider a tracer particle entering a flow cell in the packed bed. As the first approximation, this particle has a probability p to move a certain distance x_p and the probability $1-p$ to stay in the cell for a time interval T, during which it moves by $px_p = d$. The probability for the tracer to achieve r moves downstream after making n attempts is given by a binomial distribution, which provides the probability p_r that a particle moves downstream by a distance d:

$$p_r = \frac{n!}{p!(n-r)!}p^r(1-p)^r\frac{d}{p} \tag{6}$$

since the probability that the tracer stays at rest for any attempt is $(1-p)$. We consider for distance d the particle diameter, d_p. Then it is straightforward that mean migration distance after n attempts is $npx_p = nd_p$ while the variance is $\sigma^2 = np(1-p)d_p^2/p^2$ about the mean. When n increases to infinity, the binomial distribution tends toward a Gaussian distribution. The variance of this distribution under the influence of dispersion with a coefficient D, after a time t is

$$\sigma^2 = 2Dt \tag{7}$$

Accordingly, since $t = nd_p/U$, with U the average interstitial linear velocity, we have

$$np(1-p)\frac{d^2}{p^2} = 2\frac{Dn\,d}{U} \tag{8}$$

or

$$\frac{Ud}{D} = \frac{2p}{1-p} \tag{9}$$

Diffusion transfers tracer molecules from regions where the flow of the stream is slow to regions where it is fast and conversely. The probability p may be considered as a measure of the fraction of the fluid in a unit cell of the packed bed that moves fast (at a velocity $U_f = U/p$) while the fraction $1-p$ corresponds to the fraction of the fluid that moves at a slower velocity ($U_s = 0$).

A detailed discussion of the modeling of diffusion between the fast and the slow streams leads to the following equation combining the effects of convection and diffusion

$$\frac{D}{Ud} = \frac{ReSc}{\epsilon\Gamma}(1-p)^2 + \frac{Re^2Sc^2}{\epsilon^2\Gamma^2}p(1-p)^3 \times \left[\exp\left(\frac{-\epsilon\Gamma}{p(1-p)ReSc}\right) - 1\right] + \frac{\epsilon}{\tau ReSc} \tag{10}$$

where ϵ is the bed external porosity, τ its tortuosity, and Γ a characteristic of the packed bed, with $\Gamma = 4(1-\epsilon)\alpha_1^2/\epsilon$, and α_1 the first root of the zero-order Bessel function, and Re and Sc are the Reynolds and the Schmidt numbers with

$$Re = \frac{Ud\rho}{\eta} \tag{11}$$

$$Sc = \frac{\eta}{\rho D_m} \tag{12}$$

where ρ and η are the fluid density and viscosity, respectively, and D_m the molecular diffusivity of the analyte. This equation has Eq. (8) for limit when $Re\,Sc$ becomes very large (convection is much faster than diffusion). Conversely, when convection becomes slow and the limit is

$$\frac{Ud}{D} = \frac{\tau ReSc}{\epsilon} \tag{13}$$

This equation accounted fairly well to experimental data measured for the dispersion of several compounds in streams of various fluids, both gases and liquids, under different experimental conditions by several authors [68,70,71]. A more complex equation including the dispersion contribution of the fluctuations of the mobile phase velocity in non- uniform random packed beds was developed later [70].

Strangely, this work has rarely been used in liquid chromatography. It seems that knowledge of the work of Gunn on dispersion in packed bed has never reached the chromatographic community. Regretfully, we must realize that the important Eq. (10) was never been applied to investigate the velocity dependence of efficiency data. It should be emphasized that the parameter D in this equation is not the molecular diffusivity D_m but the apparent dispersion coefficient, often called D_L. It combines the contributions of axial dispersion and eddy dispersion and mixes the contributions usually considered separately, as the A and B terms of the van Deemter equation. It considers that the particles are solid, nonporous. This restricts the usefulness of this equation.

2.2. The models of chromatography

This section reports on the development of the models of chromatography based on the mass balance equations in the column, starting with the ideal model of chromatography and ending with the most sophisticated model, the general rate model.

2.2.1. The ideal model

This model assumes that there is no axial diffusion of the sample band but that equilibrium is achieved everywhere at all times. Therefore, the mass balance reduces to [13]:

$$\frac{\partial C}{\partial t} + \frac{1-\epsilon_t}{\epsilon_t}\frac{\partial q}{\partial t} + u_0\frac{\partial C}{\partial z} = 0 \tag{14}$$

where C and q are the sample concentration in the bulk and in the stationary phase, respectively, t is the time, ϵ_t is the total column porosity (or volume fraction of the column occupied by the eluent), z is the axial coordinate, and $u_0 = (F_v/\epsilon_t \pi r_c^2)$ is the chromatographic linear velocity. Equation (14) was first derived by Wicke [2] then, independently by Wilson [3] who showed that it can propagate concentration discontinuities or shocks. DeVault [4] derived a solution for the continuous part of the solution. In analytical applications, the equilibrium isotherm between the two phases of the system is linear, with $q = Kc$, so the solution of Eq. (14) is a band identical to the injection profile or inlet boundary condition, i.e., for a pulse injection, δ-Dirac, it is a pulse migrating at the constant linear velocity u_R [72]:

$$u_R = \frac{u_0}{1 + \frac{1-\epsilon_t}{\epsilon_t}K} = \frac{u_0}{1+k} \tag{15}$$

where K is the equilibrium Henry's constant and k is the retention factor.

The main property of the mathematical δ-Dirac function is its zero bandwidth. The HETP equation is then $H = 0$. This model is unrealistic since it assumes that radial diffusion is infinite (to ensure radial equilibrium) but that axial diffusion is zero. It is useless in analytical chromatography. However, it is most important in nonlinear and preparative chromatography because it results from the mathematical properties of Eq. (14) that each concentration propagates at its own velocity, which is a function of the equilibrium isotherm [13,73]. So, the ideal model predicts reasonably accurate overloaded band profiles. To account for band profiles in linear chromatography, we need a model which takes into account the sources of band broadening during the migration of analyte bands along the column.

2.2.2. The equilibrium-dispersive model

The equilibrium-dispersive model assumes that all non-equilibrium effects can be lumped into a single axial dispersion coefficient, D_a. An axial dispersion term is added to the mass balance equation of the ideal model [13], leading to the equation:

$$\frac{\partial C}{\partial t} + \frac{1-\epsilon_t}{\epsilon_t}\frac{\partial q}{\partial t} + u_0\frac{\partial C}{\partial z} = D_a\frac{\partial^2 C}{\partial z^2} \tag{16}$$

The apparent axial dispersion coefficient is directly related to the plate height H at the corresponding linear velocity u_0 by [13]:

$$H = \frac{2D_a}{u_0} \tag{17}$$

This model of chromatography is widely used for the prediction of band broadening in preparative chromatography due to its simplicity, which allows very fast calculations of elution band profiles. Because, in many if not most practical cases, the thermodynamic causes of band broadening, which are accurately accounted for in Eq. (16), are more important than those of kinetic origins, this model provides a correct description of elution band profiles and permits the calculation of reasonable estimates of the performance of a preparative system [13]. However, this model is purely empirical. It completely ignores the causes for the non-equilibrium effects taking place in actual chromatographic columns. The D_a coefficients that it provides do not give any valuable information on the sources of band broadening nor on ways to reduce their contribution.

This is why attention must be shifted toward a more sophisticated model of chromatography, the general rate model.

2.2.3. The general rate model

The general rate model considers separately the fraction of the eluent that percolates through the column bed and flows across the interstitial volume and the fraction of eluent that is stagnant in the internal volume, in the pores of the particles or mesopores of the monoliths. Obviously, all analytes partition between the percolating and the stagnant fluid with an equilibrium constant equal to unity. Separate mass balance equations are written for the stagnant and for the mobile fluids. This approach is justified by the profound differences between the mass transfer mechanisms of analytes in these two fluids.

The mass balance equation for the external bulk eluent is written [13]:

$$\frac{\partial C}{\partial t} + \frac{A_s}{\epsilon_e}j_s + u\frac{\partial C}{\partial z} = D_L\frac{\partial^2 C}{\partial z^2} \tag{18}$$

where ϵ_e is the external porosity of the column (generally $\simeq$0.4 for packed beds and $\simeq$0.7 for monolithic columns), $u = (F_v/\epsilon_e \pi r_c^2)$ is the interstitial linear velocity, D_L is the axial dispersion coefficient in the mobile phase, A_s is the ratio of the external surface area of the stationary phase to the column volume, and j_s is the mass flux density of molecules exchanged between the interstitial and internal eluents:

$$j_s = k_f\,[C - C_i(r = R_s)] \tag{19}$$

where k_f is the external film mass transfer coefficient, C_i is the sample concentration in the internal eluent, inside the mesopores of the porous stationary phase, r is the radial coordinate, and R_s is the characteristic radius of the stationary phase. For spherical particles (packed columns) and cylinders (monolithic stationary phase), we have $A_s = (3(1-\epsilon_e)/R_s)$ and $(2(1-\epsilon_e)/R_s)$, respectively.

The mass balance equation in the stagnant eluent (assume that the particles have a spherical shape, which is the general case for modern particles) is written [13]:

$$\epsilon_p\frac{\partial C_i}{\partial t} + (1-\epsilon_p)\frac{\partial q}{\partial t} = D_p\left[\frac{\partial^2 C_i}{\partial r^2} + \frac{2}{r}\frac{\partial C_i}{\partial r}\right] \tag{20}$$

where q is the solid phase concentration, ϵ_p is the internal porosity of the particles, and D_p is the effective diffusion coefficient in the

stationary phase (combining the contributions of both pore and surface diffusion).

These two mass balance equations are not independent since the eluent and analyte molecules equilibrate between them. So, these equations are linked by this exchange of molecules. Accordingly, the mass flux density of solute entering the interstitial volume when coming from the internal volume is equal to the mass flux density of solute leaving the stationary phase. Therefore:

$$k_f\,[C - C_i(r = R_s)] = D_p \left(\frac{\partial C_i}{\partial r}\right)_{r=R_s} \tag{21}$$

Additionally, if the adsorption–desorption from the mesopore volume to the solid surface is slow, the rate of variation of the sample concentration in the solid adsorbent can be written according to a first-order adsorption–desorption kinetics model [13]:

$$\frac{\partial q}{\partial t} = k_a \left(C_i - \frac{q}{K}\right) \tag{22}$$

where k_a is the adsorption rate constant.

In conclusion, the general rate model can account for four distinct sources of non-equilibrium effect: (1) The axial dispersion (kinetic parameter D_L) in the interstitial volume which combines longitudinal diffusion and eddy dispersion in the moving eluent, (2) The mass transfer resistance (kinetic parameter k_f) across the external surface area of the stationary phase, (3) The sample diffusivity across the stationary phase volume (kinetic parameter D_p), and (4) the slow adsorption–desorption rate onto the surface of the solid adsorbent (kinetic parameter k_a).

After Laplace transform of the time domain equations, Kučera [74] and Kubin [75] derived the first and second central moments of the resulting band profiles under linear conditions ($q = KC_i$) for columns packed with spherical particles. The same approach was applied by Miyabe [76] in order to derive the moments of monolithic columns (cylindrical stationary phase geometry). In the case of packed columns, the HETP was then written [13]:

$$H = \frac{2D_L}{u} + 2\frac{\epsilon_e}{1-\epsilon_e}\left(\frac{k_1}{1+k_1}\right)^2 \times \left[\frac{d_p^2}{60D_p} + \frac{d_p}{6k_f} + \frac{1}{1-\epsilon_p}\left(\frac{k_p}{1+k_p}\right)^2 \frac{1}{k_a}\right] u \tag{23}$$

where k_1 and k_p are given by [13]:

$$k_1 = \frac{1-\epsilon_e}{\epsilon_e}\left[\epsilon_p + (1-\epsilon_p)K\right] \tag{24}$$

and

$$k_p = \frac{1-\epsilon_p}{\epsilon_p}K \tag{25}$$

where k_1 is the zone retention factor. Due to the distinction made by the general rate model between the two fractions of the mobile phase, the percolating eluent (in which the analyte is not retained) and the stagnant one (in which the analyte may be retained), the conventional definition of the retention factor has to be abandoned for the concept of zone retention factor. The actual retention time gives the correspondence between these two factors

$$t_R = (1+k)t_0 = (1+k_1)t_e \tag{26}$$

where t_0 is the hold-up time in the sum of the interstitial and stagnant volumes of the eluent in the column and t_e is the hold-up time in the interstitial moving volume of the mobile phase.

Despite the excellent description of a real chromatographic column by the general rate model and its use to predict complex band profiles [77], Eq. (23) does not reveal all the physico-chemical phenomena or sources of band broadening in chromatography. The first weakness of the general rate model of chromatography concerns the expression of its axial dispersion coefficient D_L. This coefficient lumped two distinct non-equilibrium effects: the longitudinal diffusion (the classical B coefficient in the van Deemter equation), which is related to the relaxation of the concentration gradients within the sample zone during its migration, and the eddy dispersion (the classical A term in the van Deemter equation), which accounts for any type of flow unevenness in the column. These two terms can be described separately. The second weakness of the general rate model does not consider the source of band broadening caused by friction–expansion of the mobile phase when either very high pressures (in very high-pressure liquid chromatography also called vHPLC) or highly compressible mobile phases (in supercritical fluid chromatography, SFC) are applied. Finally, appropriate expressions for the kinetic parameters k_f, D_p, and k_a are needed in the specific case of chromatographic columns.

2.2.4. The stochastic-dispersive model

This model was initially suggested by Giddings and Eyring [18], who showed that the migration of molecules along a column could be modeled as a Poisson process. Considering the random migration of a series of isolated molecules along the column, they derived an expression for their residence times distribution This derivation assumed the random adsorption–desorption of the molecules on a single type of sites, ignored diffusion in the mobile phase, that all the molecules spend the same amount of time (t_0) in the mobile phase, and a pulse injection. McQuarrie extended this model to the cases of different injection inputs and to an adsorbent having multiple types of adsorption sites [23]. Using the same model as the one developed by Giddings and Eyring, he solved the stochastic model of chromatography in the case of a column having a number of types of sites with different adsorption energy distributions. He used the complex variable theory of Laplace transforms to derive exact expressions, which are usually complicated and of limited numerical utility. He also used an alternative technique that consider only the first few central moments and which proved to be of great practical use since a theorem of mathematical statistics allows one to determine moments of complex problems when those of simpler problems are known. This made it possible the derivation of expressions easy to use for the various elution profiles.

Later, Cavazzini et al. showed that the Monte Carlo model of nonlinear chromatography is equivalent to the Thomas kinetic model with a second order Langmuir kinetics [28]. Felinger et al. [78] demonstrated the equivalence between the lumped kinetic model of chromatography [13] and the microscopic model of chromatography, which combines the random migration of the solute molecules carried along the column by the mobile phase and the random adsorption–desorption of these molecules on the stationary phase. This latter process is modeled as a Poisson process that assumes exponential distributions of the residence times of the analyte molecules in both the mobile and the stationary phases. Although the stochastic model provides useful information on the behavior of molecules during the migration of a sample bolus along the column, for example, the time that they spend in a particle during their migration along the column and the number of particles that a molecule visits on the average, it has not generated a wealth of results comparable to what the development of the generalized non-equilibrium theory and its consequences has generated [13].

Felinger published an informative analysis of simple chromatograms showing how the stochastic model provides interesting and surprising details regarding the migration of analyte molecules along the column [79]. He demonstrated how the evaluation of chromatograms of nonionizable analytes shows that a molecule undergoes between 13,000 and 20,000 adsorption events when it is eluted on a 150 mm × 3.9 mm RPLC column and that this number is not strongly affected by the retention factor of the analytes

(the average residence time increases while the number of adsorption events hardly changes). Depending on the retention factor, the average fly-times in the mobile phase between a desorption and the subsequent adsorption vary roughly between 3 and 5 ms, during which time the molecule travels on the average a distance of 1.5–2.3 times the particle diameter [79]. However, for half the times, the molecule travels downstream by less than one particle diameter, probably visiting the same particle twice. Yet, it visits only a very small fraction of the particles in the column bed. The number of 5 μm particles packed in a 150 mm × 3.9 mm column is about 1.8×10^{10}. Thus, molecules visit only a tiny fraction of the stationary phase particles during their elution. One molecule visits only one out of every one million particles [79]. Since the sojourn time in the stationary phase strongly correlates with the analyte retention, the selectivity of analyte separations is mainly due to the dependence of this sojourn time on k, between 8.4 ms (for $k' = 1.75$) and 47 ms (for $k' = 12.7$) in a typical example.

In summary, the stochastic model provides useful information on the statistical behavior of molecules during their elution process. It informs on their residence times and their distribution. It can also be useful to investigate heterogeneous interactions, as exemplified in the work of Felinger at al. [24]. For example, Felinger [80] determined the number of visits and the average residence of phenol molecules eluted by methanol/water solutions on a 4.6 mm × 75 mm column packed with 5 μm particles of Symmetry C_{18} (Waters, Milford, MA). The average number of visits onto the low-energy, fast sites decreases linearly from 23,500 to 2700 when the methanol concentration increases from 10 to 70% while their average residence time on these sites decreases from 0.20 to 0.008 ms. The average number of visits onto the high-energy, slow sites decreases rapidly from ca. 2.4 to practically 0 when the methanol concentration increases from 5 to 50% while their average residence time on these sites decreases from 20 to 0.01 ms. These results are consistent with the findings of the existence of two types of sites of adsorption on this packing material [81].

2.3. Physico-chemical description of the general HETP equation

In the next subsections, we will report on the theoretical expressions of all the non-equilibrium effects that can be possibly involved in a chromatographic column. They include the contribution of the longitudinal diffusion ($H_{Long.}$), the eddy dispersion (H_{Eddy}), the external film mass transfer resistance (H_{Film}), the mass transfer resistance across the stationary phase including pore and surface diffusion ($H_{Stat.}$), the rate of adsorption–desorption at the surface of adsorbent (H_{ads}), and the friction–expansion of the mobile phase ($H_{Fric.-Expa.}$). All these physico-chemical phenomena being independent, the total HETP is then written:

$$H = H_{Long.} + H_{Eddy} + H_{Film} + H_{Stat.} + H_{ads.} + H_{Fric.-Expa.} \quad (27)$$

The HETP equation (27) accounts for all the non-equilibrium effects, which will be derived from a rigorous physico-chemical analysis. It clearly differs from the old and semi-empirical van Deemter [11] and Knox [29] HETP equations, the coefficients of which are meaningless and cannot be related to any physical description of the mass transfer mechanism in a chromatographic column. For the sake of comparison, we recall that the van Deemter plate height equation is written [11]:

$$H = \frac{B}{u_0} + A + C_s u_0 \quad (28)$$

where u_0 is the chromatographic linear velocity and B, A, and C_s are empirical parameters. The Knox reduced plate height equation is written [29]:

$$h = \frac{2\gamma_e}{\nu} + \alpha\nu^{1/3} + \omega\nu \quad (29)$$

where γ_e is the external obstruction factor (<1) and α and ω are empirical parameters.

These old HETP equations simply allows a good mathematical fit between experimental and theoretical data but ignore the actual mass transfer mechanisms involved in the column.

2.3.1. Longitudinal diffusion and the B term

The contribution of the longitudinal diffusion HETP term to the overall HETP becomes preponderant when the mobile phase velocity is such that it takes longer for a sample molecule to be displaced by convection than by diffusion at the scale of the particle (d_p) or the monolithic domain size. The time necessary for the molecules to move a distance d_p by pure convection is t_c, which is given by:

$$t_c = \frac{d_p}{u} \quad (30)$$

The time necessary to diffuse along a distance d_p is t_d, given by

$$t_d = \frac{d_p^2}{2D_{eff}} \quad (31)$$

where D_{eff} is the effective or apparent diffusion coefficient in the composite material made of porous particles in contact and dispersed in the eluent matrix. D_{eff} depends on the molecular diffusivity, D_m, but is different; it depends also on the equilibrium constant between the two phases [58,59]. It is defined by the apparent diffusion equation along the heterogeneous packed bed [34] in the absence of flow ($u = 0$):

$$\frac{\partial C}{\partial t} = D_{eff}\frac{\partial^2 C}{\partial z^2} \quad (32)$$

Accordingly, the longitudinal diffusion term is dominant when $t_c > t_d$ or when:

$$\frac{u d_p}{D_{eff}} < 2 \quad (33)$$

The longitudinal diffusion coefficient B related to the interstitial linear velocity u is defined by [34]:

$$H_{Long.} = \frac{B}{u} \quad (34)$$

By definition, the longitudinal diffusion HETP term, $H_{Long.}$, is the ratio to the column length, L, of the variance increment arising from the sample diffusion along the column bed during its elution time, $t_R = (1 + k_1)L/u$ (with L, the column length).

$$H_{Long} = \frac{2D_{eff}t_R}{L} = \frac{2(1+k_1)D_{eff}}{u} \quad (35)$$

Eq. (35) demonstrates that the calculation of the actual longitudinal diffusion term requires the knowledge of the effective diffusion coefficient of the sample component in the composite material made of the stationary phase (the adsorbent particles impregnated by the eluent, diffusion coefficient ΩD_m, volume fraction $1 - \epsilon_e$) and the bulk mobile phase (diffusion coefficient D_m, volume fraction ϵ_e). So, we need to find a suitable model in the list of various models of effective diffusion in columns packed with fully and superficially porous particles. The ratio of the core to the particle diameters is called ρ.

2.3.1.1. The time-averaged model. Until today, the *B* coefficient was primarily derived from the time-averaged diffusion model elaborated by Knox [82] and well documented in most chromatographic books devoted to mass transfer kinetics in chromatography [15,83]. This model is simply based on the additivity of the mass density fluxes in the particles and in the external eluent. It is written [34]:

$$D_{eff} = \frac{\gamma_e + \frac{1-\epsilon_e}{\epsilon_e}(1-\rho^3)\Omega}{1+k_1} D_m \quad (36)$$

Let recall that the coefficient Ω is the ratio of the sample diffusivity in the porous adsorbent to the bulk diffusion coefficient and ρ the relative diameter of the non-porous core to the that of the particle. The result for fully porous particles is directly obtained for $\rho = 0$. Note also that the zone retention factor, k_1, for columns packed with core–shell particles is written [55]:

$$k_1 = \frac{1-\epsilon_e}{\epsilon_e}\left[\epsilon_p + (1-\epsilon_p)K\right](1-\rho^3) \quad (37)$$

The time-averaged model of diffusion predicts approximate [84,85] but physically meaningful values for the effective diffusivity in packed beds of small and large molecules [34,45,39,49,74,82,86–91,93–103]. Yet, there is place for improvement because the 3D distribution of the different phases (external eluent, porous material, and solid cores) is not as simple as that of a parallel distribution. Effective medium theories are definitely needed in order to account for the actual micro-structure of packed beds.

2.3.1.2. The Landauer model. The effective medium theory (EMT) of Landauer [104] has been thoroughly applied to the determination of effective electrical conductivity of composite materials. The EMT of Landauer consider that the dispersion of different phases is strictly random. It was extended to the problem of mass diffusion by Davis [105]. The diffusion model of Davis was recently applied to the problem of effective diffusion along a chromatographic column packed with core–shell particles [58,59,106]. Equivalent results were obtained by applying the analogy between permeability properties and diffusion properties [84,85]. The effective diffusion coefficient is then written [58]:

$$D_{eff} = \frac{a + \sqrt{a^2 + \frac{1}{2}\left(1 - \frac{3}{2}\rho^3[1-\epsilon_e]\right)\Omega}}{\epsilon_e(1+k_1)} D_m \quad (38)$$

with

$$a = \frac{1}{4}[3\epsilon_e - 1 + \Omega(3[1-\rho^3][1-\epsilon_e] - 1)] \quad (39)$$

The weakness of the EMT of Landauer is that the assumption of a random distribution for the non-porous cores, the porous shells, and the external eluent. Next we report on the result of the effective diffusion in packed beds by rigorously taking into account the specific arrangement of the different homogeneous phases in a chromatographic column.

2.3.1.3. The Garnett model. The Garnett effective medium theory of composite materials [107] assumes that the different phases are arranged as cores described by one homogeneous phase and surrounded by successive concentric shells, which account for the other homogeneous phases. This theory was then directly applied to the determination of the effective diffusion coefficient in columns packed with core–shell particles [59], the particular case of fully porous particles being derived from the condition $\rho = 0$. The final expression is given by [59]:

$$D_{eff} = \frac{2}{\epsilon_e(1+k_1)} \frac{\epsilon_e(2+\rho^3) + \Omega(1-\rho^3)(3-2\epsilon_e)}{(3-\epsilon_e)(2+\rho^3) + 2\Omega(1-\rho^3)\epsilon_e} D_m \quad (40)$$

This model accounts correctly for the geometry of the particles but ignores the physical contact between the packed particles, i.e., the spatial distribution of the bulk eluent matrix surrounding these particles. By construction, it assumes that the entire interstitial void is filled with a series of smaller and smaller inclusions, down to infinitesimally small ones. This model describes the *B* coefficient of a fractal composite material, but packed chromatographic beds are not fractal objects.

2.3.1.4. The Torquato model. More realistic models of effective diffusion in packed beds can be derived by taking into account the exact micro-structural details of the composite medium which are provided by the probability (*n*-point probability function) of finding in a given point in space either one of the different homogeneous phases that combine to make the whole composite medium [108]. This approach was recently reported for the possible determination of the *B*-term in chromatography [57,109]. Among others, it was used to describe the effective properties of a composite material described by the random dispersion of impenetrable spheres in a continuum matrix [110]. Finally, if these spheres are replaced with core–shell particles in contact, one can derive the most physically consistent model of diffusion along a chromatographic bed packed with core–shell particles. This model is written [59]:

$$D_{eff} = \frac{1}{\epsilon_e(1+k_1)}\left[\frac{1 + 2(1-\epsilon_e)\beta - 2\epsilon_e\xi_2\beta^2}{1 - (1-\epsilon_e)\beta - 2\epsilon_e\xi_2\beta^2}\right] D_m \quad (41)$$

with

$$\beta = \frac{\frac{1-\rho^3}{1+\frac{\rho^3}{2}}\Omega - 1}{\frac{1-\rho^3}{1+\frac{\rho^3}{2}}\Omega + 2} \quad (42)$$

and with $\xi_2 = 0.3277$ when the core–shell particles are in physical contact [110].

This model takes into account both the geometry of the core–shell particles and their random spatial distribution inside the column.

Note that all the previous four models of effective diffusion in ternary materials cannot predict the true value of the *B* coefficient because they necessarily ignore the microstructure of the actual packed chromatographic beds. Short-range packing disorder can affect the measured value of the *B* term at a constant external porosity. Nevertheless, the Garnett and the Torquato models can provide very accurate estimates of the true longitudinal diffusion coefficients because they describe fairly well the geometry of core–shell particles packed in a chromatographic column and in close contact with each other.

2.3.1.5. Model comparison and prediction of the B-term. In this section, we compare the predictions of the *B*-term (Eq. 35) provided by the time-averaged, the Landauer, the Garnett, and the Torquato models of effective diffusion as a function of the parameter ρ ($\rho = 0$ for fully porous particles and $\rho = 1$ for nonporous particles). The coefficient *B* is written from Eq. (35):

$$B = 2(1+k_1)D_{eff} \quad (43)$$

For the sake of relevance with actual columns packed with core–shell particles, we fixed the external porosity $\epsilon_e = 0.40$. We consider first the case of a non-retained low-molecular-weight compound ($\Omega = \epsilon_p\gamma_p F(\lambda_m) = 0.40 \times 0.60 \times 0.82 = 0.20$), where γ_p is the internal obstruction factor [87], and $F(\lambda_m)$ is the internal hindrance diffusion parameter associated to the confinement of the sample within narrow mesopores and estimated from the Renkin [111] or Brenner [112] correlation. Note that in the expression of the time-averaged diffusion model Eq. (36), we assume $\gamma_e = 0.65$ as it was measured for columns packed with non-porous cores [42].

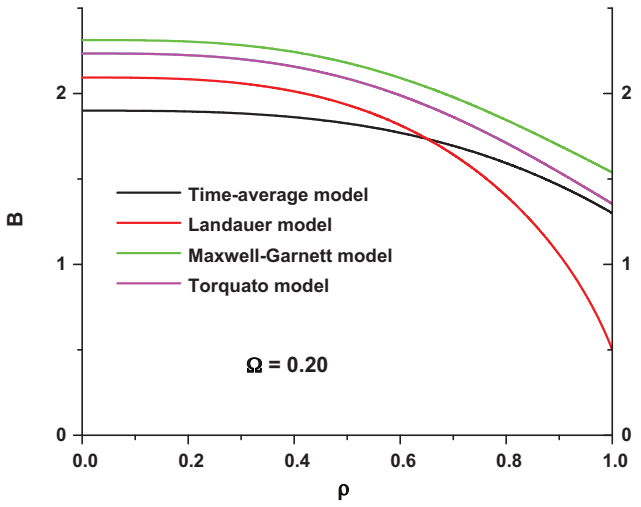

Fig. 1. Plot of the reduced longitudinal diffusion coefficient B as a function of the ratio of the core to the particle diameter, ρ, for a non-retained compound, for two models of effective diffusion coefficients in columns packed with core–shell particles. The external porosity of the bed is $\epsilon_e = 0.4$ and the relative analyte diffusivity in the shell to that in the bulk phase (D_m), Ω, is 0.20.

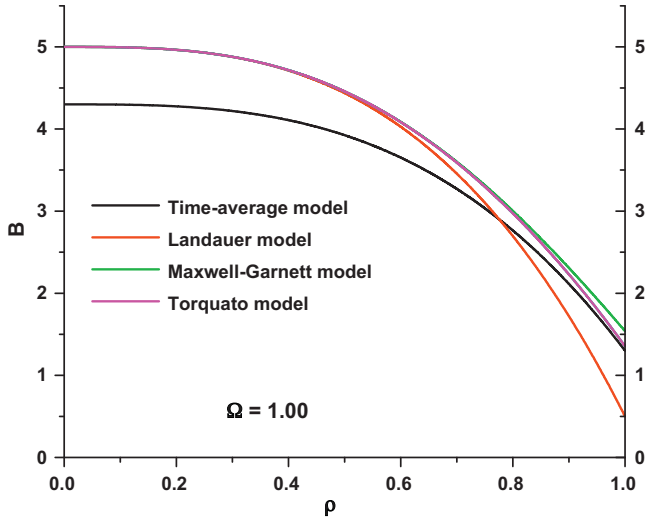

Fig. 2. Plot of the reduced longitudinal diffusion coefficient B as a function of the ratio of the core to the particle diameter ratio, ρ, for a retained compound in RPLC and for the four models of effective diffusion coefficients in columns packed with core–shell particles. The external porosity of the bed is $\epsilon_e = 0.4$ and the relative sample diffusivity in the shell to that in the bulk phase (D_m), Ω, is equal to 1.0.

Fig. 1 compares the trends of the four models described above. As expected, the B term decreases as the ratio ρ increases or when the relative size of the nonporous core to that of the particle increases. This decrease illustrates (1) the absence of sample diffusion in volume occupied by these cores and (2) the obstruction for diffusion caused by these impermeable spheres. We note first that the Landauer model makes no physical sense for ρ values close to 1. This model predicts a B term of 0.5 for nonporous particles while a value of 1.3 is expected according to the experiments [42]. The Landauer model clearly fails. We can observe that the decrease predicted by the time-averaged model of diffusion is not as steep as those of the Garnett and Torquato models because the increasing obstruction of the cores when ρ increases is not taken into account in this simple model. In contrast, the Garnett and the Torquato model of diffusion show the most realistic decrease of the B term. The Torquato appears to be the best model of diffusion because it predicts a B value of 1.35 with nonporous particles, a value in excellent agreement with the experiment (1.30). The small difference observed may be due to the fact that the actual size distribution of the cores is not infinitely narrow (RSD around 5% [99]) as is assumed in the Torquato diffusion model, and contributes to the local disorder in the real packing.

Fig. 2 shows the same figure as in Fig. 1, except that the ratio of the sample diffusivity in the porous shell to the bulk diffusion coefficient, Ω, is increased to unity. In RPLC, this illustrates the case of a small retained compound. Ω increases because surface diffusion in the adsorbed state adds up to the mesopore diffusion.

When $\Omega = 1$, the porous shell behaves just as the eluent matrix in terms of sample diffusivity. Therefore, if the particles are fully porous, the column is equivalent to a column filled with eluent, $D_{eff} = D_m$, $B = (2/\epsilon_e) = 5$. The time-averaged model is the sole diffusion model which converges to $B = 4.3$ when $\rho \to 0$ because it accounts for the external obstruction factor, γ_e, for all ρ values. Very interestingly, the Garnett and Torquato are nearly distinguishable for most ρ values. Both models account for the exact distribution of the cores, concentric porous shells, and eluent matrix existing in a chromatographic column packed with core–shell particles. They can be considered as the reference expressions for the longitudinal diffusion term in the general HETP equation (27). Finally, the Torquato diffusion model is more relevant than the Garnett model regarding the prediction of the B-term with nonporous particles.

2.3.2. Eddy dispersion and the A term

The eddy dispersion HETP term, H_{Eddy}, accounts for the source of band broadening related to any flow unevenness in the column. The flow pattern in an HPLC column is of the creeping laminar flow type [113], with a Reynolds number of the order of 0.01 or often less. So, there could not be any actual turbulence, with does rule out the formation of stable, laminar eddies in some places throughout the column, e.g., between particles. For all that, however, the presence of zones where some back-circulation (with negative velocities) takes place under viscous flow conditions and may contribute to enhance flow evenness in the column.

Initially, it was considered, as suggested by van Deemter et al. [11] that the contribution of eddy diffusion to band broadening could be accounted for by a constant term, proportional to the particle diameter. Later, Giddings recognized that numerous experimental results demonstrated that this contribution was not constant but that it was a complex function of the mobile phase flow velocity [114–116]. He explained that eddy diffusion is due to the irregularities of the stream paths in the anastomosed network of channels of the porous medium [114]. The velocity along a given streamlet persists for a length of the order of d_p, after what it changes randomly. This migration process is equivalent to a random walk process, with molecules within any stream-path stepping back and forward with respect to those migrating at the average stream velocity. The diffusion coefficient of such a process is

$$D = \frac{l^2 n_1}{2} = \frac{v^2}{2n_1} \tag{44}$$

where $l = \lambda d_p$ is the length of a step, v the average velocity, and $n_1 = v/l = v/(2\lambda d_p)$ the number of steps per unit time. Then, Giddings suggested that molecules may alter their migration velocity by diffusing from their current stream-path to a nearby one, if there is any radial concentration gradient. Let assume that a step in this direction takes place after a migration distance $l = \beta d_p$. Then, the number of steps is

$$n_2 = \frac{2D}{\beta^2 d_p^2} \tag{45}$$

Actually, eddy diffusion arose from a coupling between these two contributions because streamlines along the bed can randomly merge and split, depending on the random 3D distribution of

the particle positions in the column. The total number of steps undertaken by a molecule being $n_1 + n_2$, the apparent dispersion coefficient becomes

$$D = \frac{v^2}{v/\lambda d_p + 4D/\beta^2 d_p^2} \tag{46}$$

Since molecules are retained by interaction with the stationary phase during the fraction $1 + k$ of the time, D is correspondingly reduced and the eddy diffusion term becomes

$$H_{Eddy} = \frac{2\lambda d_p}{1 + \frac{4\lambda D}{u\beta^2 d_p}} \tag{47}$$

However, packed beds are more heterogeneous than assumed in this somewhat simplistic model. Eventually, Giddings showed that the flow heterogeneities in the inter-particle volume can be categorized into three different classes [15]. Each class is characterized by a specific length over which velocity extremes are expected. These lengths range from the trans-channel (the distance between two adjacent particles), to the short-range inter-channel (a few particle diameters), and to the trans-column (the column inner radius) distances. The size of the channels between particles in packed columns is scaled by the particle size. It is smaller than their diameter. Bird et al. [113] showed that an estimate of the average size of the flow channels in a bed of packed spheres, which is a good model of packed columns, is given by the hydraulic radius, R_h, which they define as the ratio of the volume available to the stream and the total wetted surface area:

$$R_h = \frac{d_p}{6}\frac{\epsilon_e}{1 - \epsilon_e} \tag{48}$$

So, the trans-channel distance is of the order of $d_p/6$. Actually, the two mechanisms occur simultaneously and are coupled. So, each individual HETP term, $H_{Eddy,i}$, should be written [15]:

$$H_{Eddy,i} = \frac{1}{\frac{1}{2\lambda_i d_p} + \frac{D_m}{\omega_i u d_p^2}} \tag{49}$$

where λ_i and ω_i are numerical parameters related to the structure of the bed and the particle distribution.

Finally, the eddy dispersion, H_{Eddy}, is the sum of three contributions:

$$H_{Eddy} = \sum_{i=1}^{i=3} H_{Eddy,i} \tag{50}$$

where $H_{Eddy,i}$ is the eddy dispersion term related to the type of velocity bias i, with the values of the numerical coefficients λ_i and ω_i being [15]:

$$\lambda_i = \frac{\omega_{\beta,i}^2 \omega_{\lambda,i}}{2} \tag{51}$$

and

$$\omega_i = \frac{\omega_{\beta,i}^2 \omega_{\alpha,i}^2}{2} \tag{52}$$

where $\omega_{\beta,i}$ is the ratio of the difference between the extremes values of the velocities in the type of channels considered and the corresponding mean velocity while $\omega_{\alpha,i}$ is the ratio of the characteristic diffusion length to the particle diameter and $\omega_{\lambda,i}$ is the flow-persistence length.

The values of each of these parameters could be assessed according to the initial guesses made by Giddings in the 1960s, confirmed by Magnico and Martin [117], and to the values derived from recent investigations involving the numerical reconstruction of packed beds and the calculation of flow-dispersion in the inter-particle space [118–121]. Eddy dispersion parameters can also be estimated from the data provided by the actual physical reconstruction of the bed structure using confocal laser scanning microscopy[122] or nuclear magnetic resonance [123]. The flow velocity profile along a bed can also be visualized by X-ray computed tomography [124]. A particular interest is given to new expressions of the trans-column eddy dispersion term, which was recently demonstrated to play a major role in the band broadening observed in narrow-bore columns packed with core–shell particles [125,126].

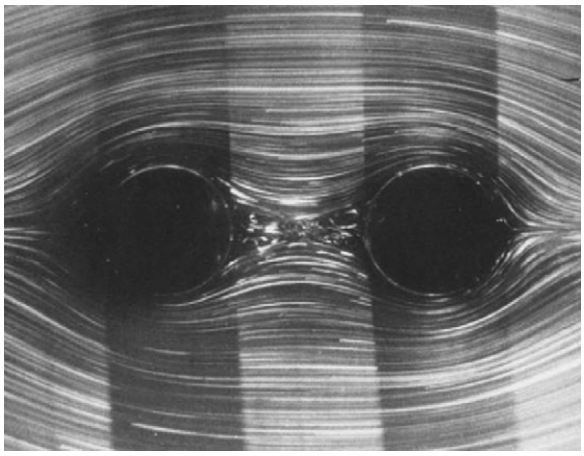

Fig. 3. Visualization of flow streamlines surrounding an impermeable sphere underlying the streamlines' merging and splitting. Reproduced with permission of Hasimoto and Sano [127].

2.3.2.1. Trans-channel (TS) eddy dispersion. This term is related to the velocity bias existing in streamlets flowing between adjacent particles. Photographs of streamlines between particles can be found in reference [127], a review paper on the flow distribution in fixed beds [128] (see Fig. 3). The local velocity of the mobile phase is strictly zero at the external surface area of the particles. At the center of inter-particle spaces, the local velocity is of the order of twice the average velocity in that channel, as indicated by the classical Poiseuille flow distribution in circular tubes. Accordingly, $\omega_{\beta,TS} = 1$. The average diffusion distance between the wall and the center of the channels is $(d_p/6)$, therefore $\omega_{\alpha,TS} = (1/6)$. Finally, Giddings estimated the flow-persistence length at about one particle diameter, so that $\omega_{\lambda,TS} = 1$. In conclusion, the kinetic parameter ω_{TS} and λ_{TS} calculated from Eqs. (51) and (52) are 0.01 and 0.5, respectively. The small value of the diffusion term ω_{TS} implies that for reduced linear velocity $v = (ud_p/D_m) < (\lambda_{TS}/2\omega_{TS}) = 25$, the trans-channel eddy dispersion term is a quasi-linear function of the velocity. In other words, the trans-channel eddy dispersion term follows Taylor–Aris behavior because the diffusion distances are extremely short.

Forty years after the publication by Giddings of the coupling theory of eddy dispersion and of his first estimates of ω_{TS} and λ_{TS}, a computational approach allowed Tallarek et al. to reconstruct a packed bed, calculate the convective-diffusive mass transport, and predict the eddy dispersion terms [118–121]. These authors investigated the influence of the packing density of the column bed, its external porosity ($0.36 < \epsilon_e < 0.46$), and the packing disorder (which they could quantify by a scalar measure) on the values of ω_{TS} and λ_{TS}. They found that, depending on this density, ω_{TS} and λ_{TS} increase from 0.004 to 0.005 and from 0.42 to 0.46, respectively. Remarkably, Giddings had overestimated the parameter ω_{TS} by only a factor two and had predicted the correct value of λ_{TS} within 20%.

In conclusion, for a column packed with spherical particles having an external porosity $\epsilon_e = 0.40$, the trans-channel eddy dispersion term can be written as [121]:

$$\frac{H_{Eddy,TS}}{d_p} = \frac{1}{\frac{1}{0.9} + \frac{1}{0.0045v}} \tag{53}$$

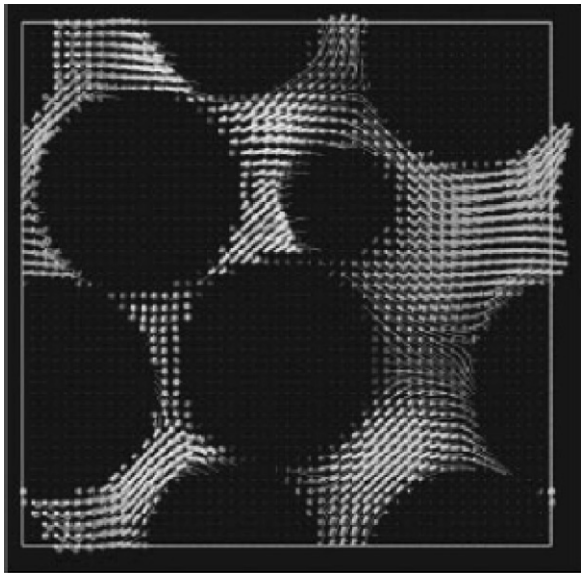

Fig. 4. Visualization of the interparticle streamlines surrounding a random array of impermeable spheres underlying the zones of low and high linear velocity at a short-range scale of a few particle diameters. Reproduced with permission of Hill et al. [129].

2.3.2.2. Short-range inter-channel (IT) eddy dispersion. This second eddy dispersion term accounts for the changes of the average trans-channel velocity over a distance of a few particle diameters (see Fig. 4). Because the spherical particles are randomly packed and have a finite size distribution (with an RSDs of ca. 10–20% for fully porous particles and 5% for core–shell particles), the local velocities vary on the short-range scale of a few particle diameters. Giddings first estimated that $\omega_{\beta,IT}$ was slightly less than unity, probably close to 0.8. The relative diffusion and the flow-persistence lengths were estimated at 1.25 and 1.50, respectively. Therefore, Giddings expected values of 0.5 for both ω_{IT} and λ_{IT}. In their recent paper, Tallarek et al. [119] found values of 0.13 and 0.25, respectively, with a bed external porosity equal to 0.4. Thus, Giddings had overestimated the short-range eddy dispersion term by a factor of nearly two. The short-range eddy dispersion term should now be written [121]:

$$\frac{H_{Eddy,IT}}{d_p} = \frac{1}{\frac{1}{0.5} + \frac{1}{0.13\nu}} \tag{54}$$

Fig. 5 compares the results of the predictions of Giddings with those of the calculations made by Tallarek et al. regarding the theoretical expressions of the trans-channel and the short-range inter-channel eddy dispersion terms. Note that the parameters considered in Tallarek's work were those obtained for an external porosity $\epsilon_e = 0.4$ and for the so-called S-packing, in which the particles are initially placed in the center of cubic cells and randomly displaced within these cells [121]. These data confirm that Giddings had overestimated the impact of the short distance velocity biases by a factor close to two. Furthermore, recent theoretical findings related to eddy dispersion in chromatographic media suggest that the sample diffusivity through porous particles could contribute to accelerate the relaxation of the concentration gradients between close inter-particle channels [130]. The same conclusion was suggested by an analysis of systematic measurements of eddy dispersion [45].

2.3.2.3. Trans-column (TC) eddy dispersion. Chromatographic columns, whether packed with particles or made of a monolith, are not radially homogeneous. The column wall is directly or indirectly at the origin of the heterogeneity. The work of Knox [131] and Eon

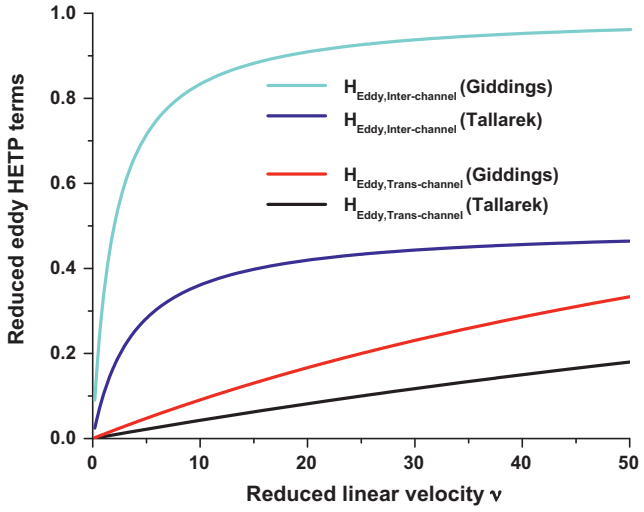

Fig. 5. Plot of the reduced eddy dispersion terms as a function of the reduced interstitial linear velocity, ν, according to the initial guess of Giddings (1960s) and the recent bed reconstruction and mass transport simulation studies of Tallarek (2000s). The external porosity of the bed was fixed at $\epsilon_e = 0.4$ in Tallarek's work.

[132], later confirmed by Farkas et al. [133], demonstrated that slurry-packed columns are radially heterogeneous, with a mobile phase velocity higher in the central region of the column than close to its wall and a local HETP larger in the wall than in the central region [134]. During the packing process shear stress takes place across the bed and is larger near the wall. Slippage of the particles alleviates this stress locally. Eventually, in slurry packing, the bed density becomes slightly smaller in the central region of the column than along its wall [135]. This explains why the local external porosity (hence, the local permeability and the local axial velocity) is slightly smaller close to the wall than in the center of the column. The velocity profile across the outlet diameter of a 4.6 mm I.D. was measured using different methods, making spectroscopic and electrochemical measurements [44,136,137]. The largest relative difference between the velocities at the center and at the wall regions of commercially available columns is typically of a few percent. A similar situation occurs in monolithic columns, with the difference that the mobile phase velocity is higher in the wall than in the central region because polycondensation of the resin is strongly exothermal, resulting in a large temperature gradient across the bed and the formation of a denser product in the warmer region. The heterogeneity of the velocity distribution warps the bands and broaden their elution profiles.

Giddings proposed a detailed theoretical analysis of the influence of the trans-column velocity biases on band broadening. Let us consider the ratio m_r of the column inner diameter to the particle diameter, call it the radial column aspect ratio, and assume that the relative velocity bias, $\omega_{\beta,TC} \simeq 10\%$. This means that the relative difference between the extreme velocities in the center and near the column wall is 20%. From the center to the wall of the column, the relative diffusion distance is $\omega_{\alpha,TC} = (m_r/2)$. Giddings estimated the relative flow-persistence length at $\omega_{\lambda,TC} = 5m_r^2$. According to the general Eqs. (51) and (52), the trans-column eddy dispersion term is written [15]:

$$H_{Eddy,TC} = \frac{d_p}{\frac{1}{0.04m_r^2} + \frac{1}{0.001m_r^2\nu}} \tag{55}$$

When Giddings was developing this theory (in the 1960s), the average particle size was 100 μm and the conventional column diameter was already 4,6 mm, giving a column aspect ratio around 50. Accordingly, the asymptotic eddy dispersion HETP term at high velocities would be as high as 100! For today's columns packed

with sub-2 μm and sub-3 μm particles the radial column aspect ratio is more likely around 1000. The numerical results suggest that Eq. (55) fails to provide a good estimate of the trans-column eddy dispersion term. A better approach is needed.

As the first step, we can resort to the general theory of dispersion of Aris [138] in a circular column. This theory was applied to solve the problem of the band broadening caused by a radial velocity distribution across open tubular columns or packed beds in electrochromatography [139] and later to solve a similar problem in packed beds [49]. The Aris-like eddy dispersion term is written [45]:

$$H_{Eddy,\,TC,\,diffusion} = C_m \frac{u_R d_c^2}{\overline{D_r}} = C_m \frac{\epsilon_e}{\epsilon_t} m_r^2 \frac{D_m}{\overline{D_r}} \frac{1}{1+k} \nu d_p \tag{56}$$

where C_m is a constant which depends on the radial flow velocity profile [45,49,139], d_c is the column inner diameter, $\overline{D_r}$ is the average radial dispersion coefficient over the column cross-section area, u_R is the linear migration velocity of the sample band, and ϵ_t is the total porosity of the column. $\overline{D_r}$ is usually expressed as the sum of a diffusive and a convective terms. It is written [45,46,139]:

$$\overline{D_r} = D_{eff} + \frac{1}{2}\gamma_r u_S d_p \tag{57}$$

where γ_r is an adjustable parameter which is of the order of 0.3 in packed beds [140,141]. For a parabolic flow profile, as in straight open tubular columns, $C_m = (1/96)$. In packed beds, the sample velocity is not zero at the wall but is close to the velocity in the column center, so the expected value of C_m is still smaller. Values between 1×10^{-8} and 1×10^{-6} were calculated [45,46,99], depending on the average dispersion coefficient (around 1×10^{-5} cm^2/s) and on the relative velocity difference between the center and the wall of the column (a few percent).

The first eddy dispersion term in Eq. (56) assumes the diffusion-controlled mechanism of Aris. Therefore, it is directly proportional to the axial velocity and can be effective only at very low flow rates and/or with very long columns, in which cases the sample molecules have enough time to statistically sample the whole column cross-section area by radial diffusion. In practice, this is rarely true, especially in the cases of ultra-fast separations.

The second eddy dispersion term is based on a flow-controlled mechanism. It needs to be determined in the absence of radial diffusion or when $\overline{D_r} = 0$. For instance, if the radial flow profile can be expressed as a polynomial of order n:

$$u(x) = u(0)[1 - \omega^*_{\beta,c} x^n] \tag{58}$$

where $\omega^*_{\beta,c}$ is the relative flow velocity difference between the center and the wall of the column, n is the polynomial order, which can vary between 2 and 16, depending on the radial extent of the flow uniformity in the center region of the column, x is the dimensionless radial coordinate, $x = (r/r_c)$, and $u(0)$ is the velocity at the center of the column ($x = 0$). The corresponding flow eddy dispersion term is written [46]:

$$H_{Eddy,\,TC,\,flow} = 2\frac{p_1}{q_1} L \omega^{*,2}_{\beta,c} \tag{59}$$

where L is the column length, and p_1 and q_1 are two integers which depend on the parameter n. The ratio (p_1/p_2) is equal to (1/24), (2/45), (8/225), (32/1377), and (128/9537) for $n = 2$, 4, 8, 16, and 32, respectively.

Because the coupling theory of eddy dispersion of Giddings can be applied to any sort of velocity biases in a chromatographic column, a simple expression for $H_{Eddy,TC}$ can be derived from a theoretical viewpoint [46]:

$$H_{Eddy,\,TC,\,diffusion} = \frac{d_p}{\frac{p_2}{2\,p_1\,m_l\,\omega^{*,2}_{\beta,c}} + \frac{\epsilon_t (D_{eff} + 0.5\epsilon_e \gamma_r D_m \nu)(1+k)}{\epsilon_e\, C_m\, m_r^2\, D_m\, \nu}} \tag{60}$$

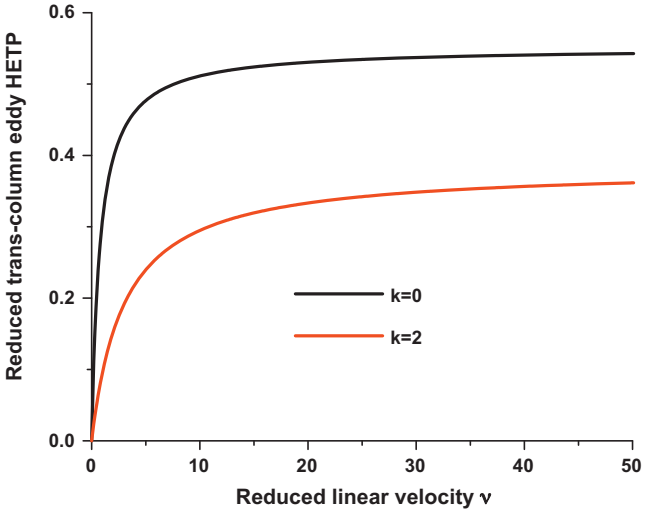

Fig. 6. Plot of the theoretical reduced trans-column eddy dispersion term as a function of the reduced interstitial linear velocity, ν, according to the model Eq. (56) for non-retained ($k = 0$) and retained ($k = 2$) species. All the parameters required for the calculations are listed in the text.

where m_l is the longitudinal aspect ratio or the ratio of the column length to the particle diameter.

Fig. 6 compares the trans-column eddy dispersion term of a non-retained ($k = 0$) and a retained ($k = 2$) compound on a RPLC column having the following characteristics: $\epsilon_t = 0.65$, $\epsilon_e = 0.40$, $p = 8$, $q = 225$ (e.g. $n = 8$ in Eq. (58)), $m_l = 37,000$, $m_r = 1700$ (e.g. $L = 100$ mm, $d_c = 4.6$ mm, and $d_p = 2.7$ μm), $\omega^*_{\beta,c} = 1.5\%$, $D_m = 1.0 \times 10^{-5}$ cm^2/s, $\gamma_r = 0.3$, $D_{eff}(k = 0) = 6.9 \times 10^{-6}$ cm^2/s, $D_{eff}(k = 2) = 5.1 \times 10^{-6}$ cm^2/s (see Torquato Eqs. (41) and (42) with $\Omega = 0.2$ for $k = 0$ or $k_1 = 0.63$, $\Omega = 1$ for $k = 2$ or $k_1 = 3.9$, and $\rho = 0$ for fully porous particles), with $C_m(k = 0) = 2.7 \times 10^{-7}$, and $C_m(k = 2) = 1.1 \times 10^{-7}$. The theoretical results are striking and predict a significant decrease of the trans-column eddy dispersion term with increasing the retention factor in RPLC, which is essentially due to the decrease of C_m with increasing retention factor.

Fig. 7 is similar to Fig. 6 but compares the trans-column eddy dispersion term between columns packed with fully porous

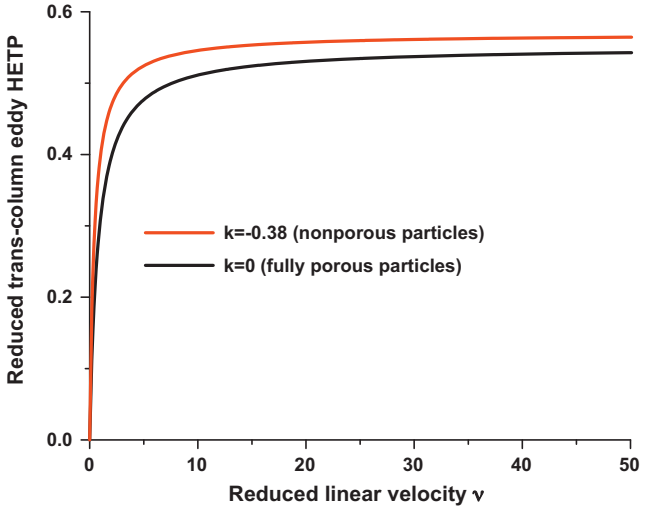

Fig. 7. Plot of the theoretical reduced trans-column eddy dispersion term as a function of the reduced interstitial linear velocity, ν, according to the model Eq. (56) for non-retained ($k = 0$) and excluded ($k = -0.38$) species. All the parameters required for the calculations are listed in the text.

($\rho = 0$) and non-porous particles ($k = -0.38$, $\rho = 1$). For a non-retained compound, $D_{eff}(k=0) = 6.9 \times 10^{-6}$ cm^2/s (see above). For a partially excluded compound, $D_{eff}(k=-0.38) = 6.8 \times 10^{-6}$ cm^2/s (see Torquato Eqs. (41) and (42) with $\rho = 1$ for nonporous particles). It is coincidental that these two values are so close. $C_m(k=0) = 2.7 \times 10^{-7}$ and $C_m(k=-0.38) = 3.0 \times 10^{-7}$.

Fig. 7 sheds light on the important role played by the particle porosity in the trans-column eddy diffusion mechanism. When molecules have access to the internal volume, the trans-column eddy diffusion is somewhat faster than when they do not. Similar results could be expected for the short-range inter-channel velocity biases but no model has yet been proposed to account for that potential effect. Anyway, the simple illustrations in Figs. 6 and 7 illustrate from a theoretical point of view how the combination of the analyte diffusivity inside the particles and the slow linear velocity can help to relax the concentration gradients taking place across the column. More accurate models of eddy dispersion are definitely needed for each type of chromatographic mode (RPLC, IEX, HILIC, SEC).

2.3.3. Mass transfer kinetics and the C term

Band broadening is also caused by the time that it takes for the mobile phase to equilibrate with the stationary phase. The molecules of analytes move at different velocities when in the eluent (average velocity u) and when in the stationary phase (zero velocity $u = 0$). So, the concentration profile of the analyte in the mobile phase always moves ahead of its concentration profile in the stationary phase. In liquid/solid chromatography, the stationary phase is made of a stagnant film of eluent surrounding the particles (in packed beds) or the skeleton (in monolithic columns), the eluent which is in the mesopore (volume fraction ϵ_p of the particles), and the surface area of the solid adsorbent. The analyte molecules escape from the stationary phase to the mobile phase by diffusion through the mesoporous network, by surface diffusion (in RPLC), and by diffusion through the external film of eluent. All these steps take a finite time that contributes to band broadening. The theoretical basis for kinetic effects in gas-solid chromatography was elucidated by Giddings [142]. This fundamental basis remains valid today, even though the details of its applications have become far more sophisticated.

2.3.3.1. Mesopore diffusion D_{pore}. Under non-retained conditions ($K = 0$), sample molecules can only diffuse across the porous adsorbent by diffusion across the open mesoporous network, referred to as pore diffusion. This diffusion takes place in the eluent phase but is hindered by the tortuosity and constriction of the mesoporous network. According to Satterfield [143] and to Brenner and Gaydos [112], the pore diffusion coefficient, D_{pore}, is written [13]:

$$D_{pore} = \gamma_p F(\lambda_m) D_m \tag{61}$$

where γ_p is the internal obstruction factor which is a complex function of the internal porosity, the tortuosity of the mesopore pathways, their constriction and their connectivity. $F(\lambda_m)$ is the hindrance diffusion factor which accounts for the confinement of the sample molecule within narrow pores. It is a function of the ratio of the size of the analyte molecules to the mesopore size, λ_m. Correlations are available in the literature, the most popular being the Brenner–Gaydos [112] and the Renkin [111] correlations. In practice, with small molecules, $\gamma_p = 0.6$, and $F(\lambda_m) = 0.8$. Therefore, the apparent sample diffusivity in the mesoporous volume is only about half the bulk diffusion coefficient.

2.3.3.2. Surface diffusion D_S. Under retained conditions, in RPLC, the sample molecules can diffuse along the hydrophobic surface and this contributes to speed up their diffusion across the porous adsorbent. Miyabe et al. have reported on the details of this diffusion phenomenon. In a recent review, they summarized the main characteristics of surface diffusion [144]. The flux of molecules is directly proportional to the local gradient of concentration in the stationary phase

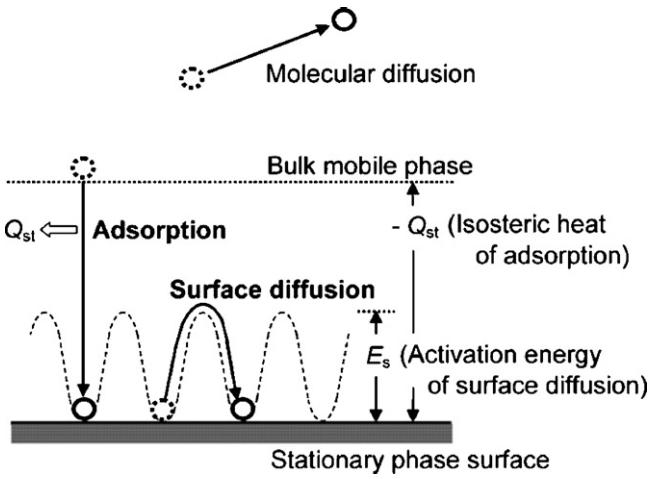

Fig. 8. Schematic illustration of the surface diffusion mechanism upon adsorption (Q_{st}) of the sample molecule. The molecule jumps along the adsorbent's surface from one adsorption site to another. It requires an activation energy of surface diffusion, $-\alpha Q_{st}$, that is less than the isosteric heat of adsorption, Q_{st}. Reproduced with permission of Miyabe et al. [144].

$$\vec{j}_{surface} = -D_S K \vec{\nabla} C \tag{62}$$

where D_S is the surface diffusion coefficient [144]:

$$D_S = D_{S,0} \exp\left[\frac{-\alpha Q_{st}}{RT}\right] \tag{63}$$

where $D_{S,0}$ is the frequency factor of surface diffusion, Q_{st} is the isosteric heat of adsorption (<0), and α is a numerical coefficient ($0 < \alpha < 1$). The activation energy of surface diffusion is smaller than the heat of adsorption, which is necessary for the transfer of a molecule from the adsorbed to the free bulk state (see Fig. 8). One important property of the surface diffusion coefficient from a chromatographic viewpoint is its continuous decrease from $D_S = D_m$ when $K = 0$ (no adsorption, $Q_{st} = 0$) to $D_S = 0$ when $K \to \infty$ (no desorption, $Q_{st} \to -\infty$). This result is illustrated in Fig. 9 taken from experimental data.

2.3.3.3. Particle diffusivity D_p. By definition, the particle diffusivity D_p of an analyte is its effective diffusion coefficient in the composite material made of open, tortuous, and narrow mesopores filled with the eluent (diffusion coefficient $\gamma_p F(\lambda_m) D_m$, concentration C, volume fraction ϵ_p) and of the surface layer on the solid adsorbent (diffusion coefficient D_S, concentration $q = KC$, volume fraction $1 - \epsilon_p$). Most of the literature devoted to particle diffusivity in liquid chromatography assumes that pore and surface diffusion fluxes are additive [13,144]. Therefore, D_p is usually written:

$$D_p = \epsilon_p \gamma_p F(\lambda_m) D_m + (1 - \epsilon_p) K D_S = \Omega D_m \tag{64}$$

An alternative estimate of particle diffusivity can be derived from the EMT of Landauer if we assume that the distribution of the open mesopores and the surface layer in the particle are random. Accordingly, D_p could also be written [106]:

$$D_p = F(\lambda_m) D_m \left(a + \sqrt{a^2 + \frac{1}{2} \frac{D_S}{D_m} \frac{K}{F(\lambda_m)}} \right) \tag{65}$$

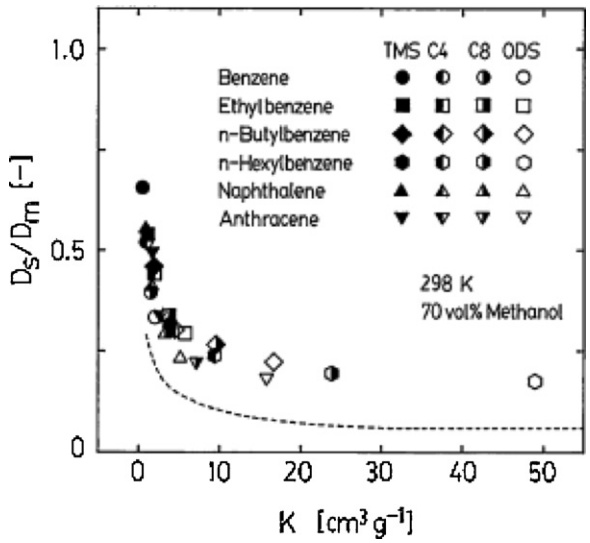

Fig. 9. Plot of the surface diffusion coefficient, D_S, as a function of the solid/bulk equilibrium constant K in RPLC conditions. Stationary phases: silica-C_1, silica-C_4, silica-C_8, and silica-C_{18}. Reproduced with permission of Miyabe et al. [144].

where a in the general Eq. (65) is equal to:

$$a = \frac{1}{4}\left[3\epsilon_p - 1 + \frac{D_S}{D_m}\frac{K}{F(\lambda_m)}(2-3\epsilon_p)\right] \tag{66}$$

However, the deconvolution of pore and surface diffusion in a porous adsorbent is still unknown. Nevertheless, the two models of particle diffusivity described above allow the derivation of physically meaningful estimates of D_S for small molecules [106,144]. We note that D_S in Eqs. (64) and (65) is an apparent diffusion coefficient in volume units while the sample must to diffuse along the adsorbent surface. Finally, the corresponding trans-particle resistance to mass transfer term provided by the Laplace transform of the general rate model of chromatography is [55]:

$$H_{Stat.} = \frac{\epsilon_e}{1-\epsilon_e}\left(\frac{k_1}{1+k_1}\right)^2\left[\frac{1+2\rho+3\rho^2-\rho^3-5\rho^4}{(1+\rho+\rho^2)^2}\right]\frac{d_p^2}{30D_p}u = C_p u \tag{67}$$

An equation similar to Eq. (67) but for a stationary phase made of a monolithic skeleton, which could be assumed to behave as cylindrical rods is written [56,145]:

$$H_{Stat.} = \frac{\epsilon_e}{1-\epsilon_e}\left(\frac{k_1}{1+k_1}\right)^2\left[1-3\rho^2-4\rho^4\frac{\ln\rho}{1-\rho^2}\right]\frac{d_p^2}{16D_p}u = C_p u \tag{68}$$

2.3.3.4. Adsorption–desorption kinetics. The concentrations of analytes in the pores filled of eluent and in the adsorbed layer are not necessarily in equilibrium because the rates of the various steps involved during adsorption and desorption of analyte molecules are not instantaneous. This issue was addressed early by Giddings [146] in the general rate model of chromatography, it is generally assumed that, for small molecular weight compounds, the adsorption rate constant k_a (see Eq. (22)) is very high and that the pore and the surface are always in equilibrium. In the case of large proteins (MW > 50 kDa), adsorption followed by unfolding and refolding of the molecule and its desorption may take a significant amount of time. Folding and unfolding of the structure of adsorbed proteins often accounts for the slow adsorption/desorption behavior observed. This phenomenon could cause serious additional band broadening under certain conditions, a phenomenon that has been modeled [13,147,148]. Under such circumstances, the corresponding HETP term, $H_{ads.}$, in the general HETP equation is written according to the Laplace transform of the general rate model of chromatography [13]:

$$H_{ads.} = 2\frac{1}{1-\epsilon_p}\frac{\epsilon_e}{1-\epsilon_e}\left(\frac{k_1}{1+k_1}\right)^2\left(\frac{k_p}{1+k_p}\right)^2\frac{1}{k_a}u = C_a u \tag{69}$$

In practice, however, and in most applications of isocratic liquid chromatography to low or medium molecular weight compounds, this term can be neglected.

2.3.3.5. External film mass transfer coefficient k_f. The final step to consider in the transfer of analyte molecules from the stationary to the mobile phase and *vice-versa* is the crossing of the stagnant film of eluent surrounding the particles (in packed columns) or the skeleton (in monolithic columns) and filling the pore openings. The density of mass flux across this barrier is controlled by the difference in concentration between the external moving eluent (C) and the internal stagnant eluent (C_i), as described above in Eq. (19). Expressions for the external film mass transfer coefficient, k_f, are available in the literature. Using the definition of the Sherwood number, Sh, they are written [13]:

- for the Wilson and Geankoplis correlation [149]

$$\frac{k_f d_p}{D_m} = Sh = \frac{1.09}{\epsilon_e}\nu^{1/3} \qquad 0.002 < Re < 55 \tag{70}$$

and

- for the Kataoka correlation [150]

$$\frac{k_f d_p}{D_m} = Sh = 1.85(1-\epsilon_e)^{1/3}\nu^{1/3} \qquad Re < 100 \tag{71}$$

These empirical correlations were derived based on studies of the rate of dissolution in water or in 40/60 solutions of water and propylene glycol, of spherical particles of a poorly soluble compound (benzoic acid) having sizes much larger (≃6.2 mm) than those used in liquid chromatography (≃5 μm) and packed in 5 cm i.d. tubes. Miyabe investigated the validity of these two correlations using 18 μm non-porous [151] and 50 μm fully porous silica-C_{18} [152] particles. Admittedly, these particle sizes are not fully representative of those currently used in HPLC ($1.7 < d_p < 5$ μm), yet they are much smaller than those which served for the derivation of Eqs. (70) and (71) and, being porous particles, the latter have a much closer internal structure.

Fig. 10 shows that the experimental data are scattered between the values given by the Kataoka (lower bound) and the Wilson–Geankoplis (upper bound) correlations. The important scatter of the data points observed in the range of low interstitial linear velocities ($\nu < 20$) is most likely in due to assumptions made for the calculation of the eddy dispersion term. In their work, Miyabe et al. assumed that the eddy dispersion HETP term was constant over the whole range of linear velocities whereas it should continuously decrease toward zero when $\nu \to 0$. For this reason, it seems impossible to validate these correlations for sub-3 and sub-2 μm particles because the precision and the accuracy which can be achieved now are insufficient.

In conclusion, it seems reasonable to use Eqs. (70) and/or (71) in order to estimate the external film mass transfer coefficient and the corresponding HETP term, H_{Film}, in the general HETP equation (27). Yet, it should be kept in mind that a relative error of about ±15% on the value of this term is probable. As a function of the Sherwood

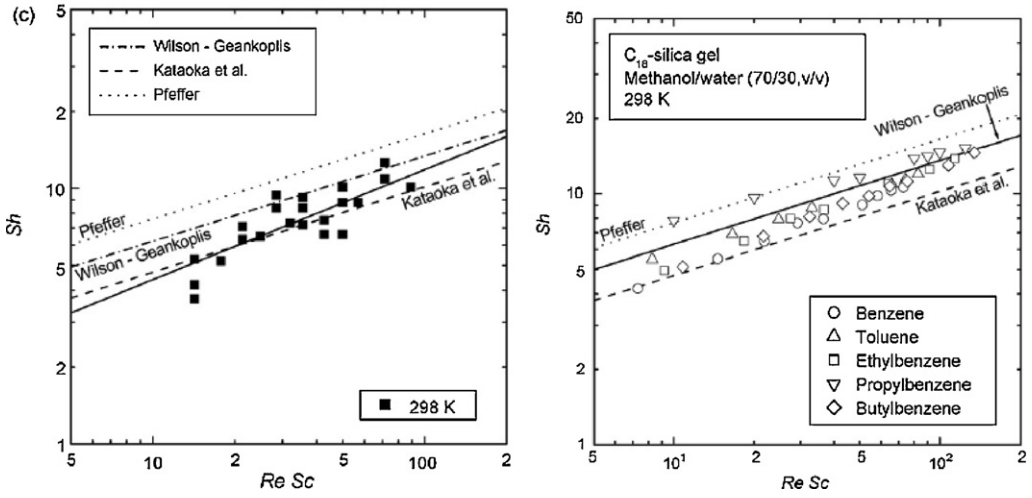

Fig. 10. Comparison between experimental (symbols) and correlations (Wilson and Geankoplis, Kataoka) for the external film mass transfer coefficient, k_f, at ambient temperature $T = 298$ K. Left graph: experiments with 18 μm nonporous particles. Right graph: experiments with 50 μm fully porous particles. Reproduced with permission of Miyabe et al. [151].

number *Sh* and according to the Laplace transform of the general rate model of chromatography, this term is written [13]:

$$H_{Film} = \frac{\epsilon_e}{1-\epsilon_e}\left(\frac{k_1}{1+k_1}\right)^2 \frac{d_p}{3k_f} u = C_f u^{2/3} \tag{72}$$

Regarding monolithic stationary phases, the film penetration theory is usually applied to predict the value of k_f [113]:

$$k_f = \sqrt{\frac{4D_m u}{\pi d_{sk.}}} \tag{73}$$

where $d_{sk.}$ is the average skeleton diameter. The corresponding HETP term for monolithic columns is written:

$$H_{Film} = \frac{\sqrt{\pi}}{4}\frac{\epsilon_e}{1-\epsilon_e}\left(\frac{k_1}{1+k_1}\right)^2 \frac{u^{1/2} d_{sk.}^{1/2}}{D_m^{1/2}} u = C_f u^{1/2} \tag{74}$$

The physico-chemical description of the analyte mass transfer between the percolating eluent, which flows under a laminar regime ($Re \approx 0.01$) in contact with the eluent stagnant inside the particles is a more complex process than can be anticipated. This mechanism of convective-diffusive mass transfer at the interface between the interstitial and the internal eluent is difficult to model at the scale of the particle and the mesopore size. Fig. 11 illustrates this situation in the simpler case of a rectangular pore size, with a Reynolds number (≃0.01) comparable to those encountered in LC but at a larger scale. Admittedly, the average mesopore size (≃100 Å) of porous silica particles is much smaller than the width of the cavity shown in Fig. 11. The back-circulation zone observed in this figure takes place in an inch wide pore. The same effect might not take place similarly in mesoporous pores.

A similar mass transfer resistance term was introduced in GC by Khan [153,154], who called it the interfacial resistance and related it to the accommodation coefficient or probability for a molecule hitting a gas–liquid interface from the gas side to penetrate through the interface and dissolve in the liquid (there is obviously a similar probability for a molecule hitting the surface from the liquid side to evaporate; at equilibrium the two rates are obviously equal). Later James et al. [155] elaborate on the accommodation coefficient and showed that the interfacial resistance should be negligible under classical GC experimental conditions. Although there is an accommodation coefficient for adsorption as well, it seems that the rational of James et al. is valid for adsorption in liquid chromatography, although specific data would be useful to put this issue to rest. The external film mass transfer resistance seems related to a reluctance of molecules to enter porous particles, for some reasons still unknown.

2.3.4. Friction–expansion term in vHPLC and SFC

In the previous three sections, we reported on the theoretical expressions of the traditional *B*, *A*, and *C* term of the van Deemter equation. As usual in chromatography, we assumed that the physico-chemical properties of the eluent and the stationary phases are uniform throughout the whole column. The recent progress in column technology, the breakthrough of vHPLC, and the regained interest in SFC, this assumption is challenged by the important heat effects that we now realize are taking place in the column under certain sets of conditions [36,89,157]. In vHPLC, the mobile phase velocity and the pressure drop along the column (1 kbar) can be so high that an important amount of heat is released, due to the friction between layers of eluent and the column bed [158,159]. At the same time, the eluent decompression

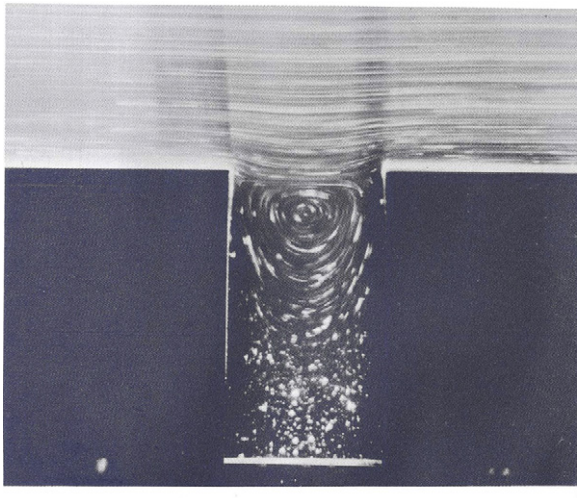

Fig. 11. Creeping flow along a smooth wall, over a rectangular cavity. The apparent equivalence with the external surface of a porous particle immersed in a moving mobile phase was not demonstrated. Streamlines are shown by aluminum dust in glycerine. The Reynolds number is 0.01 based on cavity height. The width to height ratio of the cavity is 0.5. Reproduced with permission of van Dyke [156].

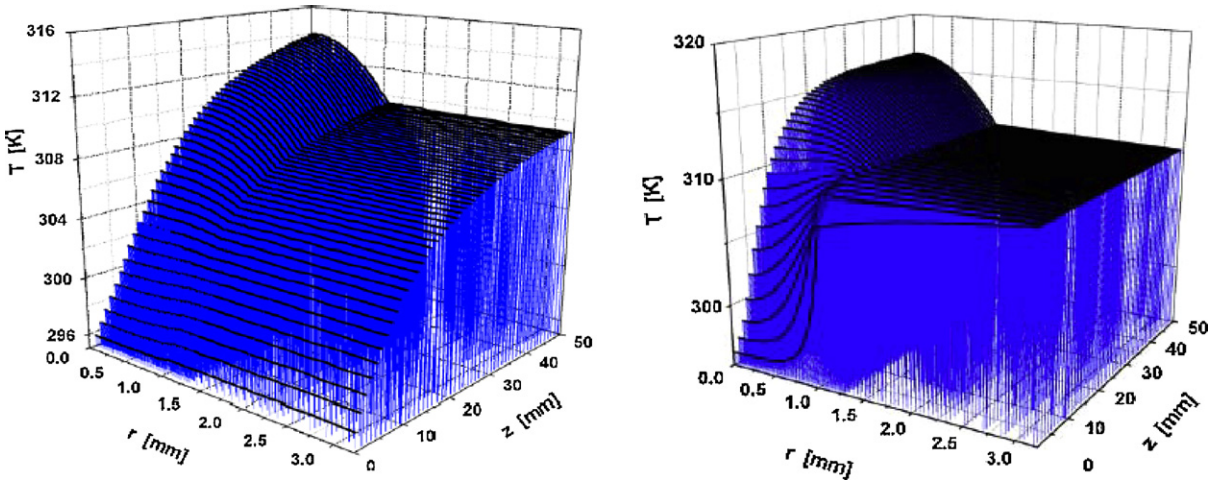

Fig. 12. Example of calculated temperature gradients formed in 2.1 mm ×50 mm columns packed with 1.7 BEH-C_{18} particles under two different external environments. Left graph: the column is left free in still-air conditions, T = 295 K, 100% CH_3CN, F_v = 2.0 mL/min (inlet pressure = 775 bar). Right graph: the column is placed in a water bath at T = 310 K in order to keep constant the temperature of the column wall, 85% CH_3CN/15% H_2O % F_v = 2 mL/min (inlet pressure = 777 bar). The r-coordinate refers to both the inner radius (r < 1.05 mm) of the packed bed and to the surrounding thickness (1.05 < r < 3.25 mm) of the stainless steel tube. Reproduced with permission of Gritti et al. [93].

is accompanied by an absorption of heat causing a temperature decrease that does not compensate for the temperature increase caused by frictional heating in HPLC. The analysis of thermal exchanges in vHPLC showed that the energy absorbed during eluent decompression accounts for ~1/3 of the energy released by friction [38]. To evacuate the heat produced, temperature gradients are formed under steady state. The temperatures is lower at the column entrance and in the wall regions whereas temperatures are higher at the column exit and in its central region.

In SFC, the balance between frictional heating and expansion cooling is different. Frictional heating is low because the pressure drops are small, due to the small viscosity of CO_2 being one order of magnitude smaller than that of liquids. On the other hand, the isobaric thermal expansion coefficient of supercritical CO_2 is an order of magnitude larger than that of most liquids. Accordingly, during the rapid decompression of supercritical CO_2 under moderate density when CO_2 compressibility is high, a significant amount of heat is absorbed by the eluent from the external environment. In this case, the temperatures are higher at the column entrance and in the wall region while they are low at the column outlet and in its center.

Next, we discuss from a theoretical point of view the quantitative impact of the temperature gradients observed in vHPLC (where friction dominates expansion) and in SFC (where expansion dominates friction).

2.3.4.1. vHPLC: friction dominates expansion. According to Horváth and Lin, the heat power (W/m) liberated per unit of column length due to the work of the friction forces is equal to [158]:

$$P_f = F_v \times \frac{\Delta P}{L} \tag{75}$$

where F_v is the flow rate, ΔP is the pressure drop, and L is the column length. Simultaneously, the eluent absorbs energy with a power, P_e, due to its expansion during decompression from the inlet to the outlet of the column [158]:

$$P_e = F_v \times \frac{\Delta P}{L} \times \overline{\alpha_p T} \tag{76}$$

where $\overline{\alpha_p T}$ is the average of the product of the expansion coefficient, α, and the temperature along the column length. Typically, the product $\overline{\alpha_p T} \simeq -1/3$ for common liquids [161]. Under steady state conditions, temperature gradients across and along the column are formed such as those that were calculated by solving the heat balance equation in the whole column volume, including the column stainless steel tube [37,162–164] and are shown in Fig. 12. The most important result is that theoretical predictions of band broadening should take into account both the radial and the longitudinal temperature gradients in the packed bed. A corresponding additional HETP term should be derived.

It is crucial to realize that the expansion term will drastically increase if the isobaric expansion coefficient, α, of the eluent increases. We now discuss this possibility in the case of supercritical fluid chromatography (SFC).

2.3.4.2. SFC: expansion dominates friction. In SFC, the viscosity of pure supercritical carbon dioxide is about one order of magnitude smaller than that of conventional liquids used in HPLC [165]. Accordingly, the pressure drop along SFC columns rarely exceeds 50 bar when pure carbon dioxide is used as the eluent, twenty times smaller than the largest pressure drops reached in vHPLC. Under such conditions, the friction power is negligible in SFC. In contrast, the isobaric expansion coefficient of supercritical CO_2 is an order of magnitude larger than that of the liquids used as eluent in HPLC and, therefore, the energy absorbed from the external environment by the decompression of the eluent is much larger in SFC than in conventional HPLC, provided that the compressibility of CO_2 under the experimental conditions selected is important. We can then expect a significant degree of cooling in SFC experiments (and not heating as in vHPLC). This conclusion was confirmed by the results of calculations of the temperature profiles in SFC columns with pure supercritical CO_2 recently published and shown in Fig. 13. The directions of the axial and radial temperature gradients are just the opposite of those calculated in vHPLC.

Interestingly, the impact of this cooling effect on the band broadening and on the column HETP could be minimized or even eliminated if the product αT is kept close to −1 (see Fig. 14) [160]. This corresponds to a specific region of the P–T phase diagram of pure CO_2 where pressures higher than 300 bar should be applied.

Recent theoretical developments were made to estimate the degree of band broadening associated with friction–expansion of the eluent whether it takes place in vHPLC or in SFC.

2.3.4.3. Friction–expansion and band broadening. As explained in the previous two sections, friction–expansion of the eluent along the column under steady-state conditions is accompanied by the formation of stationary axial and radial temperature gradients.

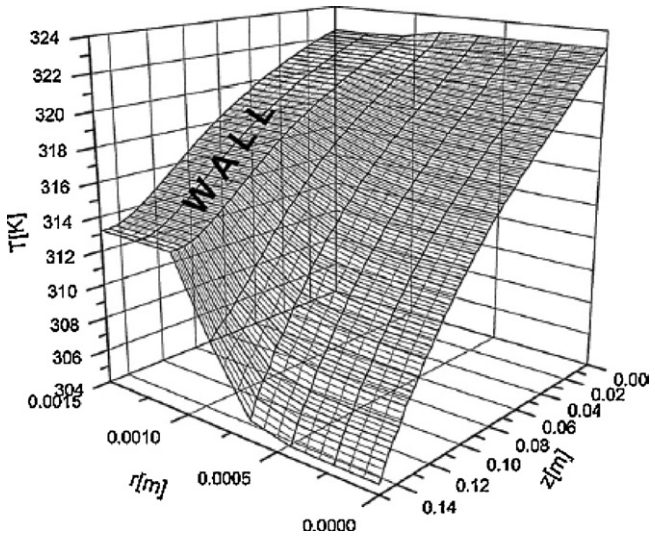

Fig. 13. Calculation of the temperature profile in a 2.0 mm × 150 mm packed with 3 μm Spherisorb C_8 at a flow rate of 1.245 mL/min. The column is let free in the oven compartment at $T = 323$ K. The r-coordinate refers to both the inner radius ($r < 1.0$ mm) of the packed bed and to the surrounding thickness ($1.0 < r < 1.5$ mm) of the stainless steel tube. Reproduced with permission of Kaczmarski et al. [160].

Accordingly, the local linear migration velocity, $u_R(x, z)$, of the analyte band depends on the cylindrical coordinate $\{x = (r/r_c), z\}$ in the column [49]:

$$u_R(x, z) = \frac{u_0}{1 + k(x, z)} \tag{77}$$

where $k(x, z)$ is the local retention factor, which is a function of the local temperature $T(x, z)$. If the van't Hoff equation applies in the range of temperature existing inside the column, then:

$$k(x, z) = \frac{1 - \epsilon_t}{\epsilon_t} K_0 \exp\left[-\frac{Q_{st}}{RT(x, z)}\right] \tag{78}$$

where K_0 is the Henry's constant at infinite temperature and R is the molar gas constant (8.31 J/K/mol).

This problem is similar to the calculation of the eddy dispersion term for the trans-column velocity biases, with the difference that now the origin of the velocity biases is not in variations of the streamline velocities due to the radial heterogeneity of the packed bed but in variations of the local mobile phase velocity due to the radial temperature gradients caused by the evacuation of the frictional heat. The Aris theory of dispersion in circular columns [138] permits the handling of the influence of the heat gradients on the column efficiency much like it was used to determine the influence of eddy dispersion. This approach gives the contributions due to the influence of heat dispersion, $H_{Fric.-Expa.,diffusion}$, and to that of the perturbation of the flow, $H_{Fric.-Expa.,flow}$. Their combination provides the HETP contribution due to friction–expansion.

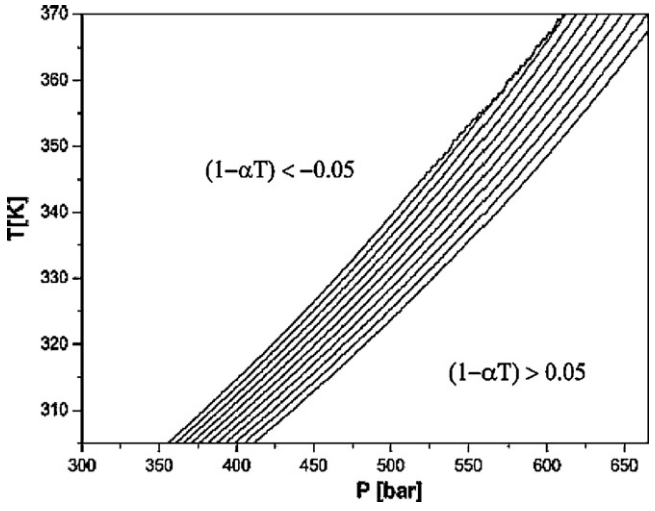

Fig. 14. Zone of the phase diagram of neat supercritical CO_2 where the coefficient αT is close to −1 and the cooling due to decompression of the eluent compensates the heating due to friction. Reproduced with permission of Kaczmarski et al. [160].

The Aris theory was extended to chromatographic columns in which the radial velocity profile, $u(x)$, is caused by a radial temperature profile, hence a radial retention factor profile [49]. In a first step, the column is divided into a series of small elementary circular slices of thickness dz, chosen so that the variation of the axial temperature profile ($T(z)$) along a slice can be considered as negligible. The local increase of the HETP between z and $z + dz$, $H(z)$, is then directly derived from Aris theory:

$$H(z) = \frac{d\sigma(z)^2}{dz} \tag{79}$$

where $d\sigma(z)^2$ is the variance increment between the axial coordinates z to $z + dz$. The detail of the mathematical procedure for the calculation of $d\sigma(z)^2$ was given in [139], where it was applied for the evaluation of band broadening in electrochromatography, a separation method in which the mobile phase moves under the influence of an electric field instead of a pressure and, as a consequence, the radial distribution of flow velocities across the column is different from the distribution observed in pressure-driven flow and so is the radial flow profile. In a second step, these variance increments are summed from $z = 0$ to $z = L$ and $H_{Fric.-Expa.,diffusion}$ is written [49]:

$$H_{Fric.-Expa.,diffusion} = \frac{\int_0^L H(z)dz}{L} \tag{80}$$

The determination of the flow-related HETP contribution is more straightforward than that of the diffusion-related one. It is based on the cross-section distribution, $t(L, x)$, of the elution time in ideal chromatography (assuming negligible axial and radial dispersion coefficients) at the column exit ($z = L$). The necessary details are given in [95,97,98]. To summarize, the first ($\bar{t}$) and the second central (σ_t^2) moments of this time distribution are computed and the HETP $H_{Fric.-Expa.,flow}$ is obtained from its general definition, giving [95]:

$$H_{Fric.-Expa.,flow} = L\frac{\sigma_t^2}{\bar{t}^2} \tag{81}$$

The overall HETP contribution due to friction–expansion of the mobile phase percolating the bed is written [15]:

$$H_{Fric.-Expa.} = \frac{1}{\frac{1}{H_{Fric.-Expa.,diffusion}} + \frac{1}{H_{Fric.-Expa.,flow}}} \tag{82}$$

3. Measurement of individual HETP term

In the previous section, we presented the current status of the theory of band broadening in chromatography, described the derivation of the theoretical expressions accounting for the various contributions to the HPLC columns, and explained their relative importance. This work would remain academic if there were no methods to accurately measure these contributions and estimate the values of their respective parameters. The results of such systematic measurements provide analysts with the approaches needed to improve the column performance and accelerate chromatographic analyses.

We now describe the methods recently developed and validated to measure each individual HETP term. This involves specific techniques for the determination of the chromatographic peak moments, which are necessary for the calculation of the correct

HETP of a column and for the measurement of the different parameters of the HETP equation. It also includes the direct measurement of several important characteristics, such as diffusion and dispersion coefficients and the parameters of the mass transfer resistances.

3.1. Measurements of true moments

The accurate determination of the coefficients of the experimental plate height equation requires first the determination of the correct value of the column HETP in a sufficiently wide range of mobile phase velocities. There are several methods available that provide different degrees of practicality, precision, and accuracy. The main ones are the half-height peak-width method, the curve fitting method, and the numerical integration method.

3.1.1. Half-height peak width method

In this method, the retention time of the peak apex, t_R, and the width of the peak at half-height, $w_{1/2}$, are systematically measured. The first and second central moments of the eluted peak are derived assuming a Gaussian peak shape, with:

$$\mu_1^{(1)} = t_R \tag{83}$$

$$\mu_2^{'(1)} = \frac{w_{1/2}^2}{5.545} \tag{84}$$

This method provides true values only if the peak has a strictly Gaussian profile. Therefore, it rarely applies, except for highly retained, nonpolar components in RPLC. Although inaccurate, however, this method is very simple and easy to apply, it is very precise and very robust.

3.1.2. Peak fit method

In this method, the experimental data points are fitted to a curve considered as a good model for elution profiles, e.g., a better model than the Gaussian curve used in the previous method. Numerous equations were suggested for this purpose. The most generally adopted curves are the five parameters EMG (Exponentially Modified Gaussian) and GMG (Gaussian Modified Gaussian) functions, which both account for an adjustable degree of peak tailing. The most popular equation is written as:

$$C(t) = \frac{a_0 \exp\left(-\frac{1}{2}\frac{(a_4 t - a_1 a_4 + a_3^2)^2}{a_4^2(a_3^2+a_2^2)}\right)\left[1+\operatorname{erf}\left(\frac{a_3(-a_2^2+a_4 t - a_1 a_4)}{\sqrt{2}a_2\sqrt{a_3^2+a_2^2}}\right)\right]}{\sqrt{2\pi}\sqrt{a_3^2+a_2^2}\operatorname{erf}\left(\frac{\sqrt{2}a_3}{2a_4}-1\right)} \tag{85}$$

where a_0 is the peak area, a_1 the elution time of its mass center, and a_3 and a_4 are distortion parameters of the EMG/GMG hybrid function. The best values of the parameters a_0, a_1, a_2, a_3, and a_4 in each particular case are determined by multi-linear regression analysis. Then, the first and the second central moments, μ_1 and μ_2', are directly calculated from the mathematical expression of the hybrid function Eq. (85):

$$\mu_1^{(2)} = \frac{\int_0^\infty C(t)t dt}{\int_0^\infty C(t)dt} \tag{86}$$

$$\mu_2^{'(2)} = \frac{\int_0^\infty C(t)\left(t-\mu_1^{(2)}\right)^2 dt}{\int_0^\infty C(t)dt} \tag{87}$$

This method is only approximate because there is no fundamental reason why the elution band profile should follow this particular profile. The method fails particularly to account properly for peaks which exhibit a severe degree of tailing or fronting. This behavior is often due to overload of the column (or in analytical applications of some particular type of adsorption sites when the adsorbent surface is heterogeneous). In such a case of thermodynamic peak tailing, the peak profile does not follow EMG/GMG behavior [13]. Failure of the method is also noteworthy when the instrument contributes significantly to the elution profile through an extra-column contribution and the peak profiles are recorded at high flow rates.

Agreement between experimental peak profiles and those calculated after any model are rarely excellent, especially in the regions of low concentration at the bottom of the recorded peaks. The reasons for the inaccuracy of the approach are detailed in [13] (see Fig. 6.10, p. 313) and in [166].

3.1.3. Numerical integration method

In this method, the elution profiles are recorded as a table (t_i, C_i) and these data points are directly used for numerical calculations of the peak moments. The true first and second central moments are then calculated according to the following numerical integration:

$$\mu_1^{(3)} = \frac{\sum_{i=1}^{i=-1}(C_i + C_{i+1})(t_i + t_{i+1})}{2\sum_{i=1}^{i=N-1} C_i + C_{i+1}} \tag{88}$$

$$\mu_2^{'(3)} = \frac{\sum_{i=1}^{i=-1}(C_i + C_{i+1})\left(\frac{t_i+t_{i+1}}{2} - \mu_1^{(3)}\right)^2}{\sum_{i=1}^{i=N-1} C_i + C_{i+1}} \tag{89}$$

This method is the most accurate among all available methods because it does not introduce any model error but works directly from the raw data. It should be preferred whenever accurate measurements of column plate heights are required [166]. The downside of this method is that its precision depends on the somewhat arbitrary decision of where the left and right cut-off points of the chromatogram should be located.

3.2. Bulk diffusion coefficient D_m

The effective diffusion coefficients of analyte molecules in the packed bed, $D_{eff} = f(\epsilon_e, \rho, \Omega)D_m$ (D_{eff} is also a function of the local disorder of the particles in the bed), their molecular diffusivities in the mesopore network, $D_{pore} = \gamma_p F(\lambda_m)D_m$, and their pore diffusion coefficients, $D_p = \Omega D_m$, are all scaled to the bulk diffusion coefficient in the mobile phase, D_m. Therefore, it is necessary to know the diffusion coefficients of the analytes of interest in the eluent. Experience teaches that empirical correlations are moderately accurate in the best of cases, so direct measurements should be preferred. Two accurate methods are available for this purpose, the Aris–Taylor and the peak-parking methods.

3.2.1. The Taylor–Golay method

The Taylor–Golay method consists of measuring the band broadening of a zone of analyte eluted at the end of an open tube. This broadening is due to the laminar parabolic flow profile (Poiseuille flow) [138,167–170] that takes place in such a tube. This method is similar to a chromatographic analysis but there is no retention. Long, straight, narrow-bore tubes are required for the results of the Taylor–Golay dispersion theory to be true. If the linear velocity is kept small enough, however, it is possible to use a wide coil tube (ca. 15–20 cm coil diameter) and avoid the perturbations due to the secondary circulation caused by the centrifugal force acting on the fluid moving along a helical tube. Under such experimental

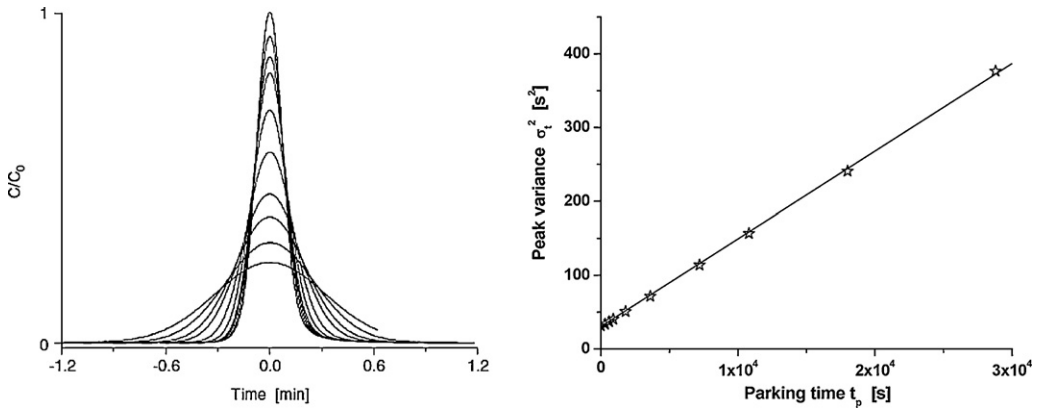

Fig. 15. Peak parking experiments. Results obtained with a 4.6 mm × 150 mm columns packed with porous 5.0 μm Symmetry-C_1 particles at room temperature with the non-retained sample thiourea. Left graph: illustration of the increase of the band spreading with increasing parking time. The successive parking times were 0, 5, 10, 15, 30, 60, 120, 180, 300, and 480 min. Right graph: plot of the corresponding peak variance as a function of the peak parking time. Note the excellent linear behavior of the plot. Reproduced with the permission of Gritti et al. [87].

conditions, the measurable peak variance, σ_t^2, in time unit is written [14,171]:

$$\sigma_t^2 = \frac{2D_m l}{u_c^3} + \frac{d^2 l}{96 D_m u_c} \tag{90}$$

where l is the length of the capillary, u_c is the fixed average linear velocity, and d is the inner diameter of the coiled capillary.

This approach was successfully used by Carr and Li [169,170] for the measurement of the true diffusion coefficients of small molecules in methanol/water and acetonitrile/water mixtures. This study allowed to assess the accuracy of several correlation equations (Wilke and Chang [172], Scheibel [173], Lusis–Ratcliff [174], and Hayduk–Laudie [175]) around ±20%. The main difficulty with the Aris–Taylor method is that its accuracy depends much on the actual dimensions of the tube used, particularly its inner diameter.

3.2.2. Peak parking (PP) in columns packed with nonporous particles

Columns packed with nonporous particles are characterized by their external obstruction factor, $\gamma_e < 1$, which is due to the tortuosity and constriction of the inter-particle channels. The apparent axial diffusion coefficient along these columns is equal to $\gamma_e D_m$. Therefore, if γ_e is known for a column, the bulk diffusion coefficient D_m can be measured, provided that we know how to measure the apparent diffusion coefficient $D_{eff} = \gamma_e D_m$. The peak parking method (PP) permits this measurement. PP was introduced by Knox, first in GC [176], later in HPLC [82]. This method was used to determine internal obstruction factors [87] and diffusion coefficients [177–179].

In the PP method, a sample zone is injected, eluted at the constant, arbitrary migration linear velocity $u_{R,PP}$ until it is at about the middle of the column, and, suddenly, the flow rate is stopped and the band left free to diffuse throughout the packed bed during a certain parking time, t_p. Then, the flow is resumed at the same flow rate and the variance of the eluted peak profile, σ_t^2, is measured by numerical integration of the whole chromatogram. This procedure is repeated for a series of parking times, keeping constant the elution flow rate throughout the series of measurements. Fig. 15 shows the typical plot of the band variance versus t_p. This plot is expected to be a straight line and it generally is [100]. Whether the particles are porous or not, the relationship between the unknown effective diffusion coefficient of the packed bed, D_{eff}, and the slope of the ratio $(\Delta\sigma_t^2/\Delta t_p)$ is given by [100]:

$$D_{eff} = \frac{1}{2}\frac{\Delta\sigma_t^2}{\Delta t_p} u_{R,PP}^2 \tag{91}$$

When the particles are nonporous, the effective diffusion coefficient $D_{eff} = \gamma_e D_m$. Therefore, using a standard sample molecule the bulk diffusion coefficient of which is known with excellent accuracy allows the derivation of the external obstruction factor of the packed column used. For instance, the diffusion coefficient of thiourea at infinite dilution in pure water, at 298.15 K, and under normal pressure (1 atm) is equal to 1.33×10^{-5} cm^2/s ±1% [180,181]. A value of $\gamma_e = 0.65 \pm 0.01$ was measured with a 4.6 mm × 100 mm column packed with 1.9 μm solid cores. Accordingly, repeating the same peak parking experiment at any temperature T, with any other compound provides a direct measurement of the bulk diffusion coefficient of this compound, at that temperature, as follows [59,179]:

$$D_m(T) = \frac{1}{2\gamma_e}\frac{\Delta\sigma_t^2(T)}{\Delta t_p} u_{R,PP}^2(T) \tag{92}$$

The accuracy of the measurements of diffusion coefficients by the PP method is excellent, with errors of 4% or less, the main source of error coming from the necessary duplication of the PP determinations, first to measure the obstruction factor (2%) and then the experimental slope, $(\Delta\sigma_t^2(T)/\Delta t_p)$ (1%). The PP method is simpler, faster, and more accurate than the Taylor–Golay method, so it should be preferred, provided that certain potential pitfalls are avoided. Note also that if the PP method is easy to use in HPLC because the eluent is practically non-compressible, the method has not been validated for SFC and that a detailed investigation of its application in this case is necessary.

3.3. Longitudinal diffusion coefficient B

We know of and use routinely two different methods to measure the longitudinal diffusion coefficient B of the van Deemter equation for a given compound, an approximate, dynamic one and a static, exact one.

3.3.1. Approximate dynamic method: elution at small flow rates

The less time consuming method consists in recording the band profile of the studied compound at a very low flow rate, the lowest possible one. The choice of this flow rate depends on the accuracy of the pressure controller of the HPLC instrument used. This accuracy should be carefully determined prior to any measurement; it should be better than 0.5%. Most conventional 400-bar instruments seem to satisfy this requirement at flow rates in excess of ca. 0.05 mL/min and flow rates as low as 0.01 mL/min could be used with vHPLC instruments. Also, due to the large retention times experienced at low flow rates (up to a few hours), the column temperature should

be carefully recorded during the whole series of experiments, to verify that it does not deviate by more than 0.5 K from the set temperature. In HPLC, D_m is of the order of 1×10^{-5} cm^2/s. So, using a 4.6 mm I.D. column with an external porosity $\epsilon_e = 0.4$ packed with 2.5 μm particles, a flow rate of 0.01 mL/min correspond to a reduced interstitial linear velocity of

$$\nu = \frac{F_v d_p}{\epsilon_e \pi r_c^2 D_m} < 0.07 \quad (93)$$

At such a small reduced velocity, the *A*, *C*, and friction–expansion terms are very small and can be considered as negligible. Therefore, the column HETP is essentially due to longitudinal diffusion along the bed, and the *B* coefficient can be directly derived from the variance of the recorded chromatogram in time unit, σ_t^2. So, *B* is equal to:

$$B = \frac{\sigma_t^2 u^3}{L(1+k_1)^3} \quad (94)$$

where *u* is the constant interstitial linear velocity applied during the low velocity run. Due to the cubic power of *u* in this equation, a high precision of measurement is required.

3.3.2. Exact static method: PP experiments

The *B* coefficient would be best measured for a zero flow rate, under static conditions than at low flow rates. The PP experiment is the most suitable method to measure the *B* coefficient. The downside of the PP method is the significant amount of time that is required to perform accurate and precise measurements, particularly for compounds that have low diffusion coefficients. It takes typically half a day (overnight) to complete the set of measurements required for low molecular weight compounds, which include five injections with parking times of 0, 1, 2, 4 and 8 h. For peptides or proteins, the necessary time would be much longer, days. As described in Section 3.2.2, the *B* coefficient in the general HETP equation, which refers to the interstitial linear velocity, is written[87,100]:

$$B = 2(1+k_1)D_{eff} = \frac{\Delta\sigma_t^2}{\Delta t_p}\frac{u_{PP}^2}{1+k_1} \quad (95)$$

where u_{PP} is the interstitial linear velocity applied during the PP experiments.

This static method was applied for the determination of the reduced *B* term of small molecules in columns packed with fully and superficially porous particles. Fig. 16 shows plots of the variations of the reduced *B* coefficient as a function of the intrinsic ratio, Ω, of the sample diffusivity in the particle ($D_p = \Omega D_m$) to the bulk diffusion coefficient (D_m). This graph demonstrates experimentally that the *B* terms of columns packed with core–shell particles are typically 20–30% smaller than those of columns packed with conventional fully porous particles. This result was expected because (1) 20% of the column's volume is occupied by the solid cores and is not accessible to analytes; and (2) the presence of the spherical cores enhance to a degree the obstruction for axial diffusion.

As it will be shown later, this static PP method can also be used for the determination of the trans-particle/trans-skeleton mass transfer resistance term, $H_{Stat.}$.

3.4. External film mass transfer resistance C_f

To the best of our knowledge, there is only one attempt to isolate and measure the external film mass transfer term in columns packed with 5 μm porous particles and no attempt with smaller ones. This approach involves the determination of the third moment of the elution peaks [182,183]. The results of this recent work have not yet been confirmed. The precision and reproducibility of the elution band moments, which must be measured by

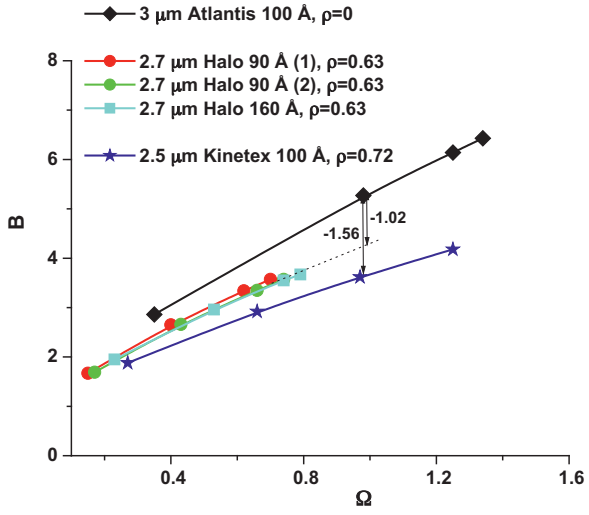

Fig. 16. Measurement of the reduced longitudinal diffusion coefficient *B* in columns packed with fully and superficially porous particles. Reproduced with the permission of Gritti et al. [103].

numerical integration, tend to rapidly decrease with increasing order of the moment because the signal becomes low and the signal to noise ratio high in the sides of the peak, regions in which the signal decreases rapidly with increasing distance to the peak center. It becomes more and more difficult to decide when the integration of the moments should start and end and this causes increasing errors [13,166,184]. Yet, the approach suggested and the results achieved make attractive this method of investigation of the external mass transfer.

We have adopted an alternative solution to this problem which seems to provide fairly precise values. By subtraction of the contributions of longitudinal diffusion, eddy dispersion, and trans-particle mass transfer resistances, it is possible to obtain an estimate of the external film mass transfer resistance contribution to the HETP:

$$H_{Film} = C_f u = H - \frac{B}{u} - A(u) - C_p u \quad (96)$$

The major difficulty of this exercise is that the eddy dispersion *A* term should be known. The theoretical variation of the external film mass transfer resistance term and that of the eddy dispersion term are proportional to $u^{2/3}$ and $u^{1/5}$, respectively. The eddy dispersion term is also sensitive to the retention factor due to the trans-column effects. Fig. 17 compares the contributions of eddy dispersion and external film mass transfer resistance to the HETP for two retention factors, $k = 0$ and 2, in a range of reduced velocity from 0 to 100. Strikingly, the eddy dispersion HETP term is significantly larger than the external film mass transfer term, whether it is derived from the Wilson and Geankoplis or the Kataoka correlation. This is particularly true for poorly retained analytes. As retention increases, the gap between the two HETP terms decreases. In conclusion, we can accept that, for the time being, measurements of the contribution of the external film mass transfer contribution remains inaccurate. This area becomes worthy of interest, particularly to better understand the column efficiency for large molecular weight compounds.

3.4.1. Packed columns

Miyabe et al. [151] observed that the error made on the measurements of H_{Film} can be minimized by using columns packed with large (18 μm), nonporous particles to measure *A* and *B*. By selecting large size particles, the precision of measurements of the experimental moments is excellent and no correction is

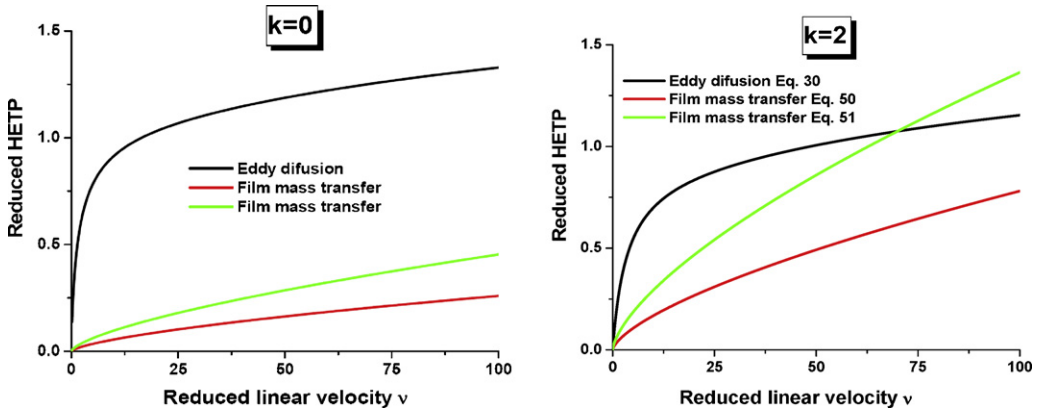

Fig. 17. Comparison between the theoretical eddy dispersion (solid black line) and the external film mass transfer resistance terms (Wilson–Geankoplis solid green line and Kataoka solid red line) . Left graph: retention factor $k = 0$. Right graph: retention factor $k = 2$. (For interpretation of the references to colour in this figure legend, the reader is referred to the web version of the article.)

required for the contributions of the extra-column volume, since this necessary correction is included in the data provided by both series of measurements. Also, the trans-particle mass transfer resistance contribution is equal to zero with nonporous particles ($C_p = 0$). Finally, making the measurements in a range of high linear velocities reduces sufficiently the contribution of the longitudinal diffusion term to make it negligible ($(B/u) \to 0$). Assuming a constant eddy diffusion A term, these authors found that the best estimate of the film mass transfer coefficient was well accounted by the Kataoka correlation at room temperature (288–298 K) but found also that the dispersion of the experimental data around the model values was large.

Miyabe et al. [152] followed a similar approach with a column packed with 50 μm fully porous particles [152]. In this case, the contribution of the trans-particle mass transfer resistance HETP term ($C_p u$) should be subtracted from the total HETP. The procedure for the determination of this term is discussed in the next section. By assuming a constant eddy dispersion term, the authors found that the experimental data were scattered between the lines defined by the classical correlations of Pfeffer [185], Wilson and Geankoplis [149], and Kataoka [150]. Yet, it remained impossible to tell which correlation could best account for the experimental data and if these results can be applied to sub-5 μm particles.

3.4.2. Monolithic columns

The external mass transfer was also studied in monolithic columns [152] by following the same experimental protocol as the one used earlier for conventional packed columns [186]. As expected, the results obtained strongly depend on the assumption made for the eddy dispersion contribution in monolithic columns. For $A = 15$ μm (the domain size of the monolithic silica rod used was 3.5 μm), the experimental results were in fair agreement with those predicted by the Wilson and Geankoplis k_f correlation (see Fig. 18).

In conclusion, the accurate measurement of the external mass transfer HETP term remains the most challenging task to accomplish in the investigations of the mass transfer mechanism in chromatographic columns. Actually, this task is as difficult to perform as the modeling of the external mass transfer is to design, and the process itself is elusive to define.

3.4.3. Suggestions for further research

It is surprising that the thickness, δ_l, of the stagnant layer of the eluent surrounding the particles was rarely investigated in any discussion of the importance of the external film mass transfer resistance in liquid chromatography. An estimate of this thickness could guide in the selection of the most suitable equation for the prediction of the external mass transfer coefficient and of the Sherwood number that are the most physically acceptable for beds of closely packed spherical particles. As indicated earlier, several correlations and equations are available in the literature. Most of them were derived in the 1960s, such as the Wilson and Geankoplis [149] and the Pfeffer (98) equations, in the 1970s, such as the Kataoka [150] and the Sircar (101) equations, and during the 1980s with the Lightfoot equation (102) for a single particle. All these equations can be written under the following form:

$$Sh = \frac{k_f d_p}{D_m} = \frac{d_p}{\delta_l} = f(\epsilon_e)\nu^{1/3} \tag{97}$$

with the function $f(\epsilon_e)$ provided by the different authors who tackled the problem being [149,150,185]:

$$f(\epsilon_e) = 1.26\left[\frac{1-(1-\epsilon_e)^{5/3}}{2-3(1-\epsilon_e)^{1/3}+3(1-\epsilon_e)^{5/3}-2(1-\epsilon_e)^2}\right]^{1/3}$$

Pfeffer (1964) (98)

$$f(\epsilon_e) = 1.09\left[\frac{1}{\epsilon_e^2}\right]^{1/3} \qquad \text{Wilson and Geankoplis (1966)} \tag{99}$$

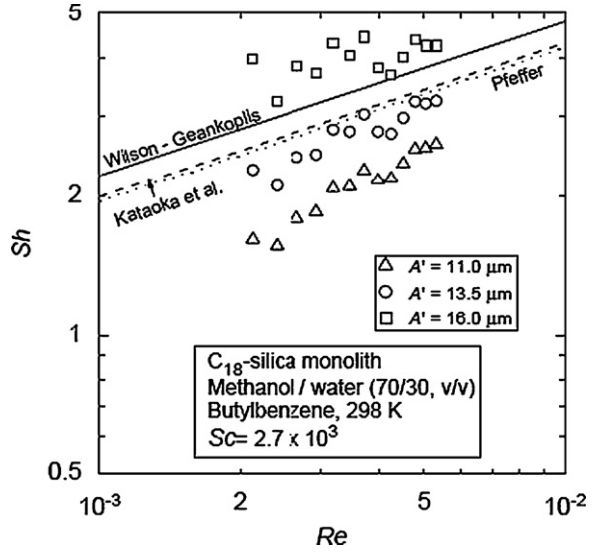

Fig. 18. Comparison between the experimental and correlation values of the Sherwood number as a function of the Reynolds number (between 1×10^{-3} and 1×10^{-2}) for a monolithic column (domain size 3.5 μm). Reproduced with the permission of Miyabe et al. [186].

$$f(\epsilon_e) = 1.85[1-\epsilon_e]^{1/3} \qquad \text{Kataoka et al. (1972)} \tag{100}$$

$$f(\epsilon_e) = 0.99\left[\frac{2+1.5(1-\epsilon_e)+1.5\left[8(1-\epsilon_e)-3(1-\epsilon_e)^2\right]^{1/2}}{\epsilon_e[2-3(1-\epsilon_e)]}\right]^{1/3} \qquad \text{Sircar (1974)} \tag{101}$$

$$f(\epsilon_e) = 1.23 \qquad \text{Lightfoot (1987)} \tag{102}$$

An approximate estimate of the maximum possible average film thickness, $\delta_{l,\max}$, of eluent surrounding a spherical particle is provided by assuming that all the eluent volume contained in the external porosity of the bed is uniformly distributed around the particles, as a concentric shell with a radius $(d_p/2)+\delta_{l,\max}$. In actual packed beds, the film thickness is not uniform but vary widely because the particles are in contact with neighbours. The distance between adjacent particles may vary from zero (at the contact point) to values that may locally exceed d_p, when particles are arching, as they some times do in 3D assemblies of particles. The volume fraction of eluent is typically $\epsilon_e \simeq 40\%$. Accordingly, the volume fraction occupied by the particles, $1-\epsilon_e$, is

$$1-\epsilon_e = \left(\frac{d_p/2}{(d_p/2)+\delta_{l,\max}}\right)^3 \tag{103}$$

Therefore, the average film thickness would be

$$\frac{\delta_{l,\max}}{d_p} = \frac{1-(1-\epsilon_e)^{1/3}}{2(1-\epsilon_e)^{1/3}} \tag{104}$$

Numerical application of Eq. (104) for $\epsilon_e = 0.4$ gives a fraction of the particle diameter equal to 9.3%. However, this is an estimate of the maximum film thickness and it is impossible that this thickness could be as large as 9% of the particle diameter. By definition, the eluent in this film is stationary and experience demonstrates that the eluent does percolate along the column at a reasonable velocity, consistent with Darcy law and the Kozeny–Carman correlation. This suggests that the film thickness could not exceed a few percent of the particle diameter.

Eq. (97) provides the ratio of the thickness of the eluent layer surrounding the particle to the particle diameter. In practical applications, HPLC columns are usually operated at high values of the Peclet number (i.e., interstitial reduced linear velocity), e.g., up to 50 in fast LC with sub-3 μm shell particles, in the analysis of small molecules. In this case, the relative film thicknesses predicted by the Pfeffer, Wilson–Geankoplis, Kataoka, Sircar, and Lightfoot models would be around 11.0%, 13.5%, 17.4%, 8.9%, and 22% of the particle diameter, respectively. The large value expected from the Lighfoot model is not surprising since this author solved the Navier–Stokes equation for a single active sphere. In contrast, the values predicted by the Pfeffer, the Wilson–Geankoplis, Kataoka, or the Sircar models do not make physical sense because the film thickness cannot exceed 10% of the particle diameters. This means that the layer of eluent surrounding the particles is very thin. Therefore, diffusion across it should be fast and the contribution to band broadening of the external film mass transfer resistance term should be negligible, unless some unexpected phenomenon takes place at the very opening of the pores and slows down solute influx.

We observe also that all former models neglect the nature of the actual external surface of the packed particles. The possible influence of the surface roughness and the intraparticle porosity (including the shape and the surface area of the pore openings) of the particles on the film thickness and on the effective diffusion of analyte molecules through this film is unknown. It should be investigated experimentally and by calculations based on bed reconstruction including a precise representation of the true topology of the particle surfaces.

3.5. Liquid–solid mass transfer resistance C_p

According to Eqs. (67) and (68), it is necessary to determine the experimental diffusivity, ΩD_m, of the analyte in the porous adsorbent to be able to obtain the trans-particle or the trans-skeleton mass transfer HETP terms ($C_p u$). Unfortunately, we do not yet have the means to accurately and precisely determine the analyte diffusivity in a single porous particle or in the shell of a superficially porous particle. A simple and indirect approach can be based on:

(1) the measurement of the true effective diffusion coefficient, D_{eff}, of the composite material made of the interstitial eluent, the porous adsorbent, and (possibly) nonporous cores, by applying the PP method and
(2) the choice of a satisfactory model of effective diffusion in a composite material, which would allow the derivation of the unknown parameter Ω. From the value of Ω, the value of the coefficient C_p is directly obtained from Eq. (67). To proceed further, we need to distinguish between packed and monolithic columns for two reasons: (1) the model of effective diffusion is not the same for a packed and for a monolithic columns; and (2) the geometry of the stationary phase (spheres in packed beds, linked cylinders in a monolithic rod) affects the expression of the coefficient C_p [15].

3.5.1. Trans-particle mass transfer resistance

As it was shown earlier in the section regarding the theoretical expression for the longitudinal diffusion coefficient B, the Torquato effective diffusion model is the most suitable model available because it accounts for the random distribution of spheres in contact ($\xi_2 = 0.3277$), immersed in a continuous matrix. The only weakness of this model is that it assumes an infinitely narrow particle size distribution (PSD) and that it ignores the actual degree of local disorder of the particles. In contrast, the relative standard deviation of the particle size is 5% for core–shell particles and between 10 and 20% for fully porous particles. However, experimental results of the PP experiments match closely those predicted by Torquato equation, which gives:

$$\frac{1}{2}\frac{\Delta\sigma_t^2}{\Delta t_p}\frac{u_{pp}^2}{(1+k_1)^2} = \frac{1}{\epsilon_e(1+k_1)}\left[\frac{1+2(1-\epsilon_e)\beta-2\epsilon_e\xi_2\beta^2}{1-(1-\epsilon_e)\beta-2\epsilon_e\xi_2\beta^2}\right]D_m \tag{105}$$

with

$$\beta = \frac{(1-\rho^3)/(1+(\rho^3/2))\Omega-1}{(1-\rho^3)/(1+(\rho^3/2))\Omega+2} \tag{106}$$

This equation in Ω has a single solution. The results of this approach designed for packed beds will be tested later (see third chapter of this review) for commercial columns packed with Halo 90 Å and Halo-ES-Peptide 160 Å core–shell particles.

3.5.2. Trans-skeleton mass transfer resistance

The micro-structure of a monolithic silica rod has not much in common with that of a packed bed. The external porosity is typically around 0.70 [41,92,187–191] for monolithic columns instead of close to 0.40 for packed columns. The shape of the elementary block of porous silica and their spatial arrangement are different for monolithic (cylinders) and packed (spheres) columns. For these reasons, the Torquato Eqs. (41) and (42), which are valid for systems of spheres should be modified for the monoliths. The

general Torquato equation of effective diffusion coefficient is written [57,110]:

$$D_{eff} = \frac{1}{\epsilon_e(1+k_1)}\left[\frac{1+n(1-\epsilon_e)\beta - n\epsilon_e\xi_2\beta^2}{1-(1-\epsilon_e)\beta - n\epsilon_e\xi_2\beta^2}\right]D_m \quad (107)$$

with

$$\beta = \frac{(1-\rho^{n+1})/(1+(\rho^{n+1}/n))\Omega - 1}{(1-\rho^{n+1})/(1+(\rho^{n+1}/n))\Omega + n} \quad (108)$$

where ξ_2 is an unknown parameters that should be determined from the experimental external obstruction factor, γ_e of a monolithic column. The shape of the porous skeleton being cylindrical, the integer is $n=1$ in both Eqs. (107) and (108) while it is $n=2$ with spheres. The monolithic skeleton is fully porous, therefore, ρ should be equal to zero in Eq. (108). Tallarek et al. [130] measured $\gamma_e = 0.73$ for $\epsilon_e = 0.704$ after morphology reconstruction of the monolithic skeleton architecture using confocal laser microscopy. Taking $\rho = 1$ (e.g. $\beta = -1$) for nonporous skeleton gives for γ_e:

$$\gamma_e = \frac{1-\xi_2}{2-\epsilon_e(1+\xi_2)} = 0.73 \quad (109)$$

Accordingly, we estimated that $\xi_2 = 0.11$.

3.6. Eddy dispersion A

The accurate measurement of the total eddy dispersion term, which includes the trans-channel, the short-range inter-channel and the trans-column velocity biases, can only be carried out with a non-invasive chromatographic method. The trans-channel and the short-range inter-channel HETP terms can also be measured after morphology reconstruction and calculation of the convective-diffusive mass transfer. These two approaches are detailed in the next sections.

3.6.1. Chromatographic method

In the absence of any friction–expansion phenomenon, the eddy dispersion term is obtained by subtracting the sum of the longitudinal diffusion term, the external film mass transfer term, and the trans-particle/trans-skeleton mass transfer resistance term from the total HETP [100]:

$$H_{Eddy} = H - H_{Long.} - H_{Film} - H_{Stat.} \quad (110)$$

The experimental determination of $H_{Long.}$ (measured by PP experiments), H_{Film} (calculated from the Kataoka and/or the Wilson and Geankoplis correlation), and $H_{Stat.}$ (obtained with PP experiment data and the diffusion coefficient calculated with Torquato model) was described in the previous sections. The total HETP is measured by numerical integration of the peak profiles to derive the first and second central moments:

$$H = L\frac{\mu_2^{\prime(3)} - \mu_{2,ex}^{\prime(3)}}{\left(\mu_1^{(3)} - \mu_{1,ex}^{\prime(3)}\right)^2} \quad (111)$$

This approach was used to compare the eddy dispersion term in columns packed with fully and superficially porous particles [103,126]. It was found that the high performance of the core–shell particles was explained for the most part by an exceptionally small eddy dispersion term compared to that of conventional columns packed with fully porous particles. For instance, Fig. 19 compares the eddy diffusion of toluene on the Atlantis-d C_{18} (fully porous particles) and on the Kinetex-C_{18} (core–shell particles) columns. The eddy dispersion is typically 30–40% smaller with core–shell than with conventional particles.

The accuracy of this chromatographic method for the determination of the eddy dispersion coefficient was recently discussed [102]. It mostly depends on the accuracy of the external film mass transfer resistance term H_{Film}, which is difficult to investigate from the sole experimental point of view. Fortunately, the contribution of this HETP term to the overall HETP term remains small, therefore, the measurement of the eddy dispersion term of small molecules remains sufficiently accurate (10–20%).

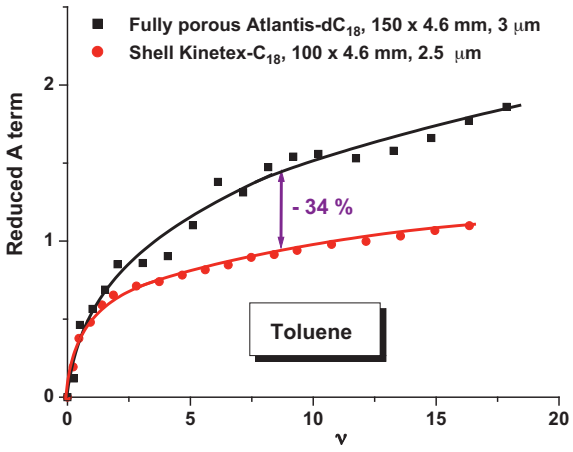

Fig. 19. Measurement of the eddy dispersion HETP term using the non-invasive chromatographic method. Comparison between the eddy dispersion term of columns packed with fully porous and shell particles. Reproduced with the permission of Gritti et al. [103].

3.6.2. Structure reconstruction method

Our understanding of eddy dispersion in packed and monolithic columns benefits now from the combination of the results of the morphology reconstruction of the actual stationary phase structure made by using confocal laser scanning microscopy (CLSM) and from the results of the calculation of transport properties in these reconstructed materials [122,130,192,193]. This task requires a pretreatment of the column. The bare silica is covalently modified by bonding a chemical dye whose maximum excitation matches the UV line of a diode laser; a small Stokes shift ensures that detection remains in the shorter wavelength part of the spectrum, an important consideration because resolution decreases with increasing excitation and emission wavelengths. This first derivatization step is followed by image acquisition using a CLSM objective, which provides a lateral and axial resolutions of about 0.2 and 0.4 µm, respectively. The structure is immersed in an eluent (glycerol/water mixture) whose refractive index matches that of silica and of the 100 µm glass capillary ($n = 1.4582$) in which the packed particles or the monolithic silica are confined. The acquired images are processed (segmentation) in order to produce a more realistic representation of the original object. The segmented images are then analyzed using the chord length distributions. Statistics for the chord lengths (average and dispersion around the mean) are collected for about a few 10^5 chords. Once the 3D structure has been reconstructed, the flow velocity field is determined based on the lattice-Boltzmann method for an incompressible fluid. The advantages of this microscopic method over the solution of the macroscopic Navier–Stokes equations are its inherent parallelism in view of computational efficiency and its ability to handle topologically complex solid–liquid interfaces. Finally, the mass transport in the reconstructed macroporous structure is simulated based on a random-walk particle-tracking model which needs to be parallelized.

Fig. 20 shows examples of reconstructed images of monolithic and particulate structures confined in 100 µm I.D. glass capillary. In these images, the contrast between the solid phase and the interstitial macropores is remarkable, which allows the visualization

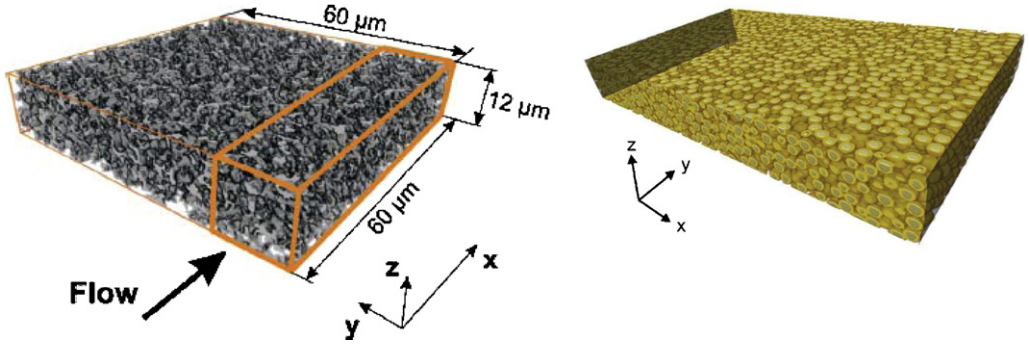

Fig. 20. Morphology reconstruction of monolithic and core–shell particulate stationary phases confined in 100 μm I.D. glass capillary using confocal laser scanning microscopy. Left graph: monolithic silica structure. Right graph: core–shell particulate structure. The sizes of the nonporous core and surrounding shells are 1.9 μm and 0.4 μm, respectively. The dimension of the reconstructed volume is 103 μm (x) × 58 μm (y) ×13 μm (z). Reproduced with the permission of Bruns et al. [130,192].

of ordered and disordered regions in the 3D structure of these two types of chromatographic support. The calculation of the mass transfer properties along these structures permits the measurement of the characteristic lengths after which the calculated axial (D_L) and/or transverse (D_t) dispersion coefficients remain invariant. The plots of the corresponding reduced HETPs, h_L and/or h_t, *versus* the average interstitial reduced linear velocity, ν, and their fit to the eddy dispersion equation of Giddings (see Section 2) allows the measurement of parameters λ_i and ω_i.

The main limitation of this morphology reconstruction method is the relatively small column aspect ratio that can be visualized by CLSM. Given the domain size of monolithic (≃3 μm) and particulate (≃2.5 μm) structures, the column aspect ratio is no larger than 50. In contrast, the aspect ratio of a 4.6 mm I.D. or even a narrow-bore 2.1 mm I.D. column exceeds 1000. It would take a considerable computational time in order for the axial dispersion coefficient to converge toward a constant value. Therefore, the morphology reconstruction method appears limited to the determination of the trans-channel and short-range inter-channel eddy dispersion terms. It can complement the chromatographic subtraction method for the measurement of the sole contribution of the trans-column eddy dispersion in packed and monolithic columns. We show later, in the third chapter, some applications to the determination of the trans-column eddy dispersion HETP term in 4.6 mm I.D. monolithic columns and in 4.6 mm I.D. columns packed with core–shell particles.

3.6.3. *Influence of the particle size distribution (PSD) on the column efficiency*

There are few investigations of this question in the literature.[1] While the influence of the average particle size was demonstrated long ago and is well understood, that of the PSD still remains obscure to this day. The commercial literature still waxes self-congratulatory statements on the supposed quality of some highly homogeneous batches of packing materials, with little experimental confirmation of their actual value. Although Purnell suggested that the nonuniformity of the packing material used might degrade the performance of gas chromatographic columns, there was no serious experimental data then to back this statement [194]. Earlier works [195–197] suggested that a narrow PSD is not essential for the achievement of efficient columns. These results had a long lasting influence and, essentially prevented further investigations. We must realize, however, that the precision of column efficiency measurements made then was generally modest, that the method used to assess it was inaccurate, and that the particles used were irregular, making their dimensions difficult to define, let alone measure. This issue was cogently developed thirty years ago by Dewaele and Verzele [198]. Although the ratio of the particle sizes below which and above which masses less than 10% of a packing material sample are found (noted as d_{90}/d_{10}) were already less than 1.5, it was not unusual to find in the optical field of a microscope more than a few particles with a diameter ratio exceeding 4 [198].

During a systematic investigation of the factors affecting column efficiency, Halaász and Naefe [197] found that, if the column efficiency depends on the average diameter of the sieve fraction of the packing material, it is not significantly affected by its d_{90}/d_{10} ratio, as long as this ratio does not exceed ca. 2. This result is consistent with the findings of Snyder [195] and Done and Knox [196]. Ten years later, Dewaele and Verzele revisited this issue in great detail [198]. They used a series of packing materials coming from batches of the same production data of C_{18} bonded porous silica particles, having average sizes of 3, 4, 5, 6, 8, and 10 μm. The PSD were derived from Coulter counter measurements, which gave ratios d_{90}/d_{10} close to 1.5 for all of them. The 100 mm ×4.6 mm column tubes were identical; the columns were packed following the same procedure, by the same person. For all columns, they derived best values of the A, B, and C coefficients of the van Deemter plots from the HETP curves. First, Dewaele and Verzele measured the efficiencies of columns packed with these pure materials and with mixtures made of equal weights of two of these materials. They found that the minimum HETPs of columns packed with binary mixtures were close to those of columns packed with the pure particles having a diameter nearly equal to the average diameter of the two materials in the mixture. For all these columns, the A and B terms were nearly the same. Then, Dewaele and Verzele measured the efficiencies of a series of ten columns packed with mixtures of the packing materials having average particle sizes of 3 and 8 μm [198]. The efficiencies of these columns increase linearly with the concentration of the material having the finer particles. In contrast, the column permeabilities did not vary linearly with this concentration but remained markedly lower than what would correspond to a linear variation. All these experimental results suggest that, as long as the PSD is reasonably narrow (e.g., with $d_{90}/d_{10} < 2$), the column HETP is determined by the average particle size and that the reduced HETP is independent of the width of the PSD, provided that the HETP is referred to the average particle size.

These results are consistent with independent theoretical findings of Dougharty [199], of Carta and Bauer [200] and of the Tallarek group [201]. Using the general rate model, Dougharty calculated the increase in the second moment of the band due to a finite PSD. He showed that this would increase the contribution due to intra-particle and to external mass transfers but that the effect would

[1] ScienceFinder queried for "Influence of the PSD of the packing material on the efficiency of chromatographic columns" returned five useful, relevant references.

be negligible for reasonably narrow PSDs, a result consistent with the findings of Kaczmarski [55]. Carta and Bauer investigated the column efficiency and calculated the elution profiles of a weakly retained compound having a very low diffusion coefficient on a column packed with a heterogeneous mixture of particles, with $d_{90}/d_{10} \simeq 10$ [200]. They found a significant but moderate difference between the elution profiles calculated for columns packed with the mixtures and for those packed with uniform-size particles. This suggests that the influence of the moderately wide PSDs of commercial packing materials which have $d_{90}/d_{10} < 2$ would be small if not negligible [200]. The Tallarek group calculated the structure of column beds randomly packed with materials having different PSDs and bed porosities, ranging from random-close to random-loose packing [201]. From these bed structures, they calculated elution chromatograms and derived the reduced HETP curves of the columns using the Sauter-mean diameter, which accounts for the surface to volume ratio of the packing and is often used in the engineering literature. Using the PSDs measured for sub-3 core–shell and sub-2 μm fully porous particles, they found no systematic differences in the bed permeabilities and only small differences in their efficiencies, corresponding to a slightly increased short-range inter-channel contribution to eddy dispersion in the bed packed with the wider PSD material. This confirms that the reduced eddy dispersion observed for core–shell packed columns [96] cannot be attributed to a narrow PSD.

Recently, these conclusions were challenged [202,203]. In a first paper a group of authors reported on investigations of the performance of series of columns packed with four different custom-made mixtures of packing materials derived from 1.9 μm HypersilGold (Thermo Fisher Scientific) modified with "different, deliberately induced PSD", which were not further defined [202]. The PSDs of these materials were subtly different. So were the HETP curves obtained. Although the authors had to conclude that the classifications of the packing materials after any characteristic of their PSDs and after their packing quality did not correlate, they suggested that the presence of low amounts of very fine particles could affect negatively the column performance, certainly the permeability, possibly the efficiency. The possibility that the presence of the fine particles in one sample was due to the "deliberately induced modifications" of the PSD was not commented upon. In a latter paper, the same group commented on a possible influence of the PSD on the column efficiency for a series of seven commercial columns [203]. Unfortunately, the column efficiencies were measured with a profoundly inaccurate method, by measuring the ratio of the retention time and the half-height of the peak and omitting to correct these experimental results for the band broadening contribution due to the extra-column volume of the instrument (see Section 3.1 and [166]). This is confirmed by the HETP curves published that exhibit minimum values markedly larger than those obtained on the same columns when the measurements are correctly done (see [102] and Fig. 8). Accordingly, both the accuracy and precision of the results are doubtful and the conclusions derived from the interpretation of these data with an obsolete set of equations (the so-called A coefficient depends on the mobile phase velocity, the C term is actually a conglomerate of several different contributions) is doubtful.

3.7. Friction–expansion

The measurement of the friction–expansion HETP term defined in Section 2 requires the acquisition of a series of data in order to solve the heat balance equation inside the column, to determine the temperature profile, $T(x, z)$, and to measure the distribution of the retention factor, $k(x, z)$, throughout the whole column volume [37,39,49,94,95,97,98,100,204]. For each mobile phase flow rate, the following data should be known with good accuracy:

1. The axial temperature profile along the external wall of the column should be measured with regularly spaced surface thermocouples [204]. The temperature of the eluent at the entrance of the column should also be known. Typically, the measurement of the local axial temperature every 1.5 cm along the column tube is sufficient.
2. The thermal conductivity of the heterogeneous chromatographic medium immersed in the eluent needs to be estimated from the thermal conductivity of the pure components, e.g. neat silica (1.4 W/m/K), octadecane (0.15 W/m/K), acetonitrile (0.20 W/m/K), methanol (0.15 W/m/K), and water (0.60 W/m/K). The apparent thermal conductivity of the chromatographic medium can be estimated from either the Zarichnyak equation [205]:

$$\lambda_{eff} = \nu_1^2 \lambda_1^T + \nu_2^2 \lambda_2^T + 4\nu_1\nu_2 \frac{\lambda_1^T \lambda_2^T}{\lambda_1^T + \lambda_2^T} \quad (112)$$

or an expression based on the effective medium theory, which yields the following relationship [206]:

$$\lambda_{eff} = \frac{1}{f-2}\left[\left(\frac{f}{2}\nu_2 - 1\right)\lambda_2^T + \left(\frac{f}{2}\nu_1 - 1\right)\lambda_1^T + \sqrt{\left[\left(\frac{f}{2}\nu_2 - 1\right)\lambda_2^T + \left(\frac{f}{2}\nu_1 - 1\right)\lambda_1^T\right]^2 + (2f-4)\lambda_1^T\lambda_2^T}\right] \quad (113)$$

Both models are based on a random distribution of two homogeneous media 1 and 2 of known thermal conductivities, λ_1^T and λ_2^T, and occupying volume fractions ν_1 and ν_2. The value recommended for the parameter f is 4.5.
3. The isosteric heat of adsorption, Q_{st}, of the sample should be determined over the range of temperature defined from the solution $T(x, z)$.
4. The dependence of the retention on the local pressure, which is negligible only for small molecular weight compounds, analyzed with conventional columns, operated with inlet pressures not exceeding a few hundred bars. Otherwise, this parameter, ΔV_m, must be measured. This is conveniently done by measuring retention at moderate flow rates (low pressure drops along the column) at successively higher average pressures by adding a high pressure resistance (i.e., a capillary restrictor) downstream the detector of the instrument. With this procedure, the average column pressure can be increased progressively while keeping low the pressure drop.

4. Applications

Earlier, we analyzed separately the mechanisms behind each contribution to the total HETP of a chromatographic column and derived equations accounting for them (Section 2). Then, we explained how these different contributions can be measured and how analysts have access to accurate values of the coefficients used in these equations (Section 3). In this last section, we show how these theoretical and experimental results can be applied to improve our understanding of the mass transfer mechanisms.

The problem of finding the best values of the two critical sets of parameters necessary for the modeling of chromatographic separations, whether at the analytical or the preparative level, is most important for any practical applications of chromatographic models. This problem has two faces, whether we want to validate a model or to apply it. Our purpose in this work is limited to the kinetic parameters but we want to validate the models, to acquire the quasi-certainty that we do understand all the phenomena involved in the elution of chromatographic peaks or bands. This requires the design of a series of appropriate

experiments for the purpose of measuring separately and accurately as many parameters as possible, making necessary numerous complex, independent measurements. This procedure is long, slow, tedious and costly. A simpler alternative approach is often used by many engineers who merely desire approximate values of these parameters in view of modeling and optimizing the experimental conditions for specific chromatographic separations. It is known as parameter optimization and consists in acquiring chromatograms and, by fitting these profiles to those calculated with a selected model, in finding the set of parameters for which the distance between the experimental and the calculated chromatograms is sufficiently small. Among others, a good example of this approach was described by Persson et al. [207,208]. This procedure is often applicable to the modeling of separations made by preparative chromatography [13]. It is valid provided that the model used has been validated by independent investigations. The results obtained are limited to the specific column and sample used and to the range of experimental conditions explored during the acquisition of the data fitted to the model. The use of the parameters that were determined by this procedure should not be extended to the modeling of other separations, even closely similar, without proper care.

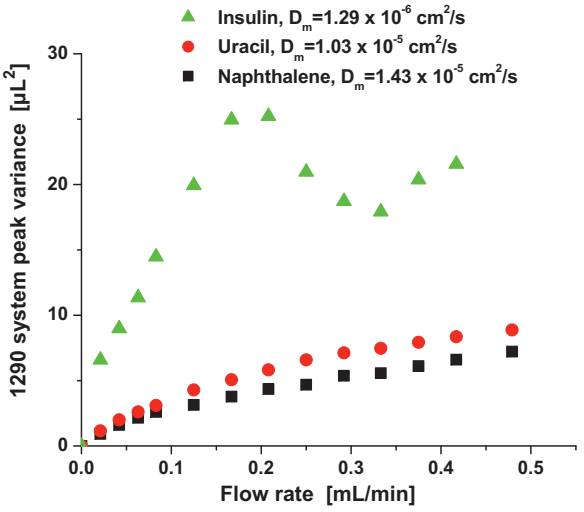

Fig. 21. Influence of the analyte bulk diffusion coefficient, D_m, on the extra-column peak variance measured with the 1290 Infinity system equipped with 115 µm connecting capillaries, a 800 nL detection cell, and after injection of 0.25 µL.

4.1. Measurement of extra-column contributions

Modern column technology has resulted in the development of new commercial columns that have markedly smaller hold-up volume, V_0, and higher efficiency, N. As a consequence, the contribution of the extra-column volumes of the instruments, $\sigma^2_{Instrument}$, to the total peak variance, σ^2_{Total}, of elution bands has continuously grown in the last few years [209,210]. The effective analytical results, the resolution between two closely eluted peaks, depends on the relative importance of the terms in the equation:

$$\sigma^2_{Total} = \sigma^2_{Instrument} + \frac{V_0^2}{N}(1+k)^2 \quad (114)$$

Instruments that were currently available at the turn of the century had not been initially designed to run columns delivering peak variances as small as a few µL^2 as it is the case today [95,96,99,126,211]. The most modern instruments show significant improvements but their contribution to the total band variance of recorded peaks is still not negligible. So, to assess actual column performance, a correction must be made [96]. Therefore, the first and the second central moments of the elution peaks and of peaks of the same compounds when the column is replaced with a zero-volume connector must be accurately determined. The subtraction of these two respective values provide the exact measurement of the inherent column HETP. Extra-column peak profiles are severely broadened at high mobile phase flow rate due to the parabolic profile of the radial distribution of laminar flow velocities (Poiseuille flow) across the connecting capillary tubes and the presence of cracks and anfractuosities everywhere two parts of the instrument plumbing are connected.

When extra-column band broadening contributions are measured, the same sample, the same eluent, and the same temperature must always be used to record the bands in the absence and in the presence of the column. To clearly illustrate the considerable influence of the diffusion coefficient of the compound (a function of the compound, the eluent and the temperature) on this contribution, Fig. 21 compares the plots of the extra-column peak variance contribution for two small (uracil and naphthalene) and one large molecule (insulin) as a function of the flow rate applied. The two small molecules were dissolved in a mixture of acetonitrile and water (65/35, v/v) and insulin in another mixture (31/69, v/v) containing 0.1% of trifluoroacetic acid (TFA).

The differences are obvious when D_m changes by a factor of approximately 10 between small and large molecules. They are even measurable when the difference in D_m does not exceed 20%.

Fig. 22 compares a typical extra-column band profile and the best Gaussian (see moments in Eq. (83)) and EMG–GMG hybrid functions (see Eq. (85)) which could be used to account for it. Obviously, a Gaussian distribution (three parameters) is inappropriate for describing such an asymmetric peak profile. A 5-parameter EMG/GMG hybrid function considerably improves the agreement between experimental and calculated profiles, yet, the agreement between the bases of the two peaks is barely acceptable. A relative difference of 10–15% between the peak variances derived from the best EMG/GMG function and the exact one measured by numerical integration of the profile is observed at high flow rates [166]. While this error does not affect much the HETP of retained compounds, the variance being proportional to $(1+k)^2$, it can have a large impact on the HETP of non-retained to poorly retained components, which are of main concern in chromatographic applications under isocratic conditions ($0.5 < k < 3$). Fig. 23 illustrates that the strategy chosen for the measurement of the first and the second central moments of the peak affects the final value found for the column HETP. In conclusion, the measurement of the correct HETPs of narrow-bore columns must involve the numerical integration method, which is the only method that can accurately account for the experimental peak tailing.

4.2. Validation of diffusion coefficient equation

In liquid chromatography, the bulk diffusion coefficient of small molecules are usually estimated from the well-known Wilke and Chang equation [172]:

$$D_m = \frac{7.4 \times 10^{-8}\sqrt{x_A\phi_A M_A + x_B\phi_B M_B}\,T}{\eta_{AB} V_b^{0.6}} \quad (115)$$

where x_A and x_B, ϕ_A and ϕ_B, M_A and M_B are the molar fractions, the associative factors (1.9 for methanol, 2.6 for water), and the molecular weights (g/mol) of the two solvents A and B used (32 g/mol for methanol, 18 g/mol for water), respectively, η_{AB} is the viscosity (cP) of the binary eluent listed in [13], and V_b is the molar volume of the compound considered at its boiling point, estimated from the LeBas group method [212]. The Wilke and Chang equation is considered to provide reasonable estimates within 20% of

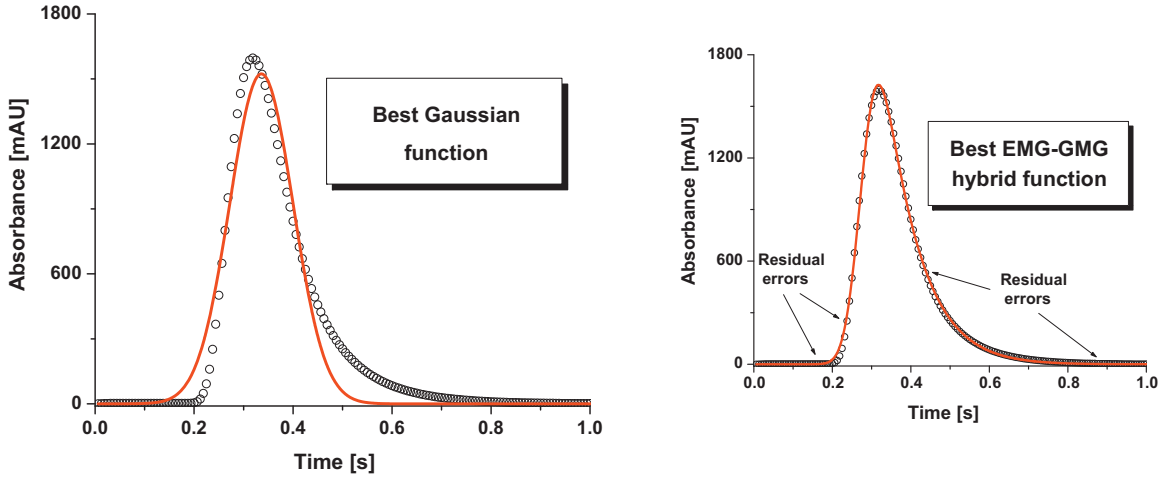

Fig. 22. Comparison between experimental (open circles) and best calculated (solid red line) extra-column band profiles. HPLC system: 1290 Infinity equipped with 115 μm connecting capillaries and a 2.4 μL detection cell volume. Injected volume: 4.8 μL. Flow rate: 3.2 mL/min. Sample: uracil. Ambient temperature. Left graph: Best Gaussian function. Right graph: Best EMG/GMG functions. (For interpretation of the references to colour in this figure legend, the reader is referred to the web version of the article.)

the diffusion coefficient D_m of small analytes in the mobile phase [212,213]. Other useful correlations are available [13,169,170].

In a recent investigation of mass transfer mechanisms in first generation monolithic columns (see later, Section 4.3), we applied the previously described PP method to a column packed with 1.9 μm nonporous particles in order to measure the diffusion coefficients of uracil, caffeine, toluene, and naphthalene in a mixture of acetonitrile and water at $T = 300$ K (see chromatograms in Fig. 24). The external obstruction factor of this column was obtained from the precisely known diffusion coefficient of thiourea in pure water, at 298.15 K [180,181], $D_m = 1.33 \times 10^{-5}$. This diffusion coefficient is corrected for the difference in temperature since the PP experiments were carried out at $T_{PP} = 292.65$ K. The viscosities of pure water at 298.15 and 292.65 K are 0.913 and 1.033 cP, respectively. Accordingly, γ_e was equal to 0.652 ± 0.007. This value was used to estimate the diffusion coefficients of uracil, caffeine, toluene, and naphthalene in a mixture of acetonitrile and water (55/45, v/v) at 300 K ($\eta = 0.724$ cP). The corresponding PP chromatograms recorded after parking times of $t_p = 1$, 60, 120, and 180 min are shown in Fig. 24. The temperature of this second series of PP experiments were 293.55 K for uracil and caffeine ($\eta = 0.835$ cP) and 293.15 K for toluene and naphthalene ($\eta = 0.855$ cP). These measurements provided diffusion coefficients of 1.12×10^{-5} cm^2/s (uracil), 9.38×10^{-6} cm^2/s (caffeine), 1.62×10^{-5} cm^2/s (toluene), and 1.37×10^{-5} cm^2/s (naphthalene). The Wilke and Chang equation estimates these coefficients at 1.29×10^{-5} cm^2/s (+13%), 8.88×10^{-6} cm^2/s (−6%), 1.17×10^{-5} cm^2/s (−38%), and 1.02×10^{-5} cm^2/s (−35%), respectively. These values are acceptable for the polar compounds uracil and caffeine (<15%) but are clearly unacceptable for the apolar compounds (>30%). Li et al. [169,170] measured the diffusion coefficients of toluene, using the Aris–Taylor method, in a 16 m long, 0.02 in I.D. PEEK tube, at a linear velocity of 0.813 cm/s and found at 303 K, for a 60/40 aqueous solution of acetonitrile $D_m = 1.71 \times 10^{-5}$ cm^2/s. Correcting this value for an acetonitrile content of 55% and a temperature of 300 K, gives a coefficient of 1.5×10^{-5} cm^2/s, within 6% of that measured with our column packed with non-porous particles.

Careful analysts who need accurate data to study mass transfer mechanisms in chromatographic columns should systematically measure the bulk diffusion coefficient of their analytes by either one of the methods described earlier to avoid the relative errors

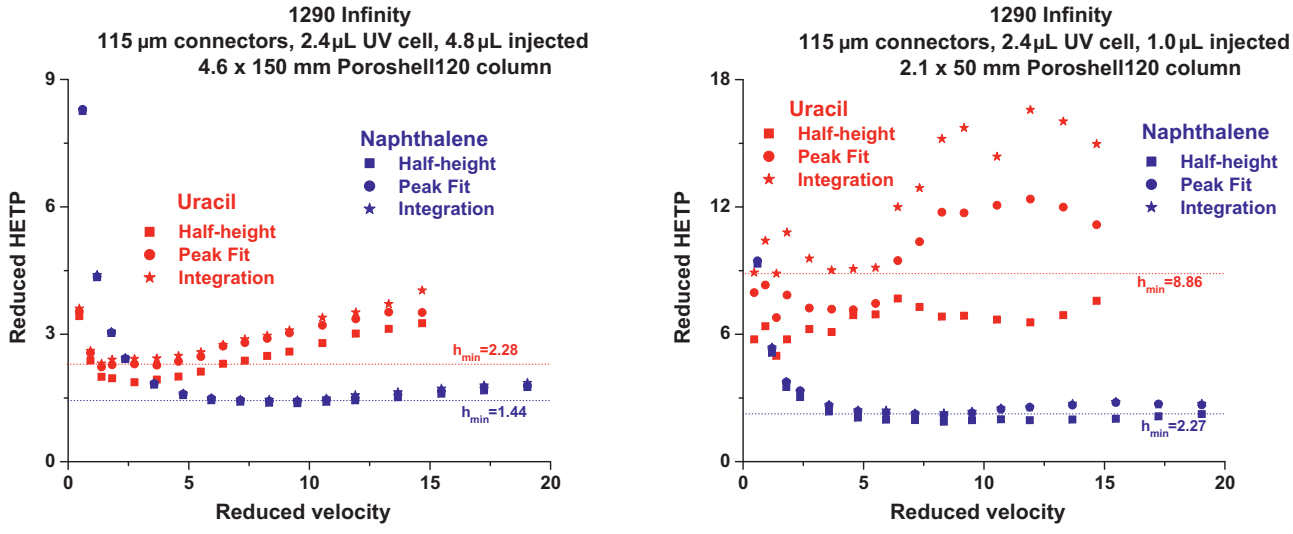

Fig. 23. Plots of the corrected reduced HETPs of two small molecules (non-retained and moderately retained) measured from the three different methods as indicated in the legend. Left graph: 150 mm ×4.6 mm I.D. column. Right graph: 50 mm ×2.1 mm I.D. column. Reproduced with the permission from Gritti et al. [166].

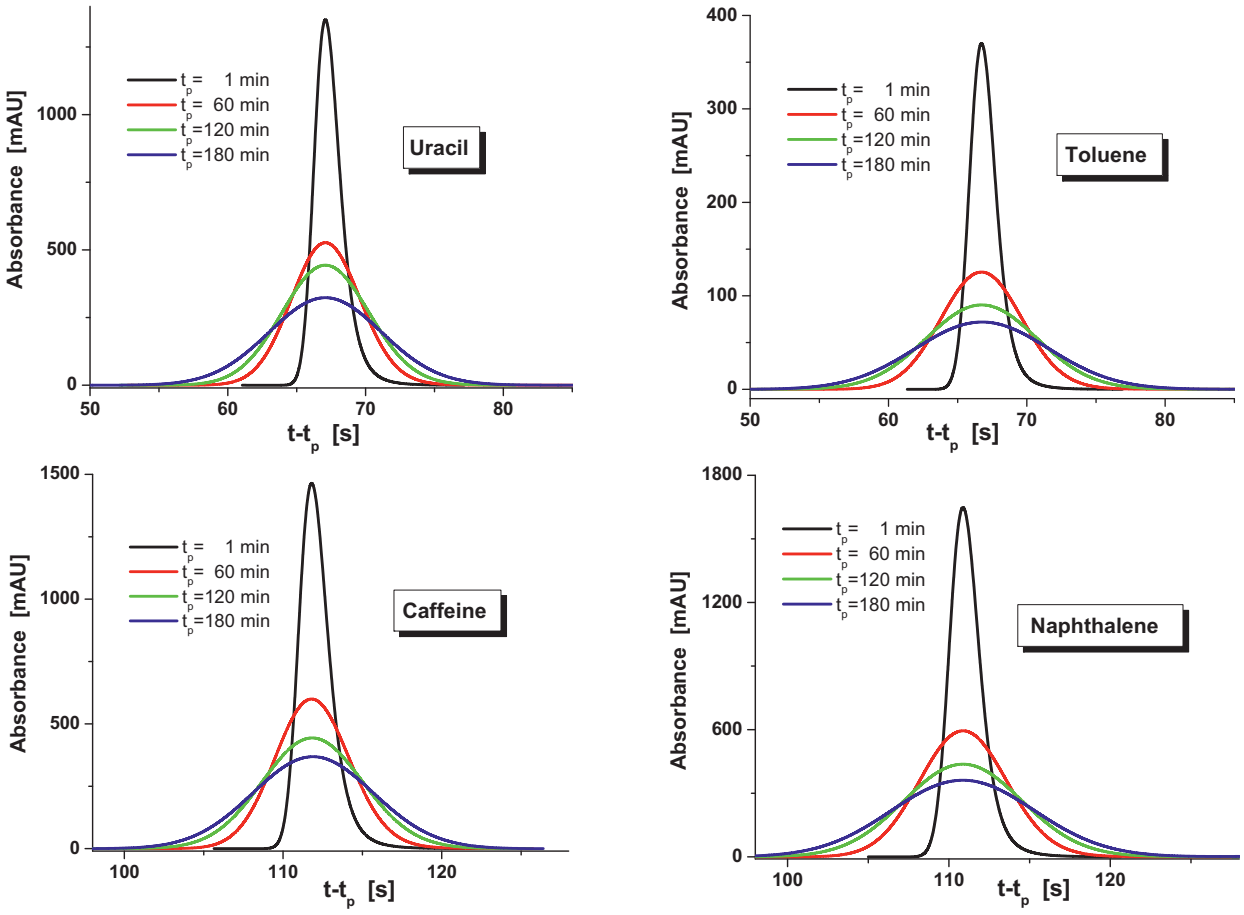

Fig. 24. Chromatograms recorded during the peak parking experiments applied to measure the diffusion coefficient of uracil, toluene, caffeine, and naphthalene in a mixture of acetonitrile and water (55/45, v/v) at $T = 300$ K. The parking times are indicated in the legend. Reproduced with the permission from Gritti et al. [42].

caused by predictions made with conventional correlation's equation, which may exceed 30%.

4.3. Eddy dispersion in a monolithic columns of the first generation

The mass transfer mechanism in a monolithic column (4.6 mm ×100 mm) of the first generation was studied according to the general protocol described in the third chapter of this work [42]. These monolithic silica rods have a typical average throughpore size of 2 μm and a skeleton size around 1 μm (the domain size is ca. 3–3.5 μm). We now know that the 4.6 mm diameter silica rods are not radially homogeneous but that their external porosity is smaller in their center than close to the wall [41,43,44,99]. Furthermore, the distribution of the injected sample at the column inlet and its collection at the column outlet may contribute to band broadening and to a loss of column efficiency. Research and development of the next generation of monolithic columns should include the design of better distributors and of rods with smaller domain sizes (≃1–2 μm).

In order to estimate the potential gain in performance of monolithic columns, it is important to measure the sole contribution of the eddy dispersion HETP term. The HETP subtraction method was recently applied to a 4.6 mm ×150 mm Onyx monolithic column [42]. Applying recent results of Miyabe et al. [186], the external film mass transfer coefficient was estimated from the Wilson and Geankoplis correlation [149]. Four compounds were used, uracil and caffeine (non-retained and poorly retained compounds), toluene and naphthalene (retained compounds). Fig. 25 compares the overall HETP and the eddy dispersion HETP term of these compounds. Obviously, the non-retained compounds have a nearly flat or even slightly decreasing overall HETP curve, consistent with as extremely fast mass transfer between the moving liquid and the stationary phase. As the retention increases to k values between 2 and 3, a larger B term (due to increasingly fast surface diffusion) and a slight linear increase of the Cu branch (due to increases of the C_p and C_f coefficients) are observed. We note first that the minimum HETP is no less than 17 μm because the peak profiles are visibly tailing (not shown here). The US Pharmacopeia (USP) tailing factors measured at 5% of the peak height range from 1.6 for the less asymmetric ones (toluene, naphthalene) to 2.4 with the most asymmetric peaks (uracil, caffeine). This confirms the relatively poor kinetic performance of these monolithic columns, compared to that of columns packed with sub-2 μm fully porous particles and/or sub-3 μm superficially porous particles, which can provide minimum HETP as low as 4 μm for retained analytes [93,95,96]. Most remarkably, Fig. 25 (right graph) reveals that eddy dispersion accounts for more than 70% of the total HETP at linear velocities larger than the optimum velocity.

In agreement with the theoretical consideration regarding the impact of the retention factor on eddy dispersion (see Figs. 6 and 7), the eddy dispersion of non-retained compounds (uracil and caffeine) is higher than that of retained compounds in the range of low velocity. The subtraction of the trans-channel and short-range inter-channel eddy dispersion contributions measured by Tallarek et al. [130] from the total eddy dispersion term shown in the right graph of Fig. 25 leaves the residual trans-column eddy dispersion term in 4.6 mm I.D. monolithic columns. Fig. 26 shows the

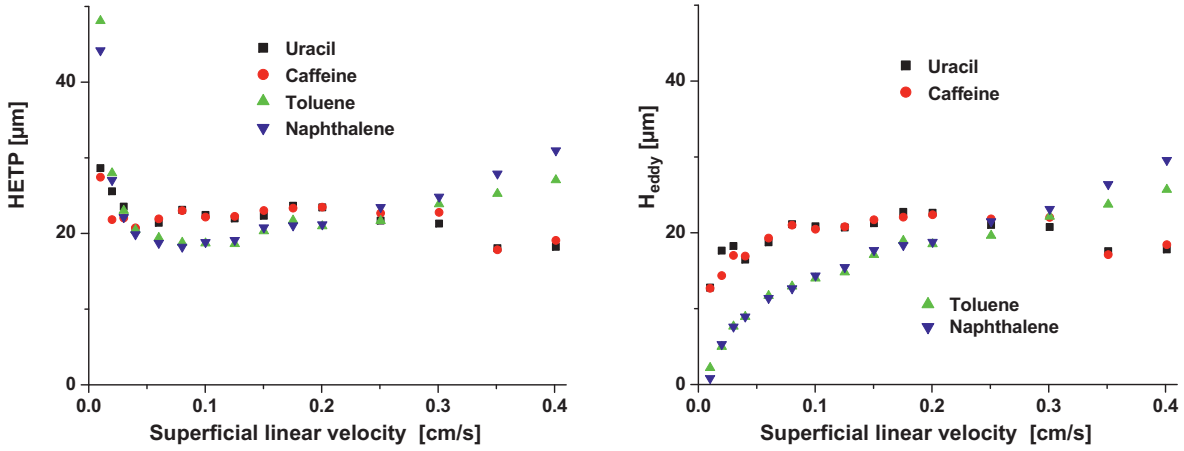

Fig. 25. HETPs of four small molecules, uracil and caffeine (non-retained and poorly retained samples), toluene and naphthalene (retained samples), measured from the numerical integration of the peak profiles recorded with a 100 mm × 4.6 mm Onyx-C−18 monolithic column. Left graph: Overall HETP curve. Right graph: Eddy dispersion term measured from the subtraction chromatographic method after removal of the B/u_S, $C_f u_S^{2/3}$, and $C_p u_S$ terms. Reproduced with the permission from Gritti et al. [42].

trans-column eddy dispersion term of uracil and toluene. Undoubtedly, the contribution of trans-channel and short-range inter-channel velocity biases plays a marginal role in the overall band spreading.

In conclusion, the subtraction method described in this work permits the measurement of eddy diffusion and the identification of the cause of the relatively poor performance of the 4.6 mm I.D. monolithic columns of the first generation. Trans-column effects should be significantly reduced in order to increase the efficiency of these highly permeable columns. This implies a more radially homogeneous structures and a better designed inlet and outlet distributors. In addition to the reduction of the trans-column flow heterogeneities, smaller domain sizes, of the order of 2 μm (instead of 3–3.5 μm) could also substantially improve the column efficiency [214], but at the cost of a lower column permeability.

4.4. Eluent friction: prediction of chromatograms in vHPLC

Frictional heating in vHPLC columns operated at high flow rates, under high pressure gradient has nefarious effects on band broadening in short (3–15 cm) narrow-bore (2.1 and 3.0 mm) columns packed with sub-2 μm particles. In order to anticipate and adjust the thermal environment of the chromatographic column under isocratic conditions, a heat balance model was derived. This model of heat transfer in and out a chromatographic column was validated based on the measurement of the surface temperature along column tubes and of the temperature of the exiting eluent [163,164,215]. Once the actual temperature distribution throughout the column was obtained, it was possible to write a mass balance model including transverse (D_t) and axial (D_a) lumped dispersion coefficients directly obtained from measurements of the actual HETP, H_a, in the absence of heat friction effects. The radial dispersion coefficient was directly taken from the transverse plate height equation of Knox et al. [216,131]:

$$D_a = \frac{H_a u_0}{2} \tag{116}$$

$$D_r = \gamma_e D_m + \frac{1}{2}\gamma_r u_0 d_p \tag{117}$$

where $\gamma_e = 0.7$ and $\gamma_r = 0.03$.

The retention factor of the sample is a complex function of the local temperature (the temperature distribution is known only after solving the heat balance equation) and of the local pressure. The axial pressure profile is calculated according to the Blake, Kozeny and Carman permeability law [113], knowing the state equation

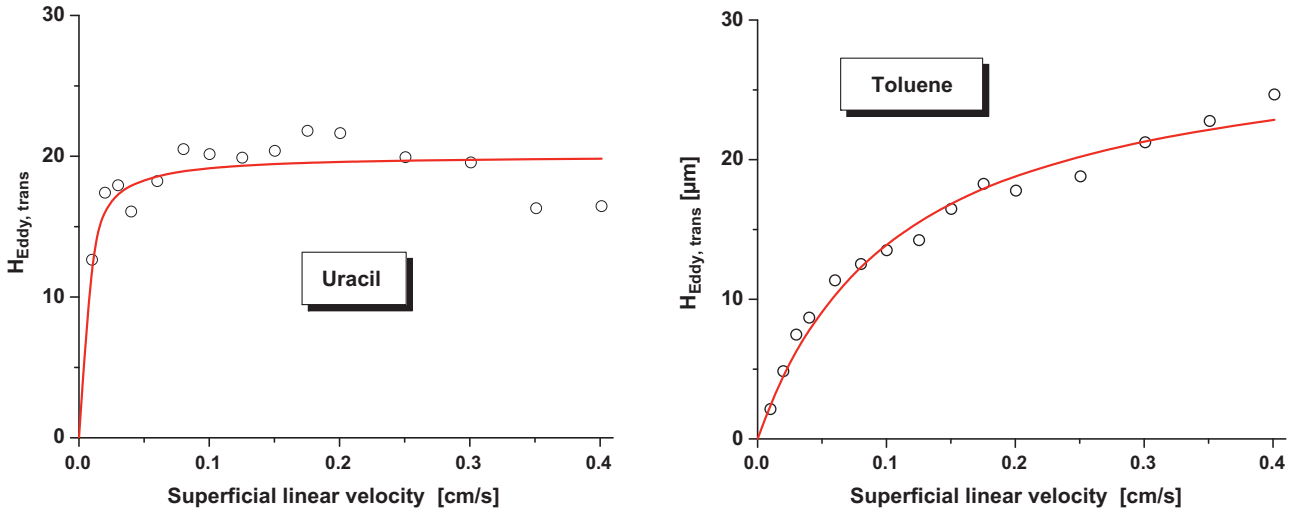

Fig. 26. Trans-column eddy dispersion of uracil (non-retained compound) and naphthalene (retained compound) measured with a 100 mm × 4.6 mm Onyx-C-18 monolithic column. Left graph: Uracil. Right graph: Toluene. Reproduced with the permission from Gritti et al. [42].

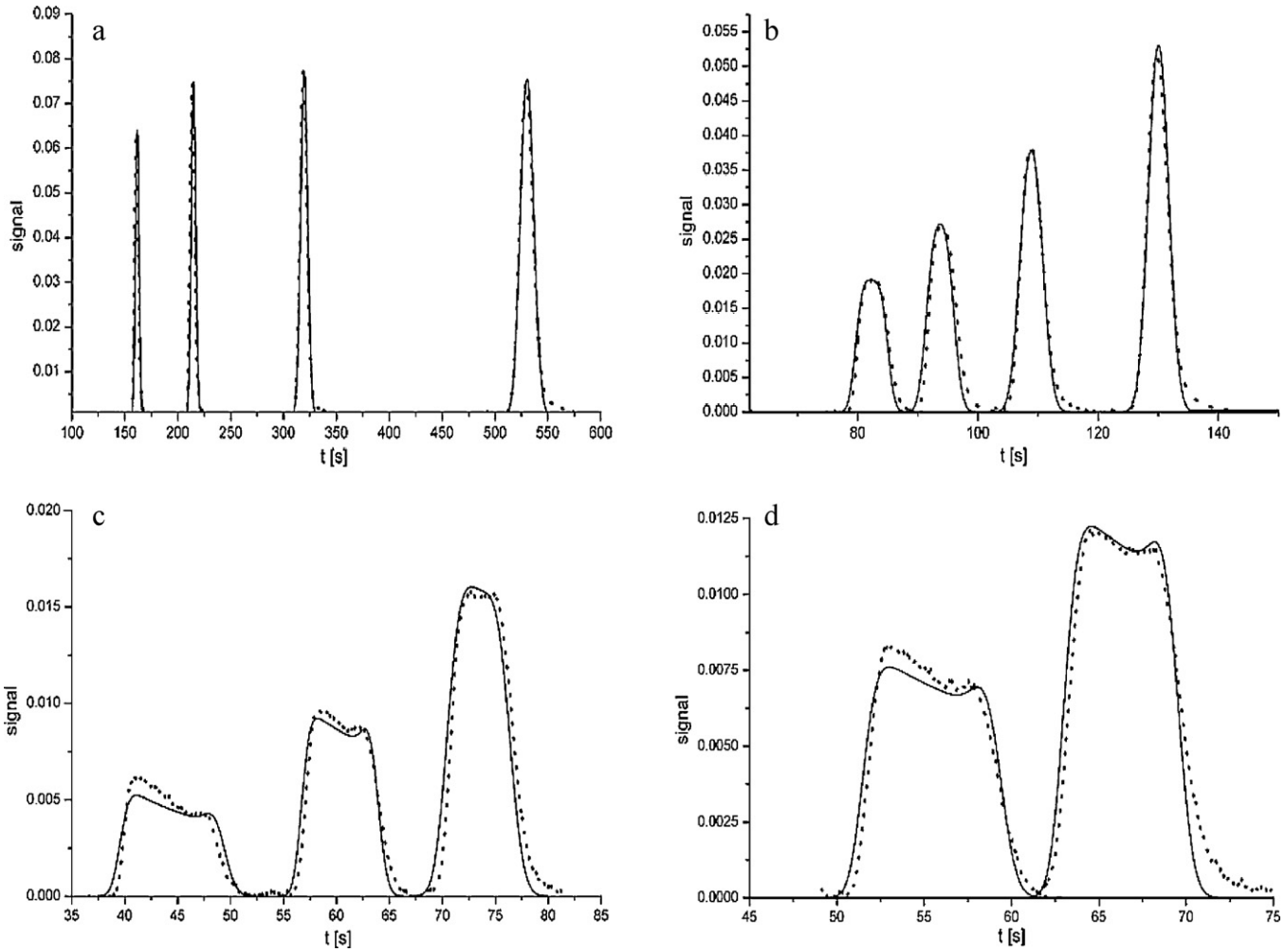

Fig. 27. Prediction (solid lines) of the nefarious heat friction effect in vHPLC and comparison to the experimental band profiles. Upper left graph: $F_v = 0.4, 0.3, 0.2, 0.12$ mL/min (from left to right) and $P = 210, 161, 114, 75$ bar, respectively. Upper right graph: $F_v = 0.8, 0.7, 0.6, 0.5$ mL/min (from left to right) and $P = 419, 365, 313, 261$ bar, respectively. Bottom left graph: $F_v = 1.5, 1.1, 0.9$ mL/min (from left to right) and $P = 808, 580, 470$ bar, respectively. Bottom right graph: $F_v = 1.2, 1.0$ mL/min (from left to right) and $P = 664, 525$ bar, respectively. See complementary experimental conditions in the text. Reproduced with the permission of Kaczmarski et al. [163].

of the eluent, $\rho(P, T)$, the viscosity law, $\eta(T, P)$, and the inlet pressure. The variations of the retention factor with the pressure at ambient temperature and with the temperature at the reference pressure P_{ref} were measured in order to estimate the isosteric heat of adsorption, Q_{st}, the Henry's constant at infinite temperature, K_0, and the difference in the partial molar volumes of the analyte in the adsorbed layer and in the liquid phase, ΔV_m. In the mass balance model, k is then written:

$$k(P, T) = \frac{1 - \epsilon_t}{\epsilon_t} K_0 \exp\left(\frac{Q_{st}}{RT}\right) \exp\left(\frac{\Delta V_m [P - P_{ref}]}{RT}\right) \quad (118)$$

Fig. 27 compares the experimental band profiles of naphtho[2,3-a]pyrene measured with a 50 mm × 2.1 mm BEH-C_{18} column thermostated in a water bath at 299 K to those calculated by solving the heat and the mass balance equations. The eluent is pure acetonitrile. As the flow rate increases, the heat friction increases, and the band becomes strongly distorted. The agreement between experimental and calculated elution profiles is excellent given the importance of the temperature and pressure inhomogeneous behavior, across and along the column. Fig. 28 illustrates the complex concentration distribution along the column when the band reaches the column exit, before it is detected [162]. Because the temperature is larger in the center than at the wall region of the column, the band moves faster along the axis than along the wall. The figure shows that the transverse dispersion coefficient is too small to fully relax the radial concentration gradients.

In conclusion, the impact of frictional heating on the band broadening of retained analytes is now deeply understood from a physico-chemical point of view. It can be predicted with great accuracy. Yet, the effect of the heat friction is not always as deleterious as is shown in Figs. 27 and 28, if the column is placed in a still-air environment which minimizes the heat exchange between the column wall and the external environment, reducing the radial temperature gradient. However, the downside of a nearly adiabatic environment is the severe variation of the average retention factor with the flow rate. Analysts must find a compromise between column efficiency and reproducible analysis time.

Next, we analyze a similar thermal problem but with a much different eluent, supercritical carbon dioxide.

4.5. Eluent expansion: prediction of chromatograms in SFC

In contrast to vHPLC, pressure drops are very small in SFC and the frictional heating remains marginal under most experimental conditions. On the other hand, the expansion of supercritical CO_2 along the column can be considerable when the average density is moderate (below ca. 0.6 g/mL) and the expansion cooling significant. Consequently, the direction of the heat flux in SFC is opposite to that observed in vHPLC, e.g. the column will eventually absorb

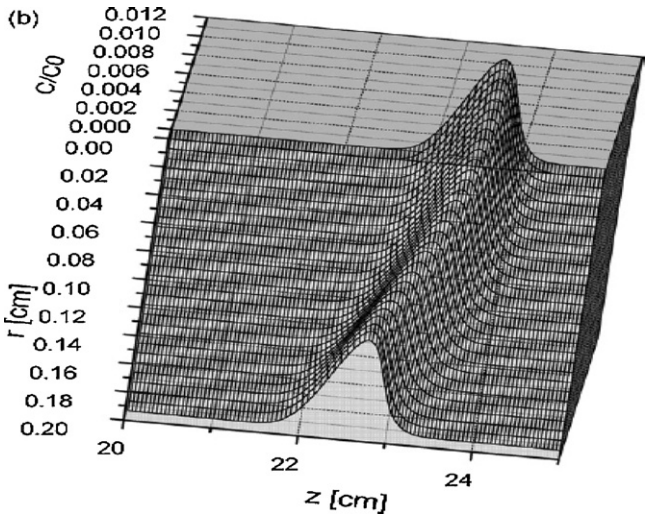

Fig. 28. Calculation and visualization of the concentration distribution across and along the column before the sample band is exiting the column. Thermostated column. Calculation made for a 250 mm × 4.0 mm column and a mobile phase (methanol–water) velocity equal to 3 mL/min at the column inlet. Reproduced with permission of Kaczmarski et al. [162].

energy from its external environment. In terms of band profiles, the result is very similar to that observed in vHPLC if the column is not insulated [217]. The central region of the column is cooler than the wall region and the part of analyte bands migrating along the wall reach the column outlet first. Fig. 29 compares the elution band profile of a series of n-alkanes under insulated (the column was covered with fiberglass and foam pipe insulation) and thermostated (the column is exposed to the oven air in typical fashion) conditions. The 150 mm × 2.0 mm column was packed with 5 μm Spherisorb-C_{18} particles.

The calculation of the heat and mass transfer under SFC conditions requires accurate knowledge of the state equation of the supercritical fluid in the ranges of pressure and temperature which are used in the experiments. This task is possible with pure CO_2, state equation of which can be easily derived numerically. Kaczmarski et al. [160] could predict the additional HETP term due to the cooling of supercritical CO_2 during its decompression along the column. Fig. 30 compares the experimental HETP and those calculated from the first and second central moments of the calculated band profiles. The agreement is excellent and the results pinpoint the importance of selecting high reduced density for CO_2 (e.g. a zone of the phase diagram distant far enough from the critical point and where the compressibility of CO_2 is low) and a very effective insulation of the column wall. SFC appears much more sensitive to the variations of the thermal environment than vHPLC.

In conclusion, despite the significant variations of the physicochemical properties (density, viscosity, thermal conductivity) of supercritical CO_2 throughout chromatographic columns, the decomposition of the column volume into elementary volumes located between the axial coordinates z and $z+dz$ and the radial coordinates r and $r+dr$ followed by the summation over the whole column volume permit the accurate prediction of the experimental band profiles in SFC conditions.

4.6. Performance of columns packed with 2.7 μm core–shell particles

Columns packed with the new sub-3 μm core–shell particles are now competing actively with those packed with sub-2 μm fully porous particles for the achievement of the fast and very efficient resolution of complex mixtures [126]. After unsuccessful beginnings in the 1970s and 1990s, the discovery of a new design for the structure of superficially porous particles and a new preparation process, the manufacturers of core–shell particles are enjoying a stunning success, as demonstrated by the attention currently invested in investigations of the performance of the 2.7 μm Halo particles (Advanced Material Technologies, Wilmington, DE), the 1.7 and 2.6 μm Kinetex particles (Phenomenex, Torrance, CA) and the 2.7 μm Poroshell120 particles (Agilent Technologies, Little Fall, DE). These columns, first offered in 2006, 2009, and 2010, respectively, have already acquired a significant part of the market. Provided that they are used with a modern instrument giving a sufficiently small extra-column volume contribution to band broadening [126,210,218], all columns packed with these core–shell particles exhibit consistently minimum reduced plate heights of 1.5 or less in the 4.6 mm I.D. format, a significant improvement compared to the minimum reduced HETP of 2.0 provided by conventional fully porous particles under similar experimental conditions.

In this section, we apply the experimental approach elaborated in Chapter 3 to measure and investigate the coefficients B, A, and C of the plate height equation and the friction–expansion term of columns packed with these new core–shell particles and to shed new light on the reasons for their exceptional performance.

4.6.1. Longitudinal B term

The B coefficient in the general HETP equation (27) was measured by applying the PP method and Eq. (95), as explained earlier. The data were acquired for four low molecular weight compounds (uracil, acetophenone, toluene, and naphthalene), one peptide molecule (β-Lipotropin), and one protein molecule (insulin). This study was done with the Halo particles that have a ratio, $\rho = 0.63$, of the core (1.7 μm) to the particle (2.7 μm) diameter. Two different shell mesopore structures were considered in this study, Halo-C_{18} 90 Å and Halo-ES-Peptide-C_{18} 160 Å [101]. The former particles were designed to separate low-molecular-weight compounds (MW <5 kDa) whereas the latter are more suited for the analyses of high-molecular-weight compounds (MW >1500 Da). The values of the B coefficients (referring to the interstitial linear velocity u) obtained on these two columns were 1.69 and 1.95 (uracil, $k = 0$), 2.66 and 2.96 (acetophenone, $k = 0.29$ and 0.20), 3.57 and 3.67 (toluene, $k = 0.89$ and 0.49), 3.35 and 3.55 (naphthalene, $k = 1.10$ and 0.61), 2.26 and 3.13 (β-Lipotropin, $k = 0.71$ and 0.80), and 1.42 and 1.81 (insulin, $k = 0.41$ and 0.92) for the Halo 90 Å and the Halo 160 Å, respectively. We note that the retention factors of the small, retained molecules are larger on the Halo 90 Å than on the Halo 160 Å which is because the surface area accessible for adsorption is larger with the former, which has a larger specific surface area (~150 m^2/g) than the latter (~90 m^2/g). In contrast, the retention factors of the more voluminous peptide and protein molecules are smaller on Halo 90 Å because these molecules are more significantly excluded from the mesoporous volume of these particles (37% for β-Lipotropin and 70% for insulin) than from the wider mesopores of Halo 160 Å (25% and 49%, only).

The B coefficients of the low molecular weight compounds increase with increasing retention factor in RPLC. The B coefficients are significantly larger with the particles that have large mesopores than with those having small ones, most likely because the diffusivity of large molecules is less hampered through large mesopores than through narrow ones. The purpose of the next section is to determine the sample diffusivity in the porous shells, $D_p = \Omega D_m$ of these particles.

4.6.2. Shell diffusivity and C_p coefficient

The measurement of the shell diffusivity, D_p, is necessary if one wants to calculate estimates of the trans-particle mass transfer resistance term. A model of effective diffusion through the packed

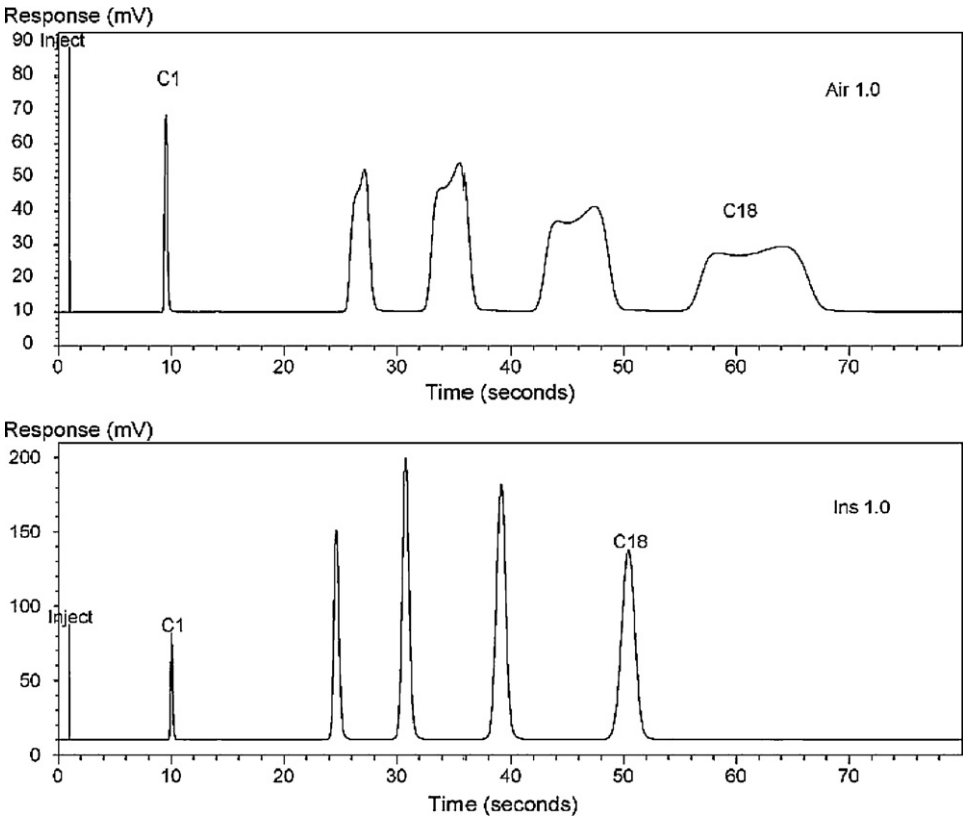

Fig. 29. Effect of thermal conditions on the peak shape of a series of n-alkanes (C_1, C_{12}, C_{14}, C_{16}, and C_{18}) in SFC (100% CO_2). Flow rate: 1.265 mL/min. Inlet pressure: 118.4 bar. Outlet pressure: 93.5 bar. Top graph: the column is placed in typical fashion in the thermostated air bath oven (323 K). Bottom graph: the column is insulated with fiberglass and foam. Reproduced with permission of Poe et al. [217].

bed is needed for this purpose. It was shown in Section 2 that the Torquato model or the Garnett model for diffusion in core–shell particles is the most relevant model of diffusion for columns packed with core–shell particles. The variable ξ_2 in Torquato equation (Eq. (41)) was set at 0.413 in order to predict the value of the external obstruction factor, $\gamma_e = 0.65$, measured by PP. The external porosity was measured at $\epsilon_e = 0.40$ and we have $\rho = 1.7/2.7 = 0.63$. Accordingly, the model yields Ω values for the two columns of 0.12 and 0.21 (uracil), 0.46 and 0.58 (acetophenone), 0.83 and 0.87 (toluene), 0.74 and 0.82 (naphthalene), 0.32 and 0.65 (β-Lipotropin), 0.04 and 0.16 (Insulin). The experimental results derived with the non-retained compound, uracil, confirm the largest hindrance for diffusion through the Halo 90 Å than through the Halo 160 Å shell particles. Given the internal porosities ($\epsilon_p = 0.22$ *versus* 0.36 measured from ISEC experiments [101]) and the hindrance diffusion factor ($F(\lambda_m) = 0.81$ *versus* 0.88 derived from the Renkin correlation [111]), the internal obstruction factors are $\gamma_p = 0.67$ and 0.66. Therefore, analyte diffusivity seems to be mostly controlled by the particle porosity. As retention increases, analyte concentration in the adsorbed layer increases, so do the concentration gradients,

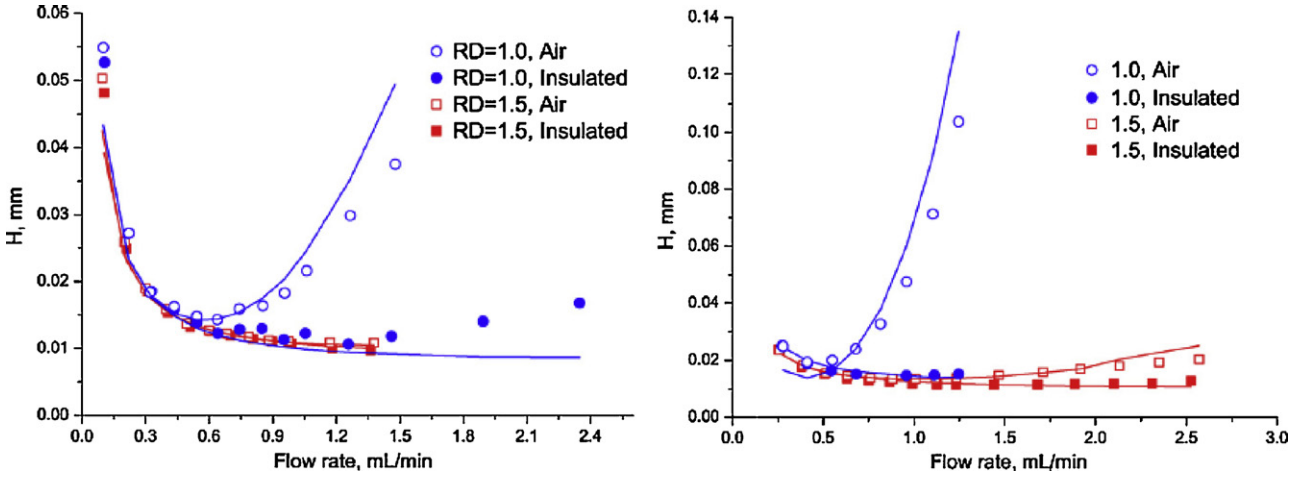

Fig. 30. Comparison between the experimental (symbols) and calculated (solid lines) HETPs for a 150 mm × 2.0 mm column packed with 5 μm (left graph) and 3 μm (right graph) Spherisorb-C_8 particles in SFC for two CO_2 reduced densities (1.0 and 1.5) and two external thermal environments (air oven and glass fiber/foam insulation). Reproduced with the permission from Kaczmarski et al. [160].

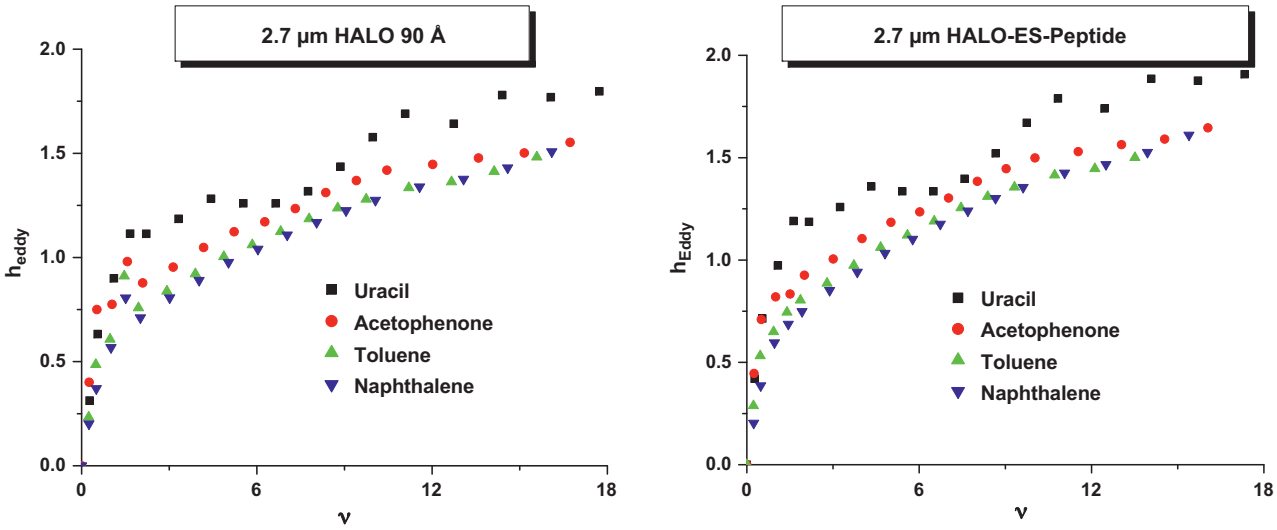

Fig. 31. Experimental eddy dispersion in 4.6 mm × 150 mm columns packed with 2.7 μm core–shell particles for four small molecules. Reproduced with the permission from Gritti et al. [101].

and surface diffusion becomes faster, compensating for the smaller pore diffusion in the small mesopores. The difference in particle diffusivity between Halo 90 Å and Halo 160 Å particles decreases. For the bulkier molecules, β-Lipotropin and insulin, the impact of the average mesopore size on D_p is large because the exclusion of these compounds from the pore volume is significant. For retained compounds, D_p is typically 10% (small molecules, D_H = 4.5 Å), 100% (peptide, D_H = 12 Å), and 300% (protein, D_H = 32 Å) larger through the particles of Halo 160 Å than through those of the Halo 90 Å particles.

The values of the trans-particle mass transfer coefficient can now be estimated using Eq. (67). They are 0.0042 and 0.0051 (uracil), 0.0041 and 0.0037 (acetophenone), 0.0052 and 0.0041 (toluene), 0.0067 and 0.0050 (naphthalene), 0.0097 and 0.0066 (β-Lipotropin), and 0.0363 and 0.0259 (insulin) for Halo 90 Å and Halo 160 Å, respectively. This information is important because it permits the determination of the contribution of the term $C_p\nu$ to the overall HETP. In the case of low molecular weight compounds on sub-3 μm core–shell particles, ν remains smaller than 25. Accordingly, in RPLC, whether these compounds are retained or not, $C_p\nu$ is on the average around 0.005 × 25 = 0.125 at ν = 25. As a comparison, the external film mass transfer term, $C_f\nu^{2/3}$ (k_f assumed from Wilson & Geankoplis correlation), varies from 0.05 for non-retained compounds to 0.56 for strongly retained ones.

These results show that the trans-particle mass transfer of low molecular weight compounds is faster than the mass transfer through the stagnant film of eluent surrounding the particles. the $C_p\nu$ term plays a minor role in the overall mass transfer resistance in chromatographic columns. In contrast, with biomolecules such as insulin, $C_f\nu$ = 0.1 ($k \simeq 1$) while $C_p\nu$ = 2.9 (Halo 90 Å) and 2.1 (Halo 160 Å) for ν = 80. The diffusion of the proteins through the porous shell controls the liquid–solid mass transfer. Regarding peptide molecules, the external film mass transfer and diffusion through the mesoporous silica medium contributes nearly equally to the overall HETP.

4.6.3. Eddy dispersion A term

The eddy dispersion *A* term of 4.6 mm I.D. columns packed with 2.7 μm core–shell particles was measured for the four same compounds for the Halo 90 Å and Halo 160 Å columns. The subtraction method described in the previous chapters was applied. As shown in Fig. 31, we observe very little differences between the eddy dispersion terms of these two columns. In fact, their external porosity are the same (ϵ_e = 0.40), the size distribution of these two packing materials are identical, and the sample diffusivity across these particles are equal within 10%. Therefore, trans-channel, short-range interchannel, and transcolumn velocity biases are very similar on both columns, which is not surprising for columns packed by the same expert using particles made with the same technology and having very similar characteristics.

Fig. 32 compares the six individual HETP terms (longitudinal diffusion, transchannel eddy diffusion, interchannel eddy diffusion, trans-column eddy diffusion, external film mass transfer, and trans-particle mass transfer terms) which control the total reduced HETP of a 150 mm × 4.6 mm column packed with 2.7 μm Halo-ES-Peptide core–shell particles. Remarkably, in a range of reduced

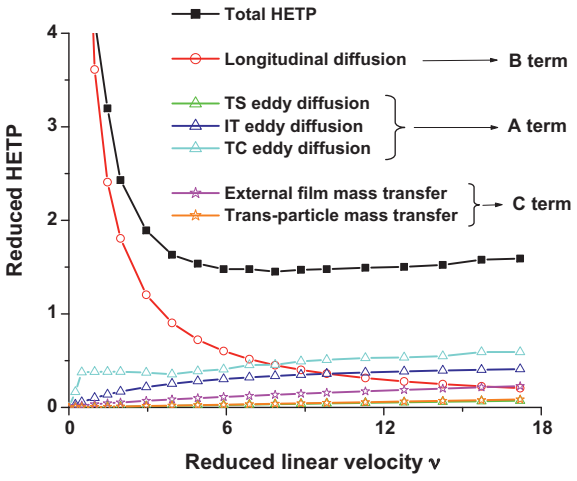

Fig. 32. Determination of each individual HETP term based on the measurement of the total HETP (full square, peak moments), of the longitudinal diffusion term (empty red circles, peak parking), of the trans-channel and short-range interchannel eddy dispersion terms (empty green and blue triangles, structure reconstruction), of the trans-column eddy dispersion term (empty cyan triangles, HETP subtraction method), of the external film mass transfer resistance term (empty pink stars, Wilson and Geankoplis), and of the trans-particle mass transfer resistance term (empty orange stars, peak parking + Torquato model of effective diffusion). (For interpretation of the references to colour in this figure legend, the reader is referred to the web version of the article.)

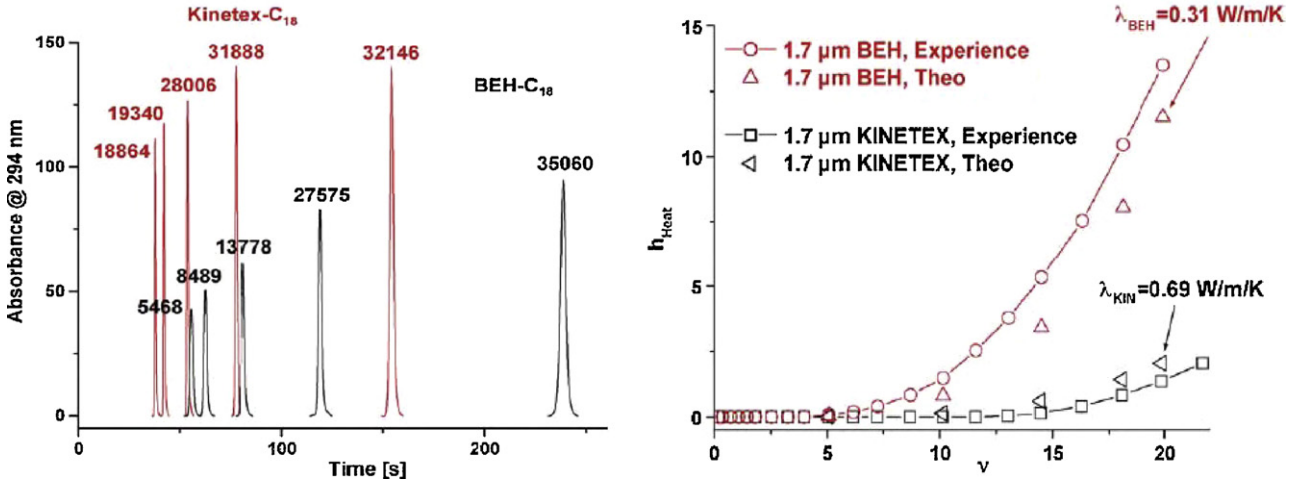

Fig. 33. Comparative performance of columns packed with 1.7 μm core–shell (Kinetex-C_{18}) and fully porous (BEH-C_{18}) particles recorded at different flow rates and under isocratic conditions. Eluent: 100% acetonitrile. T = 295 K. Sample: naphtho[2,3-a]pyrene. Flow rates: 1.10, 1.00, 0.80, 0.56, and 0.28 mL/min. Left: chromatograms. Right: experimental and theoretical additional HETP term caused by heat friction. Reproduced with the permission from Gritti et al. [97].

linear velocities around the optimal velocity, the three most important contributions to the HETP are the longitudinal diffusion, the trans-column eddy dispersion, and the short-range interchannel eddy dispersion terms. Despite the presence of the 1.7 μm solid cores and the resulting decrease of the longitudinal diffusion coefficient B [58,59], this term plays a major role in the efficiency of modern columns packed with 2.7 μm shell particles. Less than a decade ago, this contribution to band broadening was considered as practically irrelevant, mainly because the A and the overall C terms were those controlling the mass transfer kinetics in columns packed with the large particles available at the time. Were the trans-column velocity biases reduced to zero, the minimum reduced HETP would eventually be reduced to a nearly incompressible limit around 1.0 and column performance would have reached almost a final limit. Better performance could then only be reached if the packing structure could be really ordered (with no short-range inter-channel velocity biases) and if nonporous particles were used. That would bring the ultimate optimum reduced HETP around 0.5. It is amazing to realize that we are not far today from this idealized limit since minimum values of the reduced HETP between 1.0 and 1.5 (and sometimes closer to 1.0 than to 1.5) have already been measured for several brands of core–shell particles. Concerning monolithic columns, the situation is even more dramatic [130]. If the trans-column velocity biases were absent in capillary format, the minimum reduced HETP (measured according to a domain size of 3 μm) of the bulk monolithic structure would be around 0.7, i.e., a minimum plate height as small as 2 μm. This explains why some scientists are so eagerly waiting for the second generation of monolithic columns of narrower diameter (2–3 mm I.D.) with reduced trans-column eddy diffusion.

4.6.4. Friction–expansion term

Columns packed with 1.7 μm Kinetex-C_{18} core–shell particles are also available commercially in the 2.1 mm I.D. vHPLC format. When operated under certain flow rate and back pressure conditions, the power of the heat friction dissipated in the column becomes larger than 5 W/m (see Eq. (75)) and the heat released in these columns and dissipated through axial and radial diffusion is sufficient to generate significant axial and radial temperature gradients. Then, an additional HETP term, H_{heat}, must be added to the isothermal HETP. The theoretical and experimental frameworks described in the second and third chapters of this work were applied. The results are summarized in Fig. 33, which compares them with those obtained with a column of the same dimensions packed with 1.7 μm fully porous BEH-C_{18} particles.

Strikingly, it was observed that the frictional heating between the eluent and the bed through which it percolates has a significantly less detrimental impact on the efficiency of columns packed with core–shell particles than on that of columns packed with fully porous particles. It was unambiguously shown [97,98] that such a difference is due neither to a difference in the axial temperature profiles along the two column walls nor to the adsorption strength of the stationary phase (the isosteric heats of adsorption are similar). In contrast, the observations made and theoretical calculations [164] were fully consistent with a difference in the amplitude of the radial temperature gradient from the center to the wall of the column. The amplitude of this gradient is larger with the column packed with fully porous BEH-C_{18} particles than with the column packed with core–shell Kinetex-C_{18} particles. What probably explains this difference in chromatographic behavior when the amount of heat produced is the same in both cases is the difference in thermal conductivity of the two distinct packed beds. Knowing the thermal conductivities of the pure eluent (acetonitrile, 0.20 W/m/K), neat silica (1.4 W/m/K), and octadecyl silane chains (C_{18}, 0.15 W/m/K), it was possible to estimate the thermal conductivities of the packed beds at 0.69 W/m/K for the bed of C_{18}-bonded core–shell Kinetex particles and at 0.31 W/m/K for the bed packed with fully porous C_{18}-bonded BEH particles.

We might conclude from these results that the heat generated by friction diffuses radially at a smaller rate through the inner diameter of the BEH column than through that of the Kinetex column. As a result, the latter column keeps satisfactory performance at higher flow rates than the former. The results of the comparison between the performance of these two columns in gradient elution is even more striking because, as a result of the differences in the radial temperature, of the viscosity and the velocity of the mobile phase, its composition is also different at the center and close to the wall of the column [219,220]. Fig. 34 compares the chromatograms of a fragrant oil obtained with the same two columns. The peaks recorded with the column packed of fully porous particles are markedly wider than those recorded with the column packed with Kinetex particles, which is striking given that these particles are of the same size and that the heat friction released is exactly the same in both columns.

In conclusion, it seems attractive to prepare core–shell particles having a porous shell with properties similar to those of current

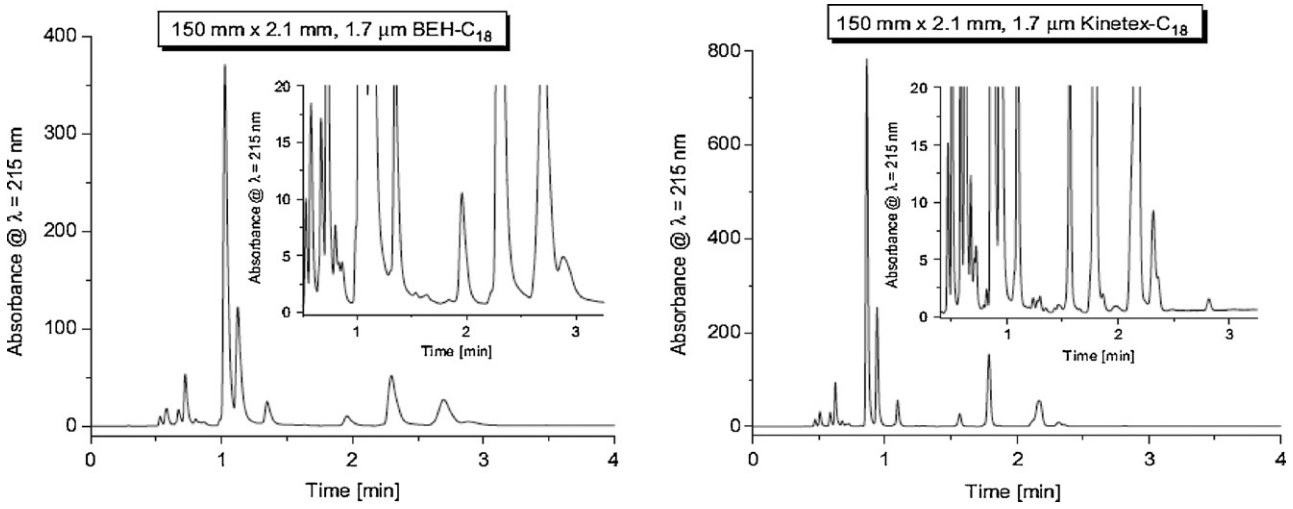

Fig. 34. Comparative performance of columns packed with 1.7 μm core–shell (Kinetex-C_{18}) and fully porous (BEH-C_{18}) in gradient elution. Sample: 1 μL of an acetonitrile solution of the oil (1/60, v/v). Solvent A: pure acetonitrile. Solvent B; pure water. Linear gradient program: from t = 0, 75/25 (v/v) A/B, to t = 4 min, 82/18 (v/v) A/B. Constant flow rate 0.75 mL/min. Initial maximum inlet pressure 1190 bar. T = 294 K. Left graph: 150 × 2.1 mm column packed with 1.7 μm BEH-C_{18} column. Right graph: 150 × 2.1 mm column packed with 1.7 μm Kinetex-C_{18}. The friction power is about 10 W/m for both columns. Reproduced with the permission from Gritti et al. [98].

similar materials available but having cores made of a material having a much higher heat conductivity. Alumina has a thermal conductivity twenty times larger than silica and seems recommended for its chemical properties of chemical inertness to most mobile phases. Metal have higher heat conductivities but stainless steel is barely eight times more conductive than silica; copper and silver are almost 200 times more conductive than silica but are too corrosive to be acceptable; gold could be but may seem difficult to bind to silica.. The use of a diamond core could permit the use of much finer particles than is presently possible but would not alleviate the consequences of the need to choose between enormous pressure drops of extremely short columns.

5. Conclusion

This review describes the considerable work made over the last eighty years to further our understanding of all the non-equilibrium effects that prevail in chromatographic columns and our ability to measure accurately and precisely their importance. The major steps in our progress were the seminal plate height concept brought by Martin and Synge [12] in the 1940s, the landmark paper of Lapidus and Amundson [9] in the 1950s that begot the whole theory of mass transfer kinetics, with the critical works of van Deemter et al. [11], Rhee et al. [72,138,221–223] and finally the generalized nonequilibrium theory of Giddings [15] in the 1960s. During the following 50 years the work of numerous groups progressively reduced these brilliant concepts, theories and ideas to practice, developing new methods of measurements of the many parameters involved, procedures to apply these tools to the solution of the innumerable practical problems encountered, and preparing better particles and packing more efficient, faster columns, all this work devoted to improving the practical usefulness of this fabulously useful separation method, chromatography. Finally, in the early 2010s, we are reaching the point where we can conceive of soon being able to understand and manipulate the phenomenon known as chromatographic band spreading by decomposing it in its element, understanding the independent physico-chemical events involved, and making them accessible to our actions.

We showed how a judicious series of measurements may successfully connect the conventional B, A, and C terms of the old van Deemter equation to the fundamental physico-chemical kinetic events involved in a chromatographic column. This includes:

1 The accurate measurement of the first and second central moments, μ_1 and μ_2', of chromatographic peaks by the numerical integration of the recorded elution data. This method is always exact and should be preferred to the approximate half-height peak width and peak fitting methods.
2 The measurement of the bulk diffusion coefficient of analytes which scales all the other diffusion coefficients along the tortuous and constricted mesopores (pore diffusion), over the hills and valleys of the adsorbent surface (surface diffusion), and through the chromatographic bed (effective bed diffusivity). The application of the peak parking method to a "calibrated" column packed with nonporous particles provides accurate measurements of D_m with a precision of ±5%.
3 The longitudinal diffusion contribution which prevails at low reduced velocities is directly and easily accessible by application of the peak parking and/or of the multi-location peak parking methods to the column studied. This last method was recently suggested to account for the possible axial heterogeneity of the packed column bed [224]. It requires between about half a day (low molecular weight compounds) and three full days (high molecular weight compounds) to record these data. The accuracy and precision are usually within a few percent.
4 The effective diffusivity of analytes through the stationary phase, ΩD_m, is obtained by combining the results of measurements of the longitudinal diffusion contribution and the Torquato model of effective diffusion in a composite material, such as monolithic or packed columns. This allows the measurement of the trans-particle mass transfer resistance term (C_p) with an error smaller than 5%. It is noteworthy that the Torquato model cannot account for the actual degree of pore disorder in packed or monolithic columns. There is still a serious need for a more reliable physical descriptors of the pore networks in packed beds. This need may be satisfied with the Voronoi or the Delaunay tessellation approaches that could potentially provide the exact diffusion model of a given column.
5 The eddy dispersion term (A) can be successfully measured under isothermal conditions using a subtraction method. This method provides good results because a fair estimate of the external film mass transfer coefficient, k_f can be made from validated correlations and the HETP contribution due to the external film

mass transfer resistance is usually small compared to that of eddy dispersion (especially in the case of poorly retained compounds). Unfortunately, this method is neither highly accurate nor very precise. Alternatively, the eddy dispersion term could be estimated from the structural reconstruction of the column, using flow calculations. The main downside of these methods is our ignorance of the contribution of the trans-column velocity biases, which have become of paramount importance in today's columns.

6 The loss of column efficiency (H_{Heat}) due to the thermal effects that are caused either by the friction of the mobile phase against the bed through which it percolates (in vHPLC) and by its expansion (in SFC) can be accurately predicted provided that we know from independent experimental data the state equation of the eluent, $\rho(P, T)$, the temperature profile along the column wall (the boundary condition needed to solve the heat balance equation), the effective thermal conductivity of the packed bed, the isosteric heat of adsorption of the analyte (which provides the temperature dependence of the retention factor), and the difference between its partial molar volumes in the adsorbed and the bulk phases (which provides the pressure dependence of the retention factor). This contribution to the HETP equation is similar to those related to the other sources of velocity biases across the column (the coupling theory of Giddings applies to them as well). It plays a major role at high velocities, when the product of the flow rate and the column pressure drop exceeds 5 W/m.

7 Finally, the nature of the physico-chemical phenomena that causes the external film mass transfer resistance is not yet understood. The corresponding HETP term (C_f) can be estimated based on the results of correlations that are only qualitatively acceptable, for the lack of a suitable model. The experimental challenges regarding future investigations of this term would consist in separating ways to separately measure the impacts of eddy diffusion and of the external film mass transfer resistance on the column efficiency.

This work shows how it is possible to accurately determine the different non-equilibrium effects in a chromatographic column, but only at the cost of long and meticulous experiments. The versatility of the protocol presented above provides a clear understanding of the mass transfer mechanisms, not only in RPLC but also in NPLC, ion-exchange chromatography (IEX), hydrophilic interaction liquid chromatography (HILIC), and largely in SFC and GC, fields in which new experimental protocols need to be developed. From a practical point of view, this review shows how our understanding of mass transfer resistance in chromatography has evolved over the ages, supported by the progressive evolutions and improvements made to the packing materials, to the column manufacturing and to the instruments. This is illustrated by the shift in the phenomenon that mainly controls column efficiency for low molecular weight compounds. It used to be diffusion through the particles. It is now trans-column eddy dispersion in columns packed with modern sub-2 μm fully porous particles and sub-3 μm superficially porous particles. The problem becomes more stringent when the column diameter is decreased from 4.6, 3.0, 2.1, and 1 mm. The wall effects become increasingly significant as the radial heterogeneity of the bed that the wall promotes seems to affect an increasingly large fraction of the column volume and this radial heterogeneity causes an important broadening of elution bands. Analysts seem to be squeezed between the needs to increase the radial homogeneity of the bed by increasing its diameter and to decrease the thermal contribution to band broadening by decreasing this diameter. Only the use of core–shell particles made with cores having a high heat conductivity could help us out of this dilemma.

This work should motivate renewed research efforts towards a better understanding of the kinetic properties of column packing materials. This work should involve simulations of the rheological problem and an investigation of new alternative packing methods. Yet, the actual performances of sub-2 μm porous particles and sub-3 μm core–shell particles already challenge the capabilities of the most recent vHPLC systems. These instruments should provide a minimum extra-column volume contribution to band broadening. Engineers who design instruments are now pressed to design new injection systems, new connections between the different parts of the instrument, more efficient, more compact arrangements of these parts, new detection cells and a better, more compact architecture of HPLC instruments. Finally, on the column front, expected improvements are in different shell structures and in the replacement of the silica cores by other solids having a higher thermal conductivity in order to alleviate the consequences of the thermal effects taking place in high efficiency columns. Diamond (2200 W/m/K), gold (318 W/m/K), alumina (40 W/m/K), and even zirconia (2 W/m/K) have a significantly larger heat conductivity than silica (1.4 W/m/K). Their use could allow analysts to perform faster separations with a lesser risk of sacrificing as much of the intrinsic column efficiency as they have to do now. In this case, the challenge lies in the difficulty in preparing chemically and mechanically stable core–shell particles using materials of different chemical natures and properties for the non-porous cores and for the surrounding porous shell. In principle, faster and more efficient columns could be prepared and heat effects pushed away by packing 1 μm diameter particles in narrow-bore columns and operating them under extremely high back pressure (up to 7 kbar). Whether this possibility, which was demonstrated by Jorgenson et al. [225–228], will become routinely practical seems remote, in view of the need for pumps that are extremely difficult to design, to manufacture, and to operate.

Acknowledgments

This work was supported in part by the cooperative agreement between the University of Tennessee and the Oak Ridge National Laboratory.

Nomenclature

Roman letters

a_i	ith parameter of the EMG/GMG function
a	Landauer parameter
A_s	Ratio of the external surface area of the solid phase to the column volume (m^{-1})
A	Eddy dispersion term (m)
B	Longitudinal diffusion coefficient
C_f	External film mass transfer coefficient
C	Sample bulk concentration (kg/m^3)
C_i	Internal sample bulk concentration (kg/m^3)
C_s	Total solid–liquid mass transfer coefficient (s)
C_m	Aris–Taylor coefficient
C_a	Adsorption–desorption mass transfer coefficient
C_p	Trans-particle solid–liquid reduced mass transfer coefficient
d	Inner diameter of the capillary tube
$d_{sk.}$	Average skeleton diameter
d_c	Inner diameter of the column stainless steel tube (m)
d_p	Mean particle diameter (m)
D_m	Bulk diffusion coefficient (m^2/s)
D_a	Apparent axial dispersion coefficient along the column (m^2/s)
D_L	Axial dispersion coefficient in the external mobile phase (m^2/s)

D_p Particle diffusivity across the porous stationary phase (m^2/s)
D_{pore} Mesopore diffusivity (m^2/s)
D_S Surface diffusion coefficient (m^2/s)
$D_{S,0}$ Frequency factor for surface diffusion (m^2/s)
D_{eff} Effective diffusivity through the packed bed immersed in the eluent (m^2/s)
D_r Radial dispersion coefficient (m^2/s)
$\overline{D_r}$ Average radial dispersion coefficient (m^2/s)
D_m Bulk molecular diffusion coefficient (m^2/s)
f Parameter in Eq. (113)
F_v Flow rate (m^3/s)
$F(\lambda_m)$ Hindrance diffusion factor
h Reduced plate height
H Column plate height (m)
H_a Axial dispersion plate height (m)
H_{Long} Longitudinal diffusion plate height (m)
H_{Eddy} Eddy dispersion plate height (m)
$H_{Eddy,i}$ Eddy dispersion plate height related to the velocity biases of type i (m)
H_{Film} External film mass transfer resistance plate height (m)
$H_{Stat.}$ Trans-particle mass transfer resistance plate height (m)
H_{Ads} Adsorption–desorption mass transfer resistance plate height (m)
$H_{Fric.-Expa.}$ Friction–expansion plate height (m)
j_s Mass flux density of molecules exchanged between the external and internal eluents ($kg\,m^{-2}\,s^{-1}$)
$j_{surf.}$ Mass flux density of molecules along the adsorbent's surface ($kg\,m^{-2}\,s^{-1}$)
k_a Adsorption–desorption rate constant (s^{-1})
k Retention factor
k_1 Zone retention factor
k_p Particle retention factor
K Henry's constant between the solid phase and the bulk phase.
K_0 Henry's constant at infinite temperature.
k_f External film mass transfer coefficient (m/s)
l Capillary length (m)
L Column length (m)
m_A Molecular weight of solvent A (g/mol)
m_B Molecular weight of solvent B (g/mol)
m_r Ratio of the inner column radius to the particle diameter
m_l Ratio of the column length to the particle diameter
n Integer
N Column efficiency
ΔP Column pressure drop (Pa)
P_e Power heat per unit of column length absorbed by the eluent during decompression (W/m)
P_f Power heat friction per unit of column length (W/m)
P_{ref} Reference pressure (Pa)
p_1 Integer
p_2 Integer
q Sample concentration in the stationary phase
Q_{st} Isosteric heat of adsorption ($J\,mol^{-1}$)
r Radial coordinate (m)
R Molar gas constant ($J\,K^{-1}\,mol^{-1}$)
R_s Characteristic radius of the stationary phase (m)
r_c Internal column radius (m)
Sh Sherwood number
t_d Diffusion time (s)
t_c Convection time (s)
t_p Parking time (s)
Δt_p Increment of the peak parking time (s)
t Time (s)
$\bar{t}$ Average elution time assuming a flow controlled mechanism (s)
T Temperature (K)
t_R Retention time (s)
u_c Average linear velocity along the open capillary (m/s)
u_S Superficial linear velocity (m/s)
u_0 Chromatographic linear velocity (m/s)
u Interstitial linear velocity (m/s)
$u(x)$ Interstitial linear velocity at the radial coordinate x (m/s)
$u(0)$ Interstitial linear velocity at the column center (m/s)
u_R Sample migration linear velocity (m/s)
$u_{R,PP}$ Sample migration linear velocity during the peak parking method (m/s)
V_0 Column hold-up volume (m^3)
V_b Molar volume of the sample at its boiling temperature (m^3/mol)
ΔV_m Difference of the sample partial molar volume in the adsorbed and bulk phase (m^3/mol)
x Reduced radial coordinate
x_A Molar fraction of solvent A
x_B Molar fraction of solvent B
z Axial coordinate along the column (m)

Greek letters

α Knox empirical parameter
α_p Isobaric thermal expansion coefficient (K^{-1})
β Torquato model parameter
ϵ_e External column porosity
ϵ_p Particle porosity
ϵ_t Total column porosity
η_{AB} Viscosity of the solvents' mixture A and B
ϕ_A Association factor of solvent A
ϕ_B Association factor of solvent B
γ_e External obstruction factor
γ_p Internal obstruction factor
γ_r Parameter related to radial dispersion through convection
λ_m Ratio of the sample diameter to the mesopore diameter
λ_{eff} Effective thermal conductivity of the packed bed immersed in the bulk eluent (W/m/K)
λ_i^T Thermal conductivity of the homogeneous medium i (W/m/K)
γ_r Coefficient related to the contribution of eluent convection to the radial dispersion of the sample
λ_i Limiting flow eddy dispersion coefficient for velocity biases of type i.
ν Reduced interstitial linear velocity
ν_i Volume fraction occupied by the homogeneous material i
$\mu_1^{(i)}$ First moment measured according to method i (s)
$\mu_{1,ex}^{(i)}$ First moment of the extra-column concentration profile measured according to method i (s)
$\mu_2^{'(i)}$ Second central moment measured according to method i (s^2)
$\mu_{2,ex}^{'(i)}$ Second central moment of the extra-column concentration profile measured according to method i (s^2)
ω Knox empirical parameter
ω_i Diffusion eddy dispersion coefficient for velocity biases of type i
$\omega_{\beta,i}$ Ratio of the difference between the extremes and the mean velocity for velocity biases of type i
$\omega_{\lambda,i}$ Flow persistence length for velocity biases of type i
$\omega_{\alpha,i}$ Ratio of the characteristic diffusion length to the particle diameter for velocity biases of type i
Ω Ratio of the effective diffusivity of the sample in the porous shell to its bulk diffusion coefficient
$\omega_{\beta,c}^*$ Relative velocity difference between the center and the wall of the column

$\omega_{1/2}$ Half-height peak width (s).
ρ Ratio of the solid non-porous core diameter to the core–shell particle diameter
$\rho(P, T)$ Density of the eluent (kg/m^3)
σ_t^2 Variance of the elution times assuming a flow controlled mechanism (s^2)
σ^2_{Total} Total volume variance (m^3)
$\sigma^2_{Instrument}$ Instrument volume variance (m^3)
$\Delta\sigma_t^2$ Increment of the peak variance measure in the peak parking method (s^2)
ξ_2 Torquato model parameter

References

[1] G.S. Bohart, E.Q. Adams, J. Am. Chem. Soc. 42 (1920) 523.
[2] E. Wicke, Kolloid Z. 86 (1939) 295.
[3] J.N. Wilson, J. Am. Chem. Soc. 62 (1940) 1583.
[4] D. DeVault, J. Am. Chem. Soc. 65 (1943) 532.
[5] H. Thomas, J. Am. Chem. Soc. 66 (1944) 1664.
[6] S. Goldstein, Proc. R. Soc. Lond. A 219 (1953) 151.
[7] E. Glueckauf, J.I. Coates, J. Chem. Soc. (1947) 1315.
[8] A.S. Michaels, Ind. Eng. Chem. 44 (1952) 1922.
[9] L. Lapidus, N.R. Amundson, J. Phys. Chem. 56 (1952) 984.
[10] J.B. Rosen, J. Chem. Phys. 20 (1952) 387.
[11] J.J. van Deemter, F.J. Zuiderweg, A. Klinkenberg, Chem. Eng. Sci. 5 (1956) 271.
[12] A.J.P. Martin, R.L.M. Synge, Biochem. J. 35 (1941) 1358.
[13] G. Guiochon, A. Felinger, A. Katti, D. Shirazi, Fundamentals of Preparative and Nonlinear Chromatography, 2nd ed., Academic Press, Boston, MA, 2006.
[14] M.J.E. Golay, in: D.H. Desty (Ed.), Gas Chromatography 1958, Butterworths, London, 1959, p. 36.
[15] J. Giddings, Dynamics of Chromatography, Marcel Dekker, New York, NY, 1965.
[16] J.C. Giddings, in: E. Heftmann (Ed.), Chromatography. A Laboratory Handbook of Chromatographic and Electrophoretic Methods, Van Nostrand Reinhold, New York, NY, 1975, p. 27.
[17] W. Feller, Probability Theory and its Application, Wiley, New York, NY, 1950 (Chap. 14).
[18] J.C. Giddings, H. Eyring, J. Phys. Chem. 59 (1955) 416.
[19] J.C. Giddings, J. Chem. Phys. 31 (1959) 1462.
[20] J.C. Giddings, J. Chromatogr. 3 (1960) 443.
[21] J.C. Giddings, J. Chromatogr. 5 (1961) 46.
[22] J.C. Giddings, J. Phys. Chem. 68 (1964) 184.
[23] D.A. McQuarrie, J. Chem. Phys. 38 (1963) 437.
[24] A. Felinger, A. Cavazzini, M. Remelli, F. Dondi, Anal. Chem. 71 (1999) 4472.
[25] A. Cavazzini, M. Remelli, F. Dondi, A. Felinger, Anal. Chem. 71 (1999) 3453.
[26] F. Dondi, P. Munari, M. Remelli, A. Cavazzini, Anal. Chem. 72 (2000) 4353.
[27] F. Dondi, A. Cavazzini, M. Remelli, A. Felinger, M. Martin, J. Chromatogr. A 943 (2002) 185.
[28] A. Cavazzini, F. Dondi, A. Jaulmes, C. Vidal-Madjar, A. Felinger, Anal. Chem. 74 (2002) 6269.
[29] J.H. Knox, J. Chromatogr. Sci. 15 (1977) 352.
[30] J.F.K. Huber, J.A.R.J. Hulsman, Anal. Chim. Acta 38 (1967) 305.
[31] J.F.K. Huber, J. Chromatogr. Sci. 7 (1969) 85.
[32] C. Horvath, H.-J. Lin, J. Chromatogr. 126 (1976) 401.
[33] J.P. Bouchaud, A. Georges, C. R. Acad. Sci. IIC 307 (1988) 1431.
[34] F. Gritti, G. Guiochon, Anal. Chem. 78 (2006) 5329.
[35] U. Neue, M. Kele, J. Chromatogr. A 1157 (2007) 236.
[36] F. Gritti, G. Guiochon, J. Chromatogr. A 1187 (2008) 165.
[37] F. Gritti, G. Guiochon, Anal. Chem. 80 (2008) 5009.
[38] F. Gritti, G. Guiochon, Anal. Chem. 80 (2008) 6488.
[39] F. Gritti, G. Guiochon, J. Chromatogr. A 1206 (2008) 113.
[40] G. Guiochon, A. Tarafder, J. Chromatogr. A 1218 (2011) 1037.
[41] G. Guiochon, J. Chromatogr. A 1168 (2007) 101.
[42] F. Gritti, G. Guiochon, J. Chromatogr. A 1218 (2011) 5216.
[43] K. Mriziq, J. Abia, Y. Lee, G. Guiochon, J. Chromatogr. A 1193 (2008) 97.
[44] J. Abia, K. Mriziq, G. Guiochon, J. Chromatogr. A 1216 (2009) 3185.
[45] F. Gritti, G. Guiochon, AIChE J. 56 (2010) 1495.
[46] F. Gritti, G. Guiochon, J. Chromatogr. A 1217 (2010) 6350.
[47] G. Guiochon, in: K.K. Unger, N. Tanaka, E. Machtejevas (Eds.), Monolithic Silicas Concepts, Syntheses, Characterization, Modeling and Applications in Liquid Phase Separations, Wiley, New York, NY, 2011, p. 127 (Chap. 7).
[48] R. Plumb, J.R. Mazzeo, E.S. Grumbach, P. Rainville, M. Jones, T. Wheat, U.D. Neue, B. Smith, K.A. Johnson, J. Sep. Sci. 30 (2007) 1158.
[49] F. Gritti, M. Martin, G. Guiochon, Anal. Chem. 81 (2009) 3365.
[50] C. Horváth, S.R. Lipsky, J. Chromatogr. Sci. 7 (1969) 109.
[51] J.J. Kirkland, Anal. Chem. 41 (1969) 218.
[52] J.J. Kirkland, Anal. Chem. 64 (1992) 1239.
[53] J.J. DeStefano, T.J. Langlois, J.J. Kirkland, J. Chromatogr. Sci. 46 (2007) 254.
[54] J.O. Omamogho, J.P. Hanrahan, J. Tobin, J.D. Glennon, J. Chromatogr. A 1218 (2011) 1942.
[55] K. Kaczmarski, G. Guiochon, Anal. Chem. 79 (2007) 4648.
[56] A. Felinger, J. Chromatogr. A 1218 (2011) 1938.
[57] S. Deridder, G. Desmet, J. Chromatogr. A 1218 (2011) 32.
[58] F. Gritti, G. Guiochon, J. Chromatogr. A 1218 (2011) 3476.
[59] F. Gritti, G. Guiochon, Chem. Eng. Sci. 66 (2011) 3773.
[60] S. Golshan-Shirazi, G. Guiochon, J. Chromatogr. 603 (1992) 1.
[61] E. Glueckauf, J. Chem. Soc. (1947) 1302.
[62] N.K. Hiester, T. Vermeulen, Chem. Eng. Progr. 48 (1952) 505.
[63] B. Lin, S. Golshan-Shirazi, G. Guiochon, J. Phys. Chem. 93 (1989) 3363.
[64] S. Golshan-Shirazi, B. Lin, G. Guiochon, J. Phys. Chem. 93 (1989) 6871.
[65] J. Giddings, Unified Separation Science, John Wiley & Sons, New York, NY, 1991.
[66] J.H. Knox, M. Saleem, J. Chromatogr. Sci. 7 (1969) 614.
[67] H. Poppe, J. Chromatogr. A 778 (1997) 3.
[68] D.J. Gunn, Trans. Inst. Chem. Eng. 47 (1969) T351.
[69] D.J. Gunn, Trans. Inst. Chem. Eng. 47 (1969) 109.
[70] D.J. Gunn, Chem. Eng. Sci. 42 (1987) 363.
[71] D.J. Gunn, R. England, Chem. Eng. Sci. 26 (1971) 1413.
[72] H.-K. Rhee, R. Aris, N. Amundson, First-Order Partial Differential Equations. II. Theory and Application of Hyperbolic Systems of Quasilinear Equations, Prentice-Hall, Englewood Cliffs, NJ, 1989.
[73] P. Rouchon, M. Schonauer, P. Valentin, G. Guiochon, Sep. Sci. Technol. 22 (1987) 1793.
[74] E. Kučera, J. Chromatogr. 19 (1965) 237.
[75] M. Kubin, Coll. Czech Chem. Commun. 30 (1965) 2900.
[76] K. Miyabe, G. Guiochon, J. Phys. Chem. B 106 (2002) 8898.
[77] K. Kaczmarski, G. Storti, M. Mazzotti, M. Morbidelli, Comput. Chem. Eng. 21 (1997) 641.
[78] A. Felinger, A. Cavazzini, F. Dondi, J. Chromatogr. A 1043 (2004) 149.
[79] A. Felinger, LC–GC North Am. 22 (7) (2004) 642.
[80] A. Felinger, J. Chromatogr. A 1126 (2006) 120.
[81] F. Gritti, A. Felinger, G. Guiochon, J. Chromatogr. A 1017 (2003) 45.
[82] J. Knox, H. Scott, J. Chromatogr. 282 (1983) 297.
[83] L. Snyder, J. Kirkland, Introduction to Modern Liquid Chromatography, Wiley and Sons, New York, NY, 1989.
[84] G. Desmet, K. Broeckhoven, J.D. Smet, S. Deridder, G. Baron, P. Gzil, J. Chromatogr. A 1188 (2008) 171.
[85] K. Broeckhoven, D. Cabooter, F. Lynen, S. Deridder, P. Sandra, G. Desmet, J. Chromatogr. A 1188 (2008) 189.
[86] A. Berthod, F. Chartier, J. Rocca, J. Chromatogr. 469 (1989) 53.
[87] F. Gritti, G. Guiochon, Chem. Eng. Sci. 61 (2006) 7636.
[88] F. Gritti, G. Guiochon, Anal. Chem. 79 (2007) 3188.
[89] F. Gritti, G. Guiochon, J. Chromatogr. A 1166 (2007) 47.
[90] F. Gritti, G. Guiochon, J. Chromatogr. A 1169 (2007) 125.
[91] F. Gritti, G. Guiochon, J. Chromatogr. A 1157 (2007) 289.
[92] F. Gritti, G. Guiochon, J. Chromatogr. A 1216 (2009) 4752.
[93] F. Gritti, G. Guiochon, J. Chromatogr. A 1216 (2009) 1353.
[94] F. Gritti, G. Guiochon, Anal. Chem. 81 (2009) 2723.
[95] F. Gritti, G. Guiochon, J. Chromatogr. A 1217 (2010) 1485.
[96] F. Gritti, I. Leonardis, D. Shock, P. Stevenson, A. Shalliker, G. Guiochon, J. Chromatogr. A 1217 (2010) 1589.
[97] F. Gritti, G. Guiochon, J. Chromatogr. A 1217 (2010) 5069.
[98] F. Gritti, G. Guiochon, Chem. Eng. Sci. 65 (2010) 6310.
[99] F. Gritti, I. Leonardis, J. Abia, G. Guiochon, J. Chromatogr. A 1217 (2010) 3219.
[100] F. Gritti, G. Guiochon, J. Chromatogr. A 1217 (2010) 5137.
[101] F. Gritti, G. Guiochon, J. Chromatogr. A 1218 (2011) 907.
[102] F. Gritti, G. Guiochon, Chem. Eng. Sci. 65 (2010) 6327.
[103] F. Gritti, G. Guiochon, J. Chromatogr. A 1217 (2010) 8167.
[104] R. Landauer, J. Appl. Phys. 23 (1952) 779.
[105] H. Davis, J. Am. Ceram. Soc. 60 (1977) 499.
[106] F. Gritti, G. Guiochon, AIChE J. 57 (2011) 346.
[107] J.C.M. Garnett, Philos. Trans. R. Soc. Lond. Ser. B 203 (1904) 385.
[108] S. Torquato, Random Heterogeneous Materials. Microstructure and Macroscopic Properties, Springer, New York, NY, 2002.
[109] S. Deridder, G. Desmet, J. Chromatogr. A 1218 (2011) 46.
[110] S. Torquato, J. Appl. Phys. 58 (1985) 3790.
[111] E. Renkin, J. Gen. Physiol. 38 (1954) 225.
[112] H. Brenner, L. Gaydos, J. Colloid Interf. Sci. 58 (1977) 312.
[113] R. Bird, W. Stewart, E. Lightfoot, Transport Phenomena, John Wiley and Sons, New York, NY, 2002.
[114] J.C. Giddings, Nature 184 (1959) 357.
[115] J.C. Giddings, R.A. Robison, Anal. Chem. 34 (1962) 885.
[116] J.C. Giddings, Anal. Chem. 34 (1962) 1186.
[117] P. Magnico, M. Martin, J. Chromatogr. 517 (1990) 31.
[118] S. Khirevich, A. Holtzel, D. Hlushkou, U. Tallarek, Anal. Chem. 79 (2007) 9340.
[119] S. Khirevich, A. Holtzel, A. Seidel-Morgenstern, U. Tallarek, Anal. Chem. 80 (2008) 5391.
[120] S. Khirevich, A. Holtzel, S. Ehlert, A. Seidel-Morgenstern, U. Tallarek, Anal. Chem. 81 (2009) 7057.
[121] S. Khirevich, A. Daneyko, A. Holtzel, A. Seidel-Morgenstern, U. Tallarek, J. Chromatogr. A 1217 (2010) 4713.
[122] D. Hlushkou, S. Bruns, U. Tallarek, J. Chromatogr. A 1217 (2010) 3674.
[123] J. Gotz, K. Zick, C. Heinen, T. Konig, Chem. Eng. Proc. 41 (2002) 611.
[124] T. Laiblin, W. Arlt, R. Kaiser, R. Kirsch, Chem. Ing. Tech. 79 (2007) 1213.
[125] F. Gritti, G. Guiochon, J. Chromatogr. A 1218 (2011) 1592.
[126] F. Gritti, G. Guiochon, J. Chromatogr. A 1218 (2011) 1915.
[127] H. Hasimoto, O. Sano, Annu. Rev. Fluid Mech. 12 (1980) 335.
[128] D. Hlushkou, U. Tallarek, J. Chromatogr. A 1126 (2006) 70.

[129] R. Hill, D. Koch, A. Ladd, J. Fluid Mech. 448 (2001) 243.
[130] D. Hlushkou, S. Bruns, A. Holtzel, U. Tallarek, Anal. Chem. 82 (2010) 7150.
[131] J.H. Knox, G.R. Laird, P.A. Raven, J. Chromatogr. 122 (1976) 129.
[132] C.H. Eon, J. Chromatogr. 149 (1978) 29.
[133] T. Farkas, G. Guiochon, Anal. Chem. 69 (1997) 4592.
[134] G. Guiochon, T. Farkas, H.G. Sajonz, J.-H. Koh, M. Sarker, B.J. Stanley, T. Yun, J. Chromatogr. A 762 (1997) 83.
[135] B.G. Yew, J. Ureta, R.A. Shalliker, E.C. Drumm, G. Guiochon, AIChE J. 49 (2003) 642.
[136] T. Farkas, G. Guiochon, Anal. Chem. 69 (1997) 4592.
[137] T. Farkas, M.J. Sepaniak, G. Guiochon, AIChE J. 43 (1997) 1964.
[138] R. Aris, Proc. R. Soc. A 235 (1956) 67.
[139] M. Martin, G. Guiochon, Anal. Chem. 54 (1982) 1533.
[140] U. Tallarek, K. Albert, E. Bayer, G. Guiochon, AIChE J. 42 (1996) 3041.
[141] U. Tallarek, E. Bayer, G. Guiochon, J. Am. Chem. Soc. 120 (1998) 1494.
[142] J.C. Giddings, Nature 188 (1960) 847.
[143] C. Satterfield, C. Colton, H. Wayne Jr., AIChE J. 19 (1973) 628.
[144] K. Miyabe, G. Guiochon, J. Chromatogr. A 1217 (2010) 1713.
[145] W. De Malsche, H. Gardeniers, G. Desmet, Anal. Chem. 80 (2008) 5391.
[146] J.C. Giddings, J. Chromatogr. 3 (1960) 443.
[147] A. Lenhoff, C. Brian, J. Chromatogr. A 1205 (2008) 46.
[148] P. Chun, C. Yang, Biophys. Chem. 9 (1979) 313.
[149] E. Wilson, C.J. Geankoplis, Ind. Eng. Chem. Fundam. 5 (1966) 9.
[150] T. Kataoka, H. Yoshida, K. Ueyama, J. Chem. Eng. Jpn. 5 (1972) 132.
[151] K. Miyabe, M. Ando, N. Ando, G. Guiochon, J. Chromatogr. A 1210 (2008) 60.
[152] K. Miyabe, Y. Kawaguchi, G. Guiochon, J. Chromatogr. A 1217 (2010) 3053.
[153] M.A. Khan, Nature 186 (1960) 800.
[154] M.A. Khan, in: M. van Swaay (Ed.), Gas Chromatography, Butterworth Inc., Washington, DC, 1962, p. 3.
[155] M.R. James, J.C. Giddings, H. Eyring, J. Phys. Chem. 68 (1964) 1725.
[156] M. van Dyke, An Album of Fluid Motion, The Parabolic Press, Stanford, CA, 1982.
[157] F. Gritti, G. Guiochon, J. Chromatogr. A 1131 (2006) 151.
[158] H. Lin, S. Horváth, Chem. Eng. Sci. 36 (1981) 47.
[159] H. Poppe, J.C. Kraak, J.F.K. Huber, J.H.M. Van Den Berg, Chromatographia 14 (1981) 515.
[160] K. Kaczmarski, D. Poe, G. Guiochon, J. Chromatogr. A 1217 (2010) 6578.
[161] M. Martin, G. Guiochon, J. Chromatogr. A 1090 (2005) 16.
[162] K. Kaczmarski, J. Kostka, W. Zapala, G. Guiochon, J. Chromatogr. A 1216 (2009) 6560.
[163] K. Kaczmarski, F. Gritti, J. Kostka, G. Guiochon, J. Chromatogr. A 1216 (2009) 6575.
[164] J. Kostka, F. Gritti, K. Kaczmarski, G. Guiochon, J. Chromatogr. A 1217 (2010) 4704.
[165] E.W. Lemmon, M. Huber, M.O. McLinden, D.G. Friend, National Institute of Standards and Technology, Standard Reference Data Program, Gaithersburg 8.0.
[166] F. Gritti, G. Guiochon, J. Chromatogr. A 1218 (2011) 4452.
[167] A. Ouano, Ind. Eng. Chem. Fundam. 11 (1972) 268.
[168] J. Atwood, J. Goldstein, J. Phys. Chem. 88 (1984) 1875.
[169] J. Li, P. Carr, Anal. Chem. 69 (1997) 2530.
[170] J. Li, P. Carr, Anal. Chem. 69 (1997) 2550.
[171] G. Taylor, Proc. R. Soc. A 186 (1953) 317.
[172] C. Wilke, P. Chang, AIChE J. 1 (1955) 264.
[173] E. Scheibel, Ind. Eng. Chem. Fundam. 46 (1954) 2007.
[174] M. Lusis, G. Ratcliff, Can. J. Chem. Eng. 46 (1968) 385.
[175] W. Hayduk, H. Laudie, AIChE J. 20 (1974) 611.
[176] J.H. Knox, L. McLaren, Anal. Chem. 36 (1964) 1477.
[177] K. Miyabe, Y. Matsumoto, G. Guiochon, Anal. Chem. 79 (2007) 1970.
[178] K. Miyabe, N. Ando, G. Guiochon, J. Chromatogr. A 1216 (2009) 4377.
[179] K. Miyabe, J.-I. Nagai, G. Guiochon, Chem. Eng. Sci. 65 (2010) 3859.
[180] D. Ludlum, R. Warner, H. Smith, J. Phys. Chem. 66 (1962) 1540.
[181] P. Dunlop, C. Pepela, B. Steel, J. Am. Chem. Soc. 92 (1970) 6743.
[182] H. Gao, X. Wu, L. Bingchang, J. Chromatogr. Sci. 48 (2010) 478.
[183] H. Gao, X. Wu, L. Bingchang, J. Chromatogr. Sci. 48 (2010) 742.
[184] C. Vidal-Madjar, G. Guiochon, J. Chromatogr. 142 (1977) 61.
[185] R. Pfeffer, Ind. Eng. Chem. Fundam. 3 (1964) 380.
[186] K. Miyabe, N. Ando, T. Nakamura, G. Guiochon, Chem. Eng. Sci. 65 (2010) 5950.
[187] M. Al-Bokari, D. Cherrak, G. Guiochon, J. Chromatogr. A 975 (2002) 275.
[188] F. Gritti, W. Piatkowski, G. Guiochon, J. Chromatogr. A 978 (2002) 81.
[189] F. Gritti, W. Piatkowski, G. Guiochon, J. Chromatogr. A 983 (2003) 51.
[190] M. Kele, G. Guiochon, J. Chromatogr. A 960 (2002) 19.
[191] K. Cabrera, J. Sep. Sci. 27 (2004) 843.
[192] S. Bruns, U. Tallarek, J. Chromatogr. A 1218 (2011) 1849.
[193] S. Bruns, T. Mullner, M. Kollmann, J. Schachtner, A. Holtzel, U. Tallarek, Anal. Chem. 82 (2010) 6569.
[194] H. Purnell, Gas Chromatography, Wiley, New York, NY, 1962, p. 185.
[195] L.R. Snyder, Anal. Chem. 39 (1967) 698.
[196] J.N. Done, J.H. Knox, J. Chromatogr. Sci. 10 (1972) 606.
[197] I. Halász, M. Naefe, Anal. Chem. 44 (1972) 76.
[198] C. Dewaele, M. Verzele, J. Chromatogr. 260 (1983) 13.
[199] N.A. Dougharty, AIChE J. 18 (1972) 657.
[200] G. Carta, G.S. Bauer, AIChE J. (1990) 147.
[201] A. Daneyko, S. Khirevich, U. Tallarek, in: 35th International Symposium and Exhibit on High Performance Liquid Phase Separations and Related Techniques, HPLC2010, Boston, June 17–22, 2010 (Poster P-2412-W).
[202] J. Billen, D. Guillarme, S. Rudaz, J.-L. Veuthey, H. Ritchie, B. Grady, G. Desmet, J. Chromatogr. A 1161 (2007) 224.
[203] D. Cabooter, J. Billen, H. Terryn, F. Lynen, P. Sandra, G. Desmet, J. Chromatogr. A 1217 (2010) 7074.
[204] F. Gritti, G. Guiochon, J. Chromatogr. A 1138 (2007) 141.
[205] Y.P. Zarichnyak, V.V. Novikov, Inzh. -Fizi. Zh. 34 (1978) 648.
[206] F. Jiang, A.C.M. Sousa, Heat Mass Transfer 43 (2007) 479.
[207] P. Persson, H. Kempe, G. Zacchi, B. Nilsson, Chem. Eng. Res. Design 82 (A4) (2004) 517.
[208] P. Persson, H. Kempe, G. Zacchi, B. Nilsson, Process Biochem. 40 (2005) 1649.
[209] C. Gritti, F. Sanchez, T. Farkas, G. Guiochon, J. Chromatogr. A 1217 (2010) 3000.
[210] F. Gritti, G. Guiochon, J. Chromatogr. A 1217 (2010) 7677.
[211] F. Gritti, G. Guiochon, J. Chromatogr. A 1217 (2010) 1604.
[212] B. Poling, J. Prausnitz, J. O'Connel, The Properties of Gases and Liquids, 5th edition, McGraw-Hill, New York, NY, 2001.
[213] X. Wang, W.E. Barber, P.W. Carr, J. Chromatogr. A 1107 (2006) 139.
[214] H. Minakuchi, K. Nakanishi, N. Soga, N. Ishizuka, N. Tanaka, J. Chromatogr. A 797 (1998) 121.
[215] K. Kaczmarski, F. Gritti, G. Guiochon, J. Chromatogr. A 1177 (2008) 92.
[216] D. Horne, J.H. Knox, L. McLaren, J. Sep. Sci. 1 (1966) 531.
[217] D. Poe, J. Schroden, J. Chromatogr. A 1216 (2009) 7915.
[218] F. Gritti, G. Guiochon, J. Chromatogr. A 1218 (2011) 4632.
[219] F. Gritti, G. Guiochon, J. Chromatogr. A 1215 (2008) 64.
[220] F. Gritti, G. Guiochon, J. Chromatogr. A 1216 (2009) 6124.
[221] H.-K. Rhee, B.F. Bodin, N.R. Amundson, Chem. Eng. Sci. 26 (1971) 1571.
[222] H.-K. Rhee, N.R. Amundson, Chem. Eng. Sci. 27 (1972) 199.
[223] H.-K. Rhee, N.R. Amundson, Chem. Eng. Sci. 28 (1973) 55.
[224] F. Gritti, G. Guiochon, J. Chromatogr. A 1218 (2011) 896.
[225] K.D. Patel, A.D. Jerkovich, J.C. Link, J.W. Jorgenson, Anal. Chem. 76 (2004) 5777.
[226] J.S. Mellors, J.W. Jorgenson, Anal. Chem. 76 (2004) 5441.
[227] J.E. MacNair, K.D. Patel, J.W. Jorgenson, Anal. Chem. 71 (1999) 700.
[228] J.E. MacNair, K.C. Lewis, J.W. Jorgenson, Anal. Chem. 69 (1997) 983.